UNIVERSIDADE FEDERAL DE PERNAMBUCO
CENTRO DE CIÊNCIAS EXATAS E DA NATUREZA
PROGRAMA DE PÓS-GRADUAÇÃO EM FÍSICA

Igor Vinícius Gomes de Oliveira

Cooperative and Affinity Effects on Majority-vote Opinion Dynamics

Recife

2025

Igor Vinícius Gomes de Oliveira

Cooperative and Affinity Effects on Majority-vote Opinion Dynamics

Dissertation presented to the Postgraduate Program in Physics of the Center for Exact and Natural Sciences of the Federal University of Pernambuco, as a partial requirement for obtaining the degree of Master in Physics.

Research area: Theoretical and computational physics

Advisor: André Luis da Mota Vilela

Recife

2025

.Catalogação de Publicação na Fonte. UFPE - Biblioteca Central

Oliveira, Igor Vinicius Gomes de.
Cooperative and affinity effects on majority-vote opinion dynamics / Igor Vinicius Gomes de Oliveira. - Recife, 2025.
131 f.: il.

Dissertação (Mestrado) - Universidade Federal de Pernambuco, Centro de Ciências Exatas e da Natureza, Programa de Pós-Graduação em Física, 2025.
Orientação: André Luis da Mota Vilela.
Inclui referências e anexo.

1. Sistemas complexos; 2. Sociofísica; 3. Redes complexas. I. Vilela, André Luis da Mota. II. Título.

UFPE-Biblioteca Central

IGOR VINÍCIUS GOMES DE OLIVEIRA

COOPERATIVE AND AFFINITY EFFECTS ON MAJORITY-VOTE OPINION DYNAMICS

Dissertation presented to the Graduate Program in Physics at Universidade Federal de Pernambuco, as a partial requirement for obtaining the title of Master's in Physics.

Area of Concentration: Theoretical and Computational Physics,

Approval date: 28/02/2025.

EXAMINING BOARD

_____

Prof. Dr. André Luis da Mota Vilela
Advisor
Universidade de Pernambuco

_____

Prof. Dr. Paulo Roberto de Araujo Campos
Internal Examiner
Universidade Federal de Pernambuco

_____

Profa. Dra. Celia Beatriz Anteneodo de Porto
External Examiner
Pontifícia Universidade Católica do Rio de Janeiro

I dedicate this work to every person with a disability who, like me, is learning to navigate a world that is still challenging for us. Statistically, we are still a minority in schools and even more resolutely a rarity in universities, research departments, master's programs, and doctoral studies. No single step in this journey is taken without true strength, perseverance, and faith in ourselves.

I myself have a bilateral genetic hearing impairment (inherited from my mother). Despite facing challenges and adaptations, I did not allow this to be an obstacle, and I have thrived academically and professionally. I am incredibly grateful for the support from my family and friends, and I am pleased to be able to help many people at the university and in the workplace. It fills me with joy to know that they see me as an inspiring, enthusiastic, positive, and persistent person.

I hope to inspire others, reassuring them that their dreams are worthy and within reach. Science flourishes because of diversity, and our perspectives are an asset. This piece of work will go some way towards reaching this goal, and many scientists work in environments where they can bring their diverse knowledge to the table and advance understanding.

To all of you who crave to burst barriers and soar to new heights: dont give up, believe in yourself and remember that what you contribute has a profound effect. Let's make the difference we wanna see in the world.

ACKNOWLEGDMENTS

In the complex network of life, we have infinite reasons to thank.

Before doing almost anything in my life, I always devoted myself to talking with God. There is no price for the peace of mind and spirit, the humility, perseverance, joy, natural curiosity, and wisdom I always got when in your presence. It is like an instantaneous passport of strength and joy. Some people often ask me where all of my energy comes from. There is no secret: Rejoice in God always. I will repeat it: Rejoice!

"Do not grieve, for the joy of the LORD is your strength."

Nehemiah 8:10

I am incredibly thankful to my family for all the support and encouragement. In particular, the incentives I got from my mother, Edenize, and my father, Marcos, my aunts, Alexandrina and Edleusa, and my uncle, Israel, are invaluable. They supported my curiosity and always believed in me. Thanks for all the comics, books, love, and patience. You taught me the importance of honesty, curiosity, hard work, and never giving up. I am extremely fortunate to have a family that supported my dreams and believed me. You gave me the whole world and a little more; I love you!

I am glad for all the love and support from my girlfriend Adriane (Quantus C.D) and her family. Thanks for being a strong partner in my trajectory, always believing in me and motivating me all these years. You made everything easier, even when everything appeared to wreak havoc. I love you!

My advisor, André Vilela, became more than a professor; he became my mentor. I am grateful for all your encouragement and for always incentivizing and pushing me to do my best. Sometimes, you believed in me even more than I did. You opened my mind with the courage to follow my dreams, and beyond professional development, you always pushed personal growth in all of us. Thanks for supporting me in my first international trip and presentation at the APS March Meeting. The Outstanding Presentation Award is all yours!

I also had the fantastic opportunity to work closely and research with Professor Paulo Campos. Thanks for all the learning and fun with the 4843 surprise tests of stochastic processes, for showing me how hard counting is for your company at the APS March meeting, and for the exciting research we did with Mateus.

I was lucky to have made big friends in the lab. Together, we always had fun and learned more. Big thanks to Mateus (Shurelby), Giuliano (Smeeeagol), my brother Cauê (Tíbio? Perônio?), Luiz Aranha (Spider-man), Caio (Student caio), Rafael (Rafinha), Duda (Dudinha), and Larissa (champion) for all the fun talks and study we did together. I am grateful to all the employees who care for the department, so we have a good place to study and research.

I cannot forget to thank my friends for all the partnerships and support: Samuel (Samuca), João Vitor (Cavalca), Raquel, Rebeca, Jessica, Netinho, Clarinha, Pedrão, Pedrinho, Reinaldo, Rodrigo, Lis, Heitor (Air Master) Diogo (Templário), Manoela (Manu). I also want to thank some big non-human friends, such as my all-time energetic dog Bolton (in memory) and my affectionate cat Marie, who typed all my documents and stayed at my side while studying at home and doing this dissertation.

While I lost contact with him, I vividly remember when I first started learning physics in a small school with my teacher, Alexandre Nogueira. His iconic physics cap, futuristic handwriting and charismatic teaching ignited my passion and curiosity. I was captivated by the power of science to explain the complexities of our world. When I started seriously reading the physics textbook and became lost in its pages, I knew I had found my way in the world.

I was generally bored in most classes and preferred reading my books quietly at my desk, something that not all teachers looked at with good eyes. However, Nogueira understood me and did everything he could to support me. He gifted me with more advanced physics textbooks and Carl Sagan DVD documentaries, encouraging me to dream big. His symbolic gesture of passing me his personalized physics cap upon high school graduation is something I will never forget. It pushed me to start rattling the bars of my cage and impacting others the same way he profoundly affected me.

"People only get really interesting when they start to rattle the bars of their cages."

Alain de Botton

I cannot forget to thank *Fundação Coordenação de Aperfeiçoamento de Pessoal de Nível Superior*, which financially supported my research. Thanks for empowering young researchers, driving knowledge production, and contributing to Brazil's scientific and technological advancement.

However, as I think of it, I depend on many other people, including those who helped and inspired the people I mentioned above. Therefore, I am grateful to all of them, but it would

be tough to mention everyone, right? Please allow me to use the power of mathematics and complex networks to thank you all.

Let us assume that the adjacency matrix of our big real-world social network comprising all individuals is A. Then, if my node on this network is i, my first neighbors that I mentioned above is the set $\{j \mid (A^1)_{ij} > 0\}$ and the neighbors of my neighbors can be described as $\bigcup_{d=1}^{2}\{j \mid (A^d)_{ij} > 0\}$, which encompasses the people who helped the ones I mentioned above. But what about the people who helped these people who helped these people? Following this argument by induction, to do the complete thanks, I would like to express my complete gratitude to all of you:

$$\lim_{k\to\infty} \bigcup_{d=1}^{k} \{j \mid (A^d)_{ij} > 0\}. \tag{1}$$

So, for you all,

$$\lim_{k\to\infty} \bigcup_{d=1}^{k} \{j \mid (A^d)_{ij} > 0\}, \tag{2}$$

thanks so much for everything!

RESUMO

Este trabalho investiga como o comportamento colaborativo social e a conectividade influenciam a formação de consenso no modelo do voto da maioria com ruído q. Agentes colaborativos experimentam uma redução efetiva no ruído social μq, onde $0 < \mu < 1$ é o parâmetro de sensibilidade ao ruído que amplifica a validação social. Usando simulações Monte Carlo, encontramos transições de fase de segunda ordem entre dissenso e consenso, com o modelo de voto da maioria cooperativo pertencendo à mesma classe de universalidade do modelo de Ising em equilíbrio 2D. Investigamos a produção de entropia social no modelo do voto da maioria em redes regulares quadradas e conjecturamos que a heterogeneidade entre indivíduos cooperativos e não cooperativos pode ser uma manifestação natural do Princípio da Produção Máxima de Entropia, no qual os estados estacionários fora do equilíbrio mais prováveis são aqueles com a maior taxa de produção de entropia. Nossos resultados destacam os efeitos de um nível de atenuação da ansiedade social na melhoria do consenso de grupo. Inspirados por redes sociais como X e Facebook, também propomos e analisamos os efeitos de redes livres de escala baseadas em afinidade na dinâmica de formação de opinião. Nesse contexto, definimos um substrato contínuo e modificamos o algoritmo de Barabási-Albert introduzindo uma probabilidade de conexão baseada na distância e no expoente de lei de potência α, definido como o parâmetro de afinidade. Essas redes baseadas em afinidade exibem a propriedade livre de escala, apresentam um coeficiente de agrupamento mais alto e geram distribuições de lei de potência côncavas, alinhando-se com dados reais de redes sociais populares. Descobrimos que a afinidade local promove o surgimento de polarização de opinião e transições de fase no modelo de voto da maioria, introduzindo uma nova classe de universalidade. Nosso trabalho evidencia como as conexões entre cooperação, afinidade e dinâmica de opinião moldam a formação de consenso em redes sociais, fornecendo perspectivas essenciais sobre o comportamento social e os mecanismos subjacentes dos sistemas complexos.

Palavras-chave: Fenômenos críticos, Sistemas complexos, Redes complexas, Simulações Monte Carlo, Teoria de Campo Médio, Sociofísica.

ABSTRACT

This work investigates how social collaborative behavior and connectivity influence consensus formation of the majority-vote model with noise q. Collaborative agents experience a reduced effective social noise μq, where $0 < \mu < 1$ is the noise sensibility parameter that enhances social validation. Using Monte Carlo simulations, we find second-order dissensus-consensus phase transitions and the cooperative majority-vote model belongs to the same universality class as the 2D equilibrium Ising model. We investigate social entropy production in the majority-vote model on regular square networks and conjecture the heterogeneity between cooperative and non-cooperative individuals could be a potential natural manifestation of the Maximum Entropy Production Principle, where the most probable non-equilibrium steady states have the highest entropy production rate. Our results highlight the effects of a social anxiety attenuation level in improving group consensus. Inspired by social media, such as X and Facebook, we also propose and examine the effects of affinity-based scale-free networks on opinion formation dynamics. In this context, we define a continuous substrate and modify the Barabási-Albert algorithm by introducing a connection probability based on distance and power law exponent α, defined as the affinity parameter. These affinity-based networks display the scale-free property, feature a higher clustering coefficient, and generate concave power law distributions, aligning with real-world data of popular social media. We find that local affinity promotes the emergence of opinion polarization and phase transitions in the majority-vote model, introducing a new universality class. Our work exhibits how the connections between cooperation, affinity, and opinion dynamics shape consensus formation in social networks, providing essential perspectives on societal behavior and the underlying mechanisms of complex systems.

Keywords: Critical Phenomena, Complex systems, Complex networks, Monte Carlo simulation, Mean-field theory, Sociophysics.

LIST OF FIGURES

LIST OF TABLES

CONTENTS

1 COMPLEX SCIENCE INTRODUCTION

"I think the next century will be the century of complexity."
Stephen Hawking

"The science of complexity is about
how interactions lead to patterns,
and patterns lead to changes."
Stephen Wolfram

This chapter introduces the basic concepts behind complex systems, complex networks, and two exciting applications: Sociophysics and Econophysics. These young multidisciplinary research fields investigate topics from "soft sciences", such as opinion formation and voting, using tools and formalism from the "hard science", such as physics, mathematics and computer science.

1.1 COMPLEX SYSTEMS

Complexity is the footprint behind highly unpredictable phenomena, not reducible to closed laws of mathematics, and that cannot be understood by studying the independent components of a system. Complex systems show emergent behavior due to many nonlinear interactions among their elements, so perturbations in one part of the system may have dramatic cascading effects elsewhere. From interactions among such systems, properties beyond the combination of their parts can arise, leading to new properties and behavior emerging from the interactions of components that can be completely different from those between the original individual elements interacting with each other (LADYMAN; LAMBERT; WIESNER, 2013).

For example, just a single stopped car on a busy highway can trigger a massive traffic jam, cascading backward as more vehicles slow down, which can change the entire city traffic flow. In an ecosystem, humans artificially introducing new plant species alter the habitat's nutrient distribution, which impacts the food web affects the behavior and population of local animals and can even lead to the extinction of some of them. In financial markets, rumors, (fake) news and political events can lead to sudden sell-offs or buying waves, amplifying market fluctuations that can trigger even more substantial volatility, affecting the value of companies, currencies and the economy of entire countries. A famous example is the 2008 global economic crisis,

Figure 1 – When panic meets euphoria, collective market decisions dance between "Sell!" and "Buy!". Rumors can generate giant financial fluctuations and affect the global economy.

Source: Illustration by Kevin Kallaugher.

where localized failures in the subprime mortgage sector in the United States had catastrophic consequences worldwide.

Similarly, in power grids, a single line failure or a sudden spike in demand can cascade through the network, overloading subsequent lines and leading to large-scale outages or even a blackout, affecting the lives of millions of people. Even the human brain can also be viewed as a complex system where neurons, synapses, and neurotransmitters interact to produce sophisticated cognition, emotions, and behavior. Indeed, activating a single new neural pathway can form new memories or generate an entirely new mood shift. The brain's emergent behaviors, like consciousness and learning, cannot be fully explained by examining neurons in isolation, as they depend on the complex network of neural interactions. Likewise, the interactions among genes, proteins, and metabolites cause the emergence of complex, organized cellular behavior necessary for life. Ultimately, some researchers consider our entire universe as a complex system (GELL-MANN, 1995).

The feedback loops are one of the most important mechanisms behind the behavior of complex systems. They are processes where the system itself affects its behavior and can

Figure 2 – In 2014, scientists from the University of Minnesota described how people move to avoid colliding with each other using models of interacting particle systems. The researchers derived a mathematical rule for an electron-like repulsive force between pedestrians, enabling them to accurately predict how a moving crowd moves when crossing a narrow passage or spontaneously forms organized directional lanes when they exit a football stadium.

Source:daily.jstor.org.

strengthen the continued behavior (positive feedback) or counteract it (negative feedback). These feedback loops help the system to self-organize, as order arises organically from the components' interactions and self-adaptation to the environmental response. A classic example that tricked scientists for a long time is the example of a flock of birds. We know that each bird tailors its flight speed and direction to match the movements of nearby birds (local feedback of closest peers), constructing macroscopically coordinated patterns (murmurations) without any form of central control, a deep signature of many complex systems (GELL-MANN, 1995).

1.2 COMPLEXITY IN NETWORK SCIENCE

We must answer two key questions to understand a complex system: How do they interact? With whom do they interact? That is, we need to know the dynamics of the system and the interaction network. For example, when one studies a social system like a community, it is necessary to not only model how and why people change their opinions but also how they are connected with each other. We must consider aspects like social media, peer groups, television, and cultural norms and figure out who influences whom and who is influenced by whom within the social network. It's impossible to know how the network behaves without charting these

relationships and exploring how different components impact one another across the network (SAVOIU; SIMAN, 2012) .

Figure 3 – The coordination of bird flocks, often seen in murmurations of starlings demonstrate how feedback can lead to emergent patterns. Even though each bird acts individually based on local feedback, the group can form intricate, beautiful patterns in the sky. These patterns are not planned; rather, they emerge from the continuous interaction of feedback loops among the birds synchronized movement.

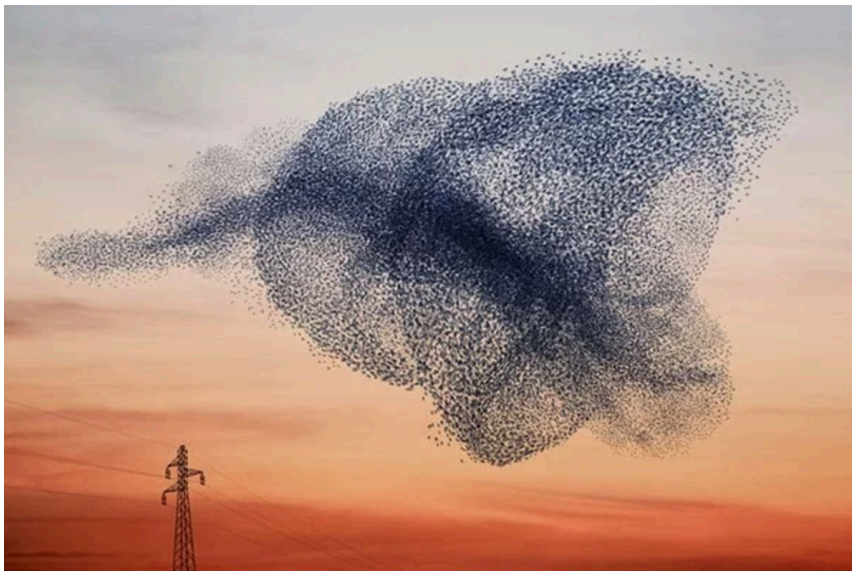

Source: Lems Levity Blog

Network Science has developed as a separate field of analysis inside complexity science and establishes a formal framework to study complex interaction structures. It is oriented towards the topology and dynamics of networks, where nodes (e.g., substations, neurons, cities, people, or webpages) and edges or links represent the relationships or interactions between them (e.g., transmission lines, synapsis, roads, social connections or hyperlinks). A profound finding in network science is the universality of system structure: from genetic and protein-protein interaction networks to cellular metabolism, social ties, and internet connectivity, several systems networks manifest similar structural characteristics. That is because some topologies, like scale-free and small worlds, play a significant role in the robustness and efficiency of how complex systems withstand perturbations, process information, and maintain emergent behaviors. Therefore, it is not a coincidence that diverse, complex systems are structured similarly (BARABASI, 2013).

Network science is at the heart of this recent data revolution; the vast advancements in data collection and computational tools that emerged at the turn of the 21st century and the increased availability of large datasets enabled researchers to map and analyze networks in

unprecedented detail. For example, organizations like the Human Connectome Project develop brain maps of neural interconnections. They look to fundamentally impact neurobiology and assist in constructing memory, mental disorders, conscience and human cognition. Similarly, due to platforms such as Facebook, LinkedIn, and large-scale social networks, researchers have access to rich datasets to study human interactions, social influence, and (des)information diffusion.

Network science can help understand how interactions at the microscopic level generate macroscopic phenomena. An example of success is that in the 2009 H1N1 pandemic, such network-based models could accurately predict the spread of the virus, showing the power of network science for real-time epidemiological forecasting (VESPIGNANI et al., 2012). By studying the network architectures that underlie complicated systems, researchers open the path for innovations to solve some of the most urgent challenges of the 21st century.

1.3 SOCIOPHYSICS

"Sociophysics is the quantitative study of societies using concepts and techniques that have been applied successfully in physics."

Serge Galam

Sociophysics is a new complex science subfield that uses physics concepts to address complex social systems. This subfield adopts techniques originally elaborated in statistical mechanics, nonlinear dynamics and complex network interaction modeling, phase transitions, and network analysis to analyze human behavior and societal dynamics. (BALL, 2002)

More precisely, Sociophysics seeks to interpret and forecast macroscopic collective and similar phenomena like opinion dynamics, crowd movement, and voting behavior. Similarly, Econophysics focuses on economic decision-making, financial markets, stock market crashes, and power laws in financial data in the Physics of Economics. Both fields offer a paradigm shift toward a more quantitative, empirical approach to social science with ambitions of bridging the gap between the "soft sciences" of sociology and economics and the "hard sciences", such as physics and chemistry.

"Econophysics is not just a buzzword; it is a new way to think about economics. It uses models from physics to explore economic systems, emphasizing complexity, collective behavior, and statistical properties rather than purely rational assumptions."

Jean-Philippe Bouchaud

Sociophysics has historical roots in the 19th-century work of Adolphe Quetelet, who started to apply statistical methods to socio-economic data in his pioneering treatise *Physique sociale*. He contended that social phenomena like marriage, birth and crime rates were not just random in the way people of the time believed. Instead, it followed more profound statistical laws, and scientists could study these social patterns just as they study the natural laws governing the physical world. After all, society is but one part of nature, governed by Nature's laws (BALL, 2002). For example, Quetelet showed that crime rates were relatively stable over time in a given population, suggesting that individual criminal acts were not merely individual choices but also reflected broader social and economic forces. Elaborating on this idea, He posited that societies have an inherent order that could be discovered via statistical analysis.

In the 20th century, scholars like Serge Galam and Dietrich Stauffer advanced the formalization of sociophysics, applying models from statistical mechanics to phenomena like opinion formation, social contagion, and crowd dynamics. They showed that the same models that describe magnetization in ferromagnetic materials can be adapted to explain how individuals align their opinions in a social network. Such models have been used to simulate opinion dynamics and show how a small initial group of individuals can influence a large groups opinions, potentially leading to consensus or polarization. For example, in the same way, people tend to agree with their friends and family because of peer pressure and social validation effects, spins in a ferromagnetic material tend to point in the same direction because of the magnetic field influence of their nearest neighbors. These striking similarities enabled scientists to adapt physical models to describe complex social systems (GALAM, 2008; STAUFFER et al., 2006).

The work of Galam, in particular, demonstrated how simple local interactions among agents can lead to global phenomena like the sudden shifts in public opinion observed during political campaigns. Indeed, a central tool that Sociophysics and Econophysics use to investigate complex systems is phase transitions, where systems undergo drastic, nontrivial macroscopic effects due to small, gradual changes in individual behavior or an external parameter. While in physics, phase transitions describe how matter changes state, such as water changing from solid to liquid phase, in response to gradual variations in external conditions such as temperature or pressure, in sociophysics, sociophysical models with phase transitions help explain phenomena like the sudden shift from moderate to extreme opinions within a population, as observed in political polarization studies. Similarly, in Econophysics, small perturbations in

trading behavior can cascade to significant, nonlinear market movements, dramatically changing asset values. These models provide a theoretical framework to understand how complex collective behaviors emerge from individual actions, capturing complex systems' nonlinear and unpredictable nature with higher precision (SAVOIU; SIMAN, 2012; GALAM; MOSCOVICI, 1991).

One of the most simple and powerful sociophysics models is the majority-vote model (OLIVEIRA, 1992). While it is common to imagine humans as fully rational beings, the experiments of Solomon Asch and Gregory Berns (ASCH, 1955; BERNS et al., 2005) show how social pressure plays a major role in human behavior and can even alter the perception of reality and cause changes in the brain (See Sec. 4.1 for a detailed explanation of Solomon Asch's and Gregory Berns' experiments). Often, the human decision-making process is not purely rational, and individuals can exhibit irrational behavior in conforming with the group, even against their personal truth and logic.

There is a parallel between the opinion dynamics described by Solomon Asch's and Gregory Berns' experiments and the magnetic behavior of ferromagnetic materials. For instance, the Ising model considers a lattice of spins, where each spin can adopt the states up or down, and each spin also interacts with its neighbors. To minimize their energy, the spins tend to align with each other, but thermal fluctuations can break their alignment.

Building on the empirical evidence from Solomon Asch's and Gregory Berns' experiment and inspired by the Ising model, the majority-vote model considers an agent-based representation of interacting individuals in a contact network where the opinion of an individual for or against some issue is represented by a stochastic variable, which assumes one of two allowed values. For instance, $+1$ or -1. Each agent agrees with the majority of its social interactions with probability $1 - q$ and disagrees with chance q. The quantity q is called the noise parameter of the model, and it measures the average nonconformity level of the individuals. In this analogy, the opinions of the individuals stand for the spin values, and the nonconformity parameter q corresponds to the temperature in the Ising model (OLIVEIRA, 1992; OLIVEIRA; MENDES; SANTOS, 1993).

1.4 ORGANIZATION AND GOALS OF THIS WORK

In this work, we explore two different problems. In the first one, we investigate how one of the most widespread social behavior, cooperation, impacts the dynamics of the majority-vote model. Collaboration still challenges scientists from several fields, often surpassing logical

assumptions. We explore how collaborative behavior affects opinion dynamics and the entropy production of social groups using Monte Carlo simulations and mean-field calculations.

The second problem we investigate is how real-world network structure affects majority-vote opinion dynamics in social networks. To accomplish that, we define a new network model that can approximate the network of social media such as X (formerly Twitter) and Meta (previously Facebook). We investigate the network properties and how this structure impacts social collective behavior.

We organize the work as follows: In Chapter 2, we review the basic theory behind network science, introduce the Barabási-Albert model for scale-free networks, discuss its limitations, and then define our new network model.

Next, in Chapter 3, we cover the mathematical background of stochastic systems dynamics and the application of the Monte Carlo method for complex systems.

In Chapter 4, we present and explain the majority-vote model, a stochastic opinion formation model for simulating social systems. Building on that, we define the cooperative majority-vote model and execute mean-field calculations for the order parameter and the entropy production.

We present the cooperative majority-vote model results in Chapter 5, and in Chapter 6, we evaluate the properties of the affinity-based Scale-Free Network we defined and how they impact the opinion dynamics of the majority-vote model.

Finally, In Chapter 7, we write our final remarks, elaborate on the work's main conclusions we found and discuss possible approaches for future research.

2 NETWORK SCIENCE

"Networks are present everywhere.
All we need is an eye for them."
Albert-László Barabási

In this chapter, we follow the discussion presented in the book Network Science of Albert-László Barabási (BARABÁSI, 2013). We discuss how to represent a network mathematically and the foundations of one of the most famous network models: the Barabási-Albert model. We also discuss the limitations and generalizations of the model to emulate real social networks such as Meta and X and introduce a new model for affinity-based scale-free networks that generate more realistic degree distributions of social networks.

2.1 BASIC NETWORK CONCEPTS

Networks (graphs) are a powerful tool for representing complex systems' structure and interaction dynamics. Essentially, a network consists of N nodes (vertices) connected by L links (edges). This mathematical abstraction offers a general framework to study numerous systems, from proteins interacting in a cell to routers connected to the internet and people interacting in social media (BARABÁSI, 2013).

The network's links can be directed or undirected. Undirected links are symmetric: if node i is connected to node j, then j is also connected to i. Some examples include romantic ties (if Alice dates Bob, then Bob dates Alice), transmission lines in power grids (electric currents can flow in both directions), friendships, protein interactions (mutual physical bonding), transport networks (two-way traffic flows), collaboration networks (if two researchers co-author a paper, there is an undirected link between them) and molecular networks (undirected links represent biochemical pathways where metabolites can transform into one another).

Directed links, however, are asymmetric: if node i is connected to node j, not necessarily j is also connected to i. For example, interactions in social media are generally directed (you can follow a rock star, but they do not follow you back). Other directed cases include phone calls and hyperlinks (URLs) pointing to websites on the internet, brain networks (the electric neuron synapsis flows in specific directions), food webs (the direction of the link shows the flow of energy or biomass, indicating predator-prey relationships) and financial networks (you can

Figure 4 – Representation of a social network and the corresponding adjacency matrix.

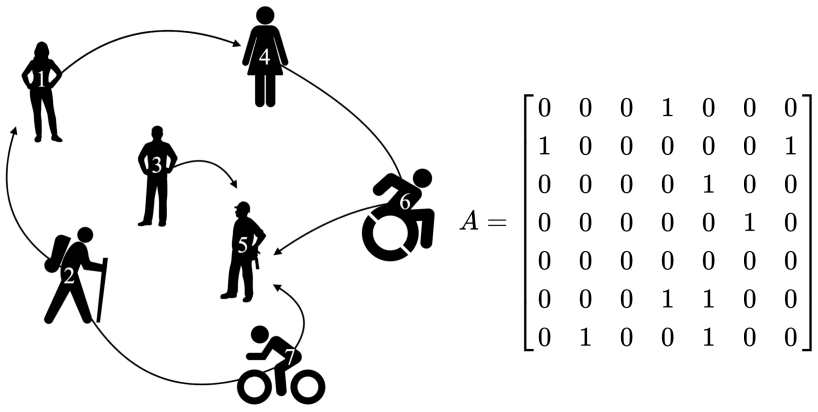

Source: Author.

make a payment to someone, or a bank can owe money to another bank) and gene regulatory responses (the gene A can influence the expression of gene B).

Mathematically, we can represent a network using an adjacency matrix A. The adjacency matrix is defined such that if there is a link from node i to node j, then $A_{ij} = 1$; otherwise, $A_{ij} = 0$. We provide a simple example of a directed network and the correspondent adjacency matrix in Fig. 4. Note that real networks often are sparse, meaning that the number of links L is much smaller than the maximum possible number of links $L_{\max}$, which is given by

$$L_{\max} = \frac{N(N-1)}{2}. \tag{2.1}$$

Using the adjacency matrix, we can calculate several network properties. A fundamental concept is the node degree, the number of links a given node i has. For undirected networks, we can calculate the degree of a node k_i as a sum over either the rows or the columns of the adjacency matrix

$$k_i = \sum_{j=1}^{N} A_{ij} = \sum_{i=1}^{N} A_{ij}, \tag{2.2}$$

we can then calculate the network average degree as

$$\langle k \rangle = \frac{1}{N} \sum_{i=1}^{N} k_i = \frac{2L}{N}, \tag{2.3}$$

where L is the total number of links in the network.

In directed networks, the incoming and outgoing degrees given by

$$k_i^{\text{in}} = \sum_{j=1}^{N} A_{ji}, \quad k_i^{\text{out}} = \sum_{j=1}^{N} A_{ij}. \tag{2.4}$$

For example, a celebrity may have many followers on social media but may not follow too many other accounts. Thus, this celebrity would have a big incoming degree but not a big outgoing degree. In direct networks, we can also calculate the node's total degree k_i

$$k_i = k_i^{\text{out}} + k_i^{\text{in}}. \tag{2.5}$$

The average degree is

$$\left\langle k^{\text{in}} \right\rangle = \frac{1}{N}\sum_{i=1}^{N} k_i^{\text{in}} = \left\langle k^{\text{out}} \right\rangle = \frac{1}{N}\sum_{i=1}^{N} k_i^{\text{out}} = \frac{L}{N}. \tag{2.6}$$

Note that we can also have weighted networks, where $A_{ij} = w_{ij}$, where some connections are stronger than others. For instance, in transport networks, the weight can represent the traffic intensity, or in social media, the amount of interactions between two individuals. While most networks are weighted, it is common only to represent unweighted networks and leave these aspects to the dynamical modeling of the complex system, which emphasizes a modular approach. Indeed, most books and papers focus on unweighted networks, and we will do the same.

The degree distribution p_k provides the probability that a randomly selected node has degree k. Given N_k is the number of nodes with degree k, then we have

$$p_k = \frac{N_k}{N}, \tag{2.7}$$

where $p_k \geq 0, \forall\ k \in \{0, 1, 2, 3, \dots\}$ and $\sum_{k=0}^{\infty} p_k = 1$.

Another important metric is the clustering coefficient, which captures the degree to which the neighbors of a given node link to each other. Thus, high clustering suggests a strong sense of local community or indicates more redundant or reliable communication channels within the network. Mathematically, for a node i with degree k_i, the local clustering coefficient is defined as

$$C_i = \frac{2L_i}{k_i(k_i - 1)}, \tag{2.8}$$

where L_i represents the number of links between the k_i neighbors of node i and we divide by the maximum number of connections the k_i neighbors of node i could have that is $k_i(k_i-1)/2$. Note that L_i can also be interpreted as the number of triangles with the node i. Hence, it is possible to calculate

$$L_i = \frac{1}{2}\sum_{j=1}^{n}\sum_{k=1}^{n} A_{ij}A_{jk}A_{ki}, \tag{2.9}$$

where the multiplication $A_{ij}A_{jk}A_{ki}$ is 1 if the nodes i, j, k form a triangle and 0 otherwise. The average clustering coefficient of the network $\langle C \rangle$ is given by

$$\langle C \rangle = \frac{1}{N} \sum_{i=1}^{N} C_i. \tag{2.10}$$

Many real-world networks have high clustering coefficients, generating more resilient networks, as they have redundant paths for information flow. Indeed, in social networks, people tend to form groups based on common interests, mutual friends, or shared environments. Friends of a person are often friends with each other, forming highly connected clusters. Rumors or innovations can rapidly propagate within a group with high clustering before spreading to the broader network. Other networks, such as power grids, intentionally have redundant connections and high clustering so the network can still function even if some transmission lines fail.

Finally, an important global measure to describe the overall network structure is the average path length $\langle d \rangle$ that represents the average number of links separating any two nodes:

$$\langle d \rangle = \frac{1}{N(N-1)} \sum_{i \neq j} d_{ij}, \tag{2.11}$$

where d_{ij} is the shortest path length between nodes i and j. Note that two web pages could be hosted on computers on opposite sides of the globe yet have a link to each other. Hence, while their physical distance may be considerable, their distance on the network is just one. At the same time, two individuals who live in the same building may not know each other but can be connected to people in another country on a phone call. Thus, in networks, the distance is a route that runs along the network links, not a physical distance. If there is no path from node i to node j, then by definition, $d_{ij} = \infty$. In Eq. (2.11), we only consider node pairs i, j where d_{ij} is finite.

In practice, we require *connected* networks, which means there is always a path between two nodes. Indeed, we need our phone to be able to call any other valid phone number and an email service that can send emails to any other email address. Note that in undirected networks, $d_{ij} = d_{ji}$, but this is not generally true for directed networks. In particular, in directed networks, there may be a path from node i to node j, but it is possible there is not a path from node j to node i. For example, if Alice follows Bob on Instagram but Bob does not follow Alice, Alice may be able to see Bob's posts, but Bob will not see Alice's posts.

The network diameter $d_{\max}$ is the longest shortest path between any two nodes in the

network:

$$d_{\max} = \max_{i,j} d_{ij}. \tag{2.12}$$

The diameter helps us measure how efficiently information or resources can travel across the network. A smaller diameter indicates the network is well-connected, and two nodes can reach each other relatively quickly. If the network has several disconnected components, it will have an infinite diameter, and this could represent several issues with a phone or email service. Here, a component is a maximal subset of nodes such that there exists a path between every pair of nodes within this subset. In other words, within a component, every node is reachable from any other node, but there are no connections to nodes outside the component. Hence, connected networks have only one big component since there is always a path between any two nodes.

In real-world networks, node failures are common, affecting the network structure and functionality. For example, in computer networks or power grids, nodes can fail due to hardware malfunction, power outages, traffic overload and environmental factors. In social networks, nodes can be removed from the network when users deactivate or delete their accounts, or when users become inactive due to loss of interest or external pressures, or even due to community migration (as when WhatsApp users move to Telegram). Additionally, some accounts can get suspended or banned, or we can have large-scale removal of bots and fake accounts or marketing campaigns.

Some networks can be totally disrupted into disconnected pieces when a relatively small fraction of the nodes are removed, while others are more resilient. We can assess the network's robustness by measuring how the removal of some nodes affects the network giant component (the biggest network component). If the size of the giant component decays dramatically, it indicates potential structural vulnerabilities. Thus, the robustness of a network is given by

$$R(f) = \frac{S(f)}{S(f=0)}, \tag{2.13}$$

where $S(f)$ is the size of the giant component after a fraction f of the network nodes are removed, and $R(f)$ is the fraction of nodes that remain functional after the failures.

2.2 SCALE-FREE NETWORKS

The discovery of scale-free networks reveals that hubs, or highly connected nodes, play a crucial role in the structure and resilience of networks,

whether biological, social, or technological.

Albert-László Barabási

2.2.1 Why do we need scale-free networks?

One of the first attempts to model real-world networks was the random network model by Paul Erdös and Alfréd Rényi. In fact, at first inspection, many real networks look as if they were totally random. In this spirit, the model constructs a random network as follows:

1. Start with N isolated nodes.
2. For each $N(N-1)/2$ possible pair of nodes, link them with probability p. Otherwise, leave them disconnected.

Observe that each random network generated is generally different, even if you use the same values of N and p. Also, the total number of links L may differ for each generated network. Indeed, the probability p_L the network has L links can be calculated using the binomial theorem

$$p_L = \binom{\frac{N(N-1)}{2}}{L} p^L q^{\frac{N(N-1)}{2}-L}, \tag{2.14}$$

where $q = 1 - p$. Thus, the expected number of links is

$$\langle L \rangle = \sum_{L=0}^{\frac{N(N-1)}{2}} L p_L = \sum_{L=0}^{\frac{N(N-1)}{2}} p \frac{\partial}{\partial p} \left[\binom{\frac{N(N-1)}{2}}{L} p^L q^{\frac{N(N-1)}{2}-L} \right]. \tag{2.15}$$

Applying the binomial theorem,

$$\langle L \rangle = p \frac{\partial}{\partial p} (p+q)^{\frac{N(N-1)}{2}} = p \frac{N(N-1)}{2}, \tag{2.16}$$

where we used $p+q=1$, this result is intuitive because it means the expected number of links is the maximum possible number of links multiplied by the connection probability. Similarly, we can obtain the degree distribution of the random network. A given node i can connect with $N-1$ other nodes. Hence, the probability that i has k links is

$$p_k = \binom{N-1}{k} p^k (1-p)^{n-1-k}. \tag{2.17}$$

With that, we can obtain the degree first moment similarly as we calculated the expected number of links

$$\langle k \rangle = \sum_{k=0}^{\infty} k p_k = (N-1)p, \tag{2.18}$$

in the second moment, apply the same trick twice:

$$\left\langle k^2 \right\rangle = \sum_{k=0}^{\infty} k^2 p_k = p\frac{\partial}{\partial p}\left(p\frac{\partial}{\partial p}(p+q)^{N-1}\right) = p(1-p)(N-1) + p^2(N-1)^2. \tag{2.19}$$

Therefore, the standard deviation is given by

$$\sigma_k = \sqrt{\langle k^2 \rangle - \langle k \rangle^2} = \sqrt{p(1-p)(N-1)}. \tag{2.20}$$

In the 90s, there was a general expectation that a random network could approximate the WWW network. In practice, real-world networks have many nodes and few connections (sparse networks) so that $N \gg k$ and $p \ll 1$. In these limits, we can make some approximations in Eq. (2.17). First, note that.

$$\binom{N-1}{k} = \frac{(N-1)(N-1-1)(N-1-2)\cdots(N-1-k+1)}{k!} \approx \frac{N^k}{k!}. \tag{2.21}$$

Additionally,

$$(1-p)^{N-1-K} = \left(1 - \frac{\langle k \rangle}{N-1}\right)^{N-1-K} \approx (1 - \frac{\langle k \rangle}{N})^N, \tag{2.22}$$

where we used Eq. (2.18). Using the exponential limit definition,

$$e^x = \lim_{N\to\infty}\left(1 + \frac{x}{N}\right)^N, \tag{2.23}$$

we got that

$$(1-p)^{N-1-K} \approx e^{-\langle k \rangle}. \tag{2.24}$$

Therefore, we can write the degree distribution as

$$p_k = \frac{(N)^k}{k!} p^k e^{-\langle k \rangle} = \frac{(pN)^k}{k!} e^{-\langle k \rangle}. \tag{2.25}$$

Applying Eq. (2.18) again, we get the Poisson Distribution:

$$p_k = \frac{\langle k \rangle^k}{k!} e^{-\langle k \rangle}. \tag{2.26}$$

Hence, if the WWW is a random network, it would follow a Poisson distribution. Indeed, as the content of each web document reflects the diverse personal and professional interests of its creators, from individuals to organizations, it seems a reasonable assumption that the WWW is a random network. In 1998, Hawoong Jeong from the University of Notre Dame generated the first WWW mapping to understand the WWW structure and make a comparison with the random network model.

Figure 5 – Sample Snapshots of the World Wide Web (WWW) mapped out by Hawoong Jeong in 1998. The sequence of images shows zooms of specific regions of the network. The the first photo displays a global view of the 1998 WWW with all its 325,729 nodes. Nodes with more than 50 links are represented in red and nodes with more than 500 links in purple. These snapshots reveal that there are a few highly connected nodes (hubs), a signature of scale-free networks.

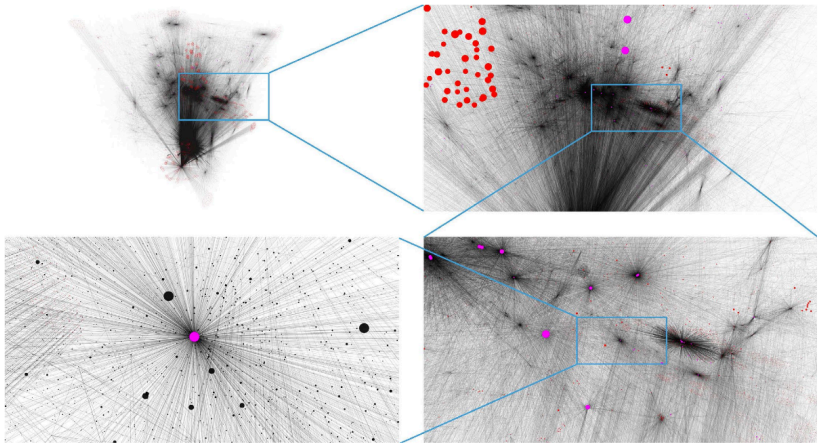

Source: (ALBERT; JEONG; BARABASI, 1999).

However, Fig. 5 reveals that the WWW has extremely highly connected nodes, hubs, and several small-degree nodes. The problem is that, in a random network, highly connected nodes are extremely improbable. Indeed, using the Stirling approximation, we know that

$$k! \approx \sqrt{2\pi k}\left(\frac{k}{e}\right)^k. \tag{2.27}$$

Hence, we can write the degree distribution as

$$p_k = \frac{e^{-\langle k\rangle}\langle k\rangle^k}{k!} = \frac{e^{-\langle k\rangle}}{\sqrt{2\pi k}}\left(\frac{e\langle k\rangle}{k}\right)^k. \tag{2.28}$$

Therefore, the chance of observing a degree $k > e\langle k\rangle$ decreases quickly. Indeed, let's estimate how the maximum degree increases with the network size. If N_k as the number of nodes with degree k, then the expected value of N_k is given by

$$E[N_k] = Np_k = N\frac{(Np)^k e^{-Np}}{k!}. \tag{2.29}$$

Hence, to find the largest degree $k_{\max}$, we need to estimate the degree k for which $E[N_k] \approx 1$, as this corresponds to the expected degree of the highest-degree node in the network. Thus,

$$N\frac{(Np)^k e^{-Np}}{k!} \approx 1. \tag{2.30}$$

Taking the logarithm of both sides, we obtain

$$\ln N + k\ln(Np) - Np - \ln(k!) \approx 0. \tag{2.31}$$

Using Stirling's approximation $\ln(k!) \approx k \ln k - k$ for large k, we get

$$\ln N + k \ln(Np) - Np - (k \ln k - k) \approx 0. \tag{2.32}$$

$$k \ln \left(\frac{Np}{k} \right) + k - Np + \ln N \approx 0. \tag{2.33}$$

Since we know we have a Poisson distribution, the largest degree is expected to be close to the average degree Np. Thus, lets write $k = Np + \delta$, where δ is a small deviation term. We can substitute $k = Np + \delta$ and expand $\ln \left(\frac{Np}{k} \right)$ around $k = Np = \langle k \rangle$ using a Taylor expansion:

$$\ln \left(\frac{Np}{Np + \delta} \right) \approx -\frac{\delta}{Np}. \tag{2.34}$$

Thus,

$$(Np + \delta) \left(-\frac{\delta}{Np} \right) + (Np + \delta) - Np + \ln N \approx 0. \tag{2.35}$$

$$-\frac{\delta^2}{Np} + \delta + \ln N \approx 0. \tag{2.36}$$

Solving the quadratic equation for δ, we have:

$$\delta \approx \frac{Np}{2} \pm \sqrt{\frac{(Np)^2}{4} + Np \ln N}. \tag{2.37}$$

For large N, the term $\sqrt{Np \ln N}$ dominates, so we approximate

$$\delta \approx \sqrt{2Np \ln N}. \tag{2.38}$$

Therefore, the largest degree scales as

$$k_{\max} \approx Np + \sqrt{2Np \ln N}. \tag{2.39}$$

This means the maximum degree of a random network grows slowly with the network size. In fact, Fig. 6 shows that the Poisson fit does not capture the empirical data pattern. Instead, the actual distribution is well approximated by a power-law fit.

This discovery suggests that the degree distribution of the WWW follows a power-law distribution

$$p_k = k^{-\gamma}. \tag{2.40}$$

It turns out that hubs are not unique to the WWW but are present in several real-world networks, from social media to biological networks. We call the networks that follow Eq. (2.40) as scale-free networks because, as we will see, these networks lack a finite scale, which enables them to have hubs.

Figure 6 – Here, we show the incoming (a) and outgoing (b) degree distribution of the 1999 WWW sample in the study (ALBERT; JEONG; BARABASI, 1999). In this log-log degree distribution plot, the circles represent the empirical data, the green curve is the Poisson distribution with an average degree of the WWW sample, and the purple line is a power-law fit.

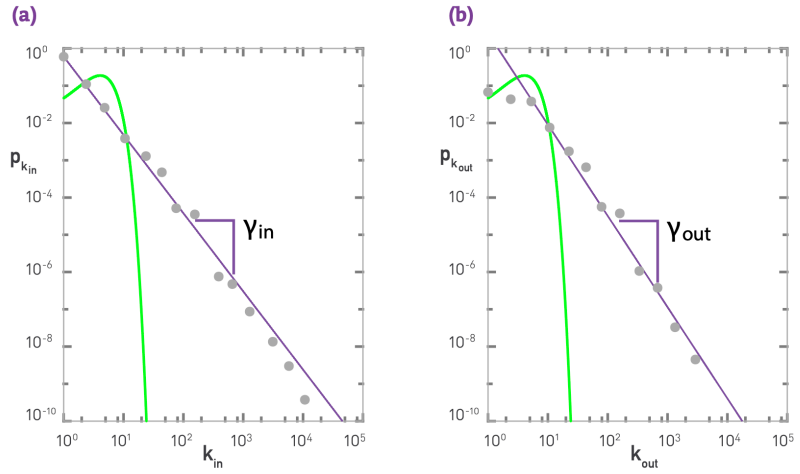

Source: (BARABASI, 2013).

2.2.2 Scale-free networks

In this section, we will analyze scale-free networks in detail. To begin with, the power-law distribution $p_k = Ck^{-\gamma}$ can be analyzed using both discrete and continuum formalisms.

In the discrete case, we determine the normalization constant C by the condition:

$$\sum_{k=1}^{\infty} p_k = 1 \quad \text{hence, } p_k = \frac{k^{-\gamma}}{\zeta(\gamma)}, \tag{2.41}$$

where $\zeta(\gamma)$ is the Riemann-zeta function.

In the continuum formalism, the degree k is approximated as a continuous variable, and we use the normalization condition:

$$\int_{k_{\min}}^{\infty} p(k)\, dk = 1. \tag{2.42}$$

Thus,

$$p(k) = \frac{\gamma - 1}{k_{\min}^{\gamma-1}} k^{-\gamma}, \tag{2.43}$$

where $k_{\min}$ is the smallest degree for which the power law holds. Note that, in the discrete formalism, p_k precisely describes the probability that a node has degree k. However, in continuous

formalism, only the integral of p_k has a physical meaning. In this case, the integral

$$\int_{k_{min}}^{k_{max}} p(k)dk, \tag{2.44}$$

is the probability that a node has degree between k_{min} and k_{max}.

Verifying the presence of hubs, or highly connected nodes, is essential because hubs are a defining feature of scale-free networks. To assess the network's ability to generate hubs, let's estimate the largest degree $k_{\max}$ for a network of size N. First, note that the cumulative distribution function $P(k \geq K)$ gives the probability that a randomly chosen node has a degree at least K:

$$P(k \geq K) \sim K^{-(\gamma-1)}. \tag{2.45}$$

For the largest degree $k_{\max}$, the expected number of nodes with a degree larger than $k_{\max}$ should be approximately 1. Thus,

$$P(k \geq k_{\max}) \approx \frac{1}{N}. \tag{2.46}$$

Hence, substituting the cumulative distribution, we get

$$k_{\max}^{-(\gamma-1)} \approx \frac{1}{N} \longrightarrow k_{\max} \approx N^{\frac{1}{\gamma-1}}. \tag{2.47}$$

This implies that if $\gamma > 1$, as the network size grows, the largest hubs become significantly more connected, unlike in random networks where the largest degree grows with $O(\sqrt{N \ln N})$.

2.2.3 Barabási-Albert (BA) model

The big question is, how can we generate scale-free networks in practice? That would allow us to run simulations and experiments and study how scale-free networks impact complex real-world systems. One of the most famous models is the Barabasi-Albert (BA) model, based on the preferential attachment principle for producing scale-free networks. The model is composed of the following steps:

1. Initialization: Generate an initial (fully connected) network of size z_0.

2. Growth: A new node is added into the network at each time step.

3. Preferential Attachment: The new node connects to z existing nodes, where the probability that the new node connects to an existing node i is proportional to the degree of

node i:

$$\Pi(i) = \frac{k_i}{\sum_j k_j}, \tag{2.48}$$

where k_i is the degree of node i, the sum is taken over all previously existing nodes in the network.

Does this model give rise to a scale-free network? To find out, we apply the rate equation method to derive the exact shape of the degree distribution. Denote by $N(k,t)$ the number of degree nodes k at time t and $N(t)$ is the total of nodes at time t. The degree distribution $p_k(t)$ is related to this quantity through

$$p_k(t) = \frac{N(k,t)}{N(t)}, \tag{2.49}$$

since we start with z_0 nodes and a new node is added to the network at each time step, we have $N(t) = z_0 + t$. The initial fully connected network of m_0 nodes has a total degree sum of $z_0(z_0 - 1)$. As each new node adds z edges to the network, the total degree of the network at time t becomes

$$\sum_j k_j(t) = z_0(z_0 - 1) + 2zt. \tag{2.50}$$

Thus, the preferential attachment mechanism can be expressed as:

$$\Pi(k) = \frac{k}{z_0(z_0 - 1) + 2zt}, \tag{2.51}$$

where the $2z$ term accounts for each link contributing to two nodes in an undirected network.

When a new node is added, the number of nodes with degree k can change due to two events

- A new link to a degree-k node turns it into a degree-$(k+1)$ node, decreasing $N(k,t)$.
- A new link to a degree-$(k-1)$ node turns it into a degree-k node, increasing $N(k,t)$.

The rate equation for nodes with degree $k > m$ becomes

$$(N+1)p_k(t+1) - Np_k(t) = -\frac{k}{z_0(z_0-1)+2zt} zNp_k(t) + \frac{k-1}{z_0(z_0-1)+2zt} zNp_{k-1}(t). \tag{2.52}$$

Here, the left term in the right side of the equation indicates the probability that one of the $Np_k(t)$ nodes with degree k are selected for attachment in one of the new z links hence turns into degree-$(k+1)$ node while the right term indicates the probability that a degree-$(k-1)$ node gets a link and turns into degree-k one.

For nodes with degree z, the rate equation is

$$(N+1)p_z(t+1) - Np_z(t) = 1 - \frac{z}{z_0(z_0-1)+2zt} zNp_z(t), \tag{2.53}$$

where 1 represents the addition of a new node with z connections at each time step.

We are interested in the limit $t \to \infty$, assuming that the degree distribution has reached a stationary state: $p_k(t) = p_k(t+1) = p_k$. Hence, applying this limit to Eq. (2.52) and considering $z_0(z_0-1)+2zt \approx 2zt$, we obtain the recursive relation

$$p_k = \frac{k-1}{k+2} p_{k-1}, \; k > z. \tag{2.54}$$

Similarly, from Eq. (2.53), we get

$$p_z = \frac{2}{z+2}. \tag{2.55}$$

Using these recurrence relations iteratively gives us the following

$$p_{z+1} = \frac{z}{z+3}\, p_z = \frac{2z}{(z+2)(z+3)}, \tag{2.56}$$

$$p_{z+2} = \frac{z+1}{z+4}\, p_{z+1} = \frac{2z(z+1)}{(z+2)(z+3)(z+4)}, \tag{2.57}$$

$$p_{z+3} = \frac{z+2}{z+5}\, p_{z+2} = \frac{2z(z+1)(z+2)}{(z+3)(z+4)(z+5)}, \tag{2.58}$$

$$p_{z+4} = \frac{z+3}{z+6}\, p_{z+3} = \frac{2z(z+1)(z+2)}{(z+4)(z+5)(z+6)}. \tag{2.59}$$

Now, we can spot the pattern and generalize to find the probability of a node with degree k:

$$p_k = \frac{2z(z+1)}{k\,(k+1)(k+2)}. \tag{2.60}$$

This is the exact degree distribution equation of the Barabási-Albert model. For large k, this looks like this:

$$p_k \sim k^{-3}, \tag{2.61}$$

which is a power-law decay with exponent $\gamma = 3$, showing that a network produced from the Barabási-Albert model is indeed of scale-free degree distribution.

2.2.4 Estimating the exponent of a scale-free network

Empirical scale-free networks can have different values of the power-law decay exponent. For example, in Fig. 6, the exponent of the incoming (outgoing) degree distribution of the

WWW is 2.1 (2.45). We can use the Maximum Likelihood Estimation (MLE) method to estimate the degree exponent of a scale-free network.

Given a set of observed node degrees $\{k_1, k_2, \ldots, k_n\}$ from empirical data, the likelihood function assuming the data follows a power-law distribution can be written as the joint probability of observing these degrees under the distribution

$$L(\gamma; k_1, k_2, \ldots, k_n) = \prod_{i=1}^{n} p_{k_i}, \tag{2.62}$$

where p_k is assumed to be a power-law distribution

$$p_k = \frac{\gamma - 1}{k_{\mathsf{min}}^{1-\gamma}} k^{-\gamma}, \tag{2.63}$$

and $\gamma - 1/k_{\mathsf{min}}^{1-\gamma}$ is the normalization constant.

The logarithm of the likelihood function, or the log-likelihood, simplifies the product of probabilities into a sum, making it easier to handle mathematically:

$$\ln L(\gamma; k_1, k_2, \ldots, k_n) = \sum_{i=1}^{n} \ln p_{k_i}. \tag{2.64}$$

Substituting p_k from above, we obtain

$$\ln L(\gamma; k_1, k_2, \ldots, k_n) = \sum_{i=1}^{n} \left[\ln(\gamma - 1) - (1 - \gamma) \ln k_{\mathsf{min}} - \gamma \ln k_i\right]. \tag{2.65}$$

Simplifying further, we get

$$\ln L(\gamma; k_1, k_2, \ldots, k_n) = n \ln(\gamma - 1) - n(1 - \gamma) \ln k_{\mathsf{min}} - \gamma \sum_{i=1}^{n} \ln k_i. \tag{2.66}$$

To find the most probable exponent, we maximize the likelihood by taking the derivative of the log-likelihood with respect to γ and setting it to zero:

$$\frac{d}{d\gamma} \ln L(\gamma; k_1, k_2, \ldots, k_n) = \frac{n}{\gamma - 1} + n \ln k_{\mathsf{min}} - \sum_{i=1}^{n} \ln k_i = 0. \tag{2.67}$$

Solving for γ, we get

$$\hat{\gamma} = 1 + n \left(\sum_{i=1}^{n} \ln \frac{k_i}{k_{\mathsf{min}}} \right)^{-1}. \tag{2.68}$$

Here, $\hat{\gamma}$ is the MLE estimate of the degree exponent γ, assuming that the data follows a power-law distribution.

One challenge is that the degree distribution of many actual networks does not follow a pure power law, not even the WWW. Empirical networks often have low-degree saturations, high-degree cutoffs and outliers. Due to this, estimating the degree exponent is still not yet an exact science, but a practical approach involves discarding points that deviate from the power law to estimate the exponent for the region $k \gg 1$.

2.2.5 Why the name "scale-free"?

The degree exponent γ plays a crucial role in determining the properties of a scale-free network. Here, we examine three regimes based on the value of γ and discuss their impact on network characteristics. First, note that the average degree $\langle k \rangle$ is given by

$$\langle k \rangle = \sum_{k=k_{\text{min}}}^{\infty} k p_k. \tag{2.69}$$

Substituting $p_k = Ck^{-\gamma}$, where C is the normalization constant, we have

$$\langle k \rangle = C \sum_{k=k_{\text{min}}}^{\infty} k^{1-\gamma}. \tag{2.70}$$

This sum converges for $\gamma > 2$, giving a finite average degree. However, the sum diverges for $\gamma \leq 2$, implying an infinite average degree as the network grows.

The variance $\langle k^2 \rangle - \langle k \rangle^2$ is calculated from the second moment:

$$\langle k^2 \rangle = \sum_{k=k_{\text{min}}}^{\infty} k^2 p_k = C \sum_{k=k_{\text{min}}}^{\infty} k^{2-\gamma}. \tag{2.71}$$

This sum converges for $\gamma > 3$, leading to a finite variance. However, the variance diverges for $\gamma \leq 3$, indicating that degree distribution fluctuations are significant and dominated by large hubs. Hence, we can classify three different regimes as follows.

(i) Anomalous Regime

For $\gamma < 2$, the exponent in Eq. (2.47) $1/(\gamma - 1)$ is larger than one, meaning that the number of links connected to the largest hub grows faster than the size of the network. This implies that as the network grows, the largest hubs degree must eventually exceed the total number of nodes, which is unsustainable. Additionally, for $\gamma < 2$, the average degree $\langle k \rangle$ diverges as $N \to \infty$, highlighting the extreme concentration of links on the largest hubs. For networks in this range, the largest hub grows faster than the network size, and without multi-links (multiple links between 2 nodes) and self-links, there will be no additional nodes for the most significant hub to connect to once its degree surpasses $N - 1$. Hence, scale-free networks with $\gamma < 2$ cannot exist unless there are multi-links.

(ii) Scale-Free Regime

In the range $2 < \gamma < 3$, the first moment (average degree) is finite, but higher moments diverge as $N \to \infty$. The term "scale-free" originates from the absence of a characteristic scale in the network's degree distribution since the variance diverges. This lack of a characteristic scale is what gives the network its "scale-free" nature, as the structure looks similar regardless of the scale at which it is observed. The divergence of the second moment (variance) indicates that fluctuations in the degree distribution are dominated by a small number of highly connected nodes or hubs. Empirical scale-free networks like the WWW and social media apps have an exponent in this regime.

(iii) Weak Scale-Free Regime

For $3 < \gamma < 3.5$, the network still follows a power-law degree distribution, but hubs are less dominant than in the classical scale-free regime. The second moment of the degree distribution (variance) is now finite, meaning that extreme hubs become rarer. Networks in this regime often display a mix of scale-free and random network properties, with hubs still playing a role but with decreasing influence as γ increases.

(iv) Random Network Regime

For $\gamma > 3.5$, the degree distribution p_k decays rapidly, limiting the presence and influence of hubs. As a result, the connectivity is more evenly distributed among nodes, leading to a network topology that is structurally closer to classical random graphs, such as Erdös-Rényi networks.

2.2.6 Limitations and Generalizations

Although the Barabási-Albert (BA) model reproduces some of the key attributes of real-world networks, it suffers some drawbacks regarding the versatility of its network construction. For instance, we notice in Figure 7 that the data as separate circles for Twitter (purple) and Facebook (green) significantly deviate from the power-law prediction, meaning they differ from the scale-free network, especially for small values of connectivity. In fact, extensive empirical

data often shows concave power-law degree distributions and a high clustering coefficient, which is absent in the standard Barabási-Albert model.

Figure 7 – Degree distribution of Twitter (purple) and Facebook (green) social online networks. The transparent hollow circles represent the degree distribution, while the filled circles represent the binned data. The black line is the power-law degree distribution fit equal to 3.

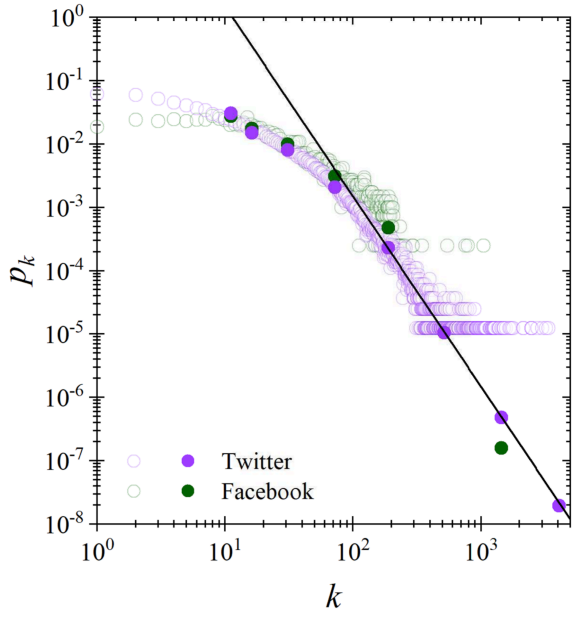

Source: (PORCIUNCULA et al., 2024)

The degree distribution of real social networks is naturally saturated at a low degree because of individual limitations, such as time and resources to maintain proximity relationships. Indeed, using the 2012 datasets from Facebook and Twitter, Figure 7 shows a deviation from the pure power law at lower degrees, where the degree distribution flattens. The BA model does not consider this saturation effect but considers that the network's highly connected nodes (hubs) can accumulate links indefinitely without restrictions (MCAULEY; LESKOVEC, 2012a; MCAULEY; LESKOVEC, 2012b).

In addition, the properties of the standard BA model network yield a low clustering coefficient, which indicates a low probability of two neighbors of a node being related. But, in reality, social networks, in particular, usually exhibit high clustering because people form tightly-knit communities in which their connections are also connected to each other. For example, on Twitter and Facebook, the existence of communities shows individuals interacting frequently within their internal groups, which significantly increases the network clustering coefficient.

In fact, homophily (the tendency for nodes to connect with other nodes that are similar to each other) is an intrinsic property of social networks. Users on such networks as Twitter and

Facebook are more likely to be linked to other users with similar interests, demographics, or geographic locations. Therefore, there is a high chance of interacting with and developing relationships with this local attachment that the Barabási model cannot explain. This phenomenon plays a major role in the development and connectedness of social networks, determining the propagation of information, diffusion of behavior, and formation and disintegration (when two individuals are not similar anymore) of social links among community members, leading to mutual reinforcement of social ties and the formation of similarity clusters. In contrast, the BA model adopts a standard random preferential attachment mechanism as the probability of connecting the new link is only a function of the degree of existing nodes without considering any similarity between nodes. The absence of homophily hinders the model's capability to mimic realistic social network configurations that depend on shared characteristics for connections.

2.3 AFFINITY-BASED SCALE-FREE NETWORK

Spatial social networks incorporate the geographical dimension into the study of social interactions. In these networks, the physical proximity of individuals plays a crucial role in forming and maintaining social ties. Prior research has modified the preferential attachment rule by introducing links generated among existing nodes and considering preferences according to the geographical distance between nodes to reflect empirical networks more precisely and achieve convex and concave shapes of cumulative degree distributions. Some studies proposed a network generation method based on social circles where agents are located on a social map according to some socio-demographic properties. While some consider a city-block-based distance measure, others apply an Euclidean measure. In these studies, Agents connect with other individuals within a radius around their position (BOGUÑÁ et al., 2004; FARZAM; SAMAL; HOST, 2020).

Empirically, studies have shown that the number of in-person memorable interactions is inversely proportional to the distance value, suggesting a connection probability given by $p \propto d^{-1}$. Analyzing mobile phone data, researchers detected a link probability function decaying with the square of the distance. Onnela et al. investigated mobile phone call data of 3.4 million users in Finland and found a connection-distance power law with exponent -1.5. This suggests that people tend to establish closer connections over shorter distances because of the reduced costs and because closer proximity increases the likelihood of interaction and accountability. Even when technology enables one to call anyone, some of the strongest relationships of an

individual have a local nature (ONNELA et al., 2007).

Building on that, in this work, we propose a simple algorithm to generate networks with a connection distance power law exponent α that displays the scale-free property and can generate concave power law distributions, aligning with real-world data on popular social media like Facebook (Meta) and Twitter (X). We also investigate the effects of these affinity-based scale-free networks on opinion formation dynamics. We consider a continuous substrate to create the network and modify the Barabási-Albert model for scale-free networks by introducing a connection probability based on distance with power law exponent α, defined as the affinity parameter.

Figure 8 – Snapshot of a small Affinity-Based Scale-Free Network with $N = 15$ nodes, $z = 3$, $\alpha = 1$, $\xi = 0.9$. Note that the periodic boundary conditions of the substrate allow for connections between nodes positioned in opposite coordinates since their distance is small due to the periodicity. Here, the size of the node is proportional to the node degree. We highlight a particular node as green and paint its connections as blue nodes.

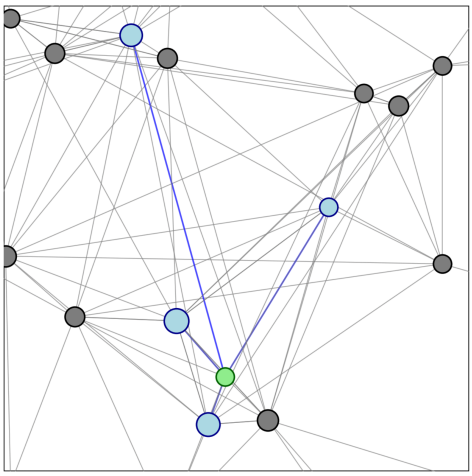

Source: Author.

Our model considers the baseline homophily in the social connections, considering that individuals who live nearby naturally have a higher likelihood of building relationships. We also consider the inbreeding homophily effect as people tend to live with similar individuals around their neighborhood, leisure, and workplaces. Indeed, individuals tend to live in neighborhoods with similar socioeconomic status and race, and people often form connections with colleagues who share similar backgrounds or interests (PINCHAK et al., 2021; THOMAS, 2019). However, this is not deterministic since individuals living nearby can still build relationships and connect with people living far away but with similar views, opinions or occupations. To account for

this, we define the probability of individual i connecting with individual j as

$$p_{ij} \propto \xi_i k_j + \frac{(1-\xi_i)}{[(x_i - x_j)^2 + (y_i - y_j)^2]^{\alpha/2}}, \tag{2.72}$$

where k_j is the degree of individual j, ξ_i is the globalization factor of individual i and x_i and y_i are the coordinate locations of individual i (generated using a random uniform distribution in this work). In that way, we simulate a competition between popularity and baseline and inbreeding homophily in the connection probability, mediated by the globalization parameter. Note that if the globalization factor $\xi_i = 1$, we recover the usual Barabási-Albert model, and if $\xi_i = 0$, we have the gravity model with exponent α. Hence, people have a high probability of connecting with popular persons living nearby, such as their city's mayor. They also have a good probability of connecting with popular individuals living far away, such as the USA president, and have a good probability of linking with non-famous nearby individuals, such as family, neighbors, and professionals of the local institutions such as schools, bakeries, restaurants, gyms, barbershops, and so on. However, they have a minimal probability of connecting with non-famous individuals living far away.

We illustrate this in Fig. 8, where we generated a small network using Eq. (2.72). We highlight a particular individual as green and his social connections as blue nodes. Observe that the model favors connecting closer individuals (homophily) and popular agents (preferential attachment). Indeed, some of the connections are close individuals, but some close people are not connected, and instead, the agent links with some popular individuals who are a little farther away.

Note that, in general, every individual has its own globalization parameter ξ, and primitive societies have a smaller ξ. As societies develop communication and transport technologies such as mobile phones, the World Wide Web, airplanes and cars, they yield a higher globalization factor ξ, and people make more connections with people living far away from them.

In this work, for simplicity, we consider $\xi_i = \xi, \forall\ i$, such ξ is the average globalization factor of the society. We distribute the location coordinates of the individuals randomly using a uniform distribution in a square space of side $L = 1$ with periodic boundary conditions. We start with a core of z individuals in a clique (a network where all nodes are connected with each other) and construct a growing network where each new individual makes z links with previous individuals with a connection probability given by Eq. (2.72).

3 STOCHASTIC DYNAMICS

"The beauty of theoretical physics
is that it allows us to see order in chaos
and chaos in order."
Murray Gell-Mann

In this chapter, we closely follow the development made by Tomé and Oliveira in the book Stochastic Dynamics and Irreversibility (TOMÉ; OLIVEIRA, 2015). We shall present the mathematical formalism of stochastic systems and prove the master equation, a powerful equation for studying the dynamics of stochastic systems. We will also discuss the Monte Carlo method for numerically simulating complex systems and the ergodicity condition.

3.1 RANDOM VARIABLES AND STOCHASTIC SYSTEMS

A random variable is any quantity whose value depends on random processes, making it impossible to exactly and deterministically predict it a priori. For example, the outcome of rolling a die, the amount of rainfall on a given day, the price of a stock at the end of a trading day and the final score of a basketball game are random variables.

In this context, a stochastic process is a mathematical model describing a sequence of random variables, typically indexed by time. For example, we can define a stochastic process as a collection of random variables $\{X_t : t \in T\}$, where T represents the set of time frames. If the set T is discrete, the process is said to be discrete-time, whereas if T is a continuous interval, the process is continuous-time. The state space S of a stochastic process is the set of all possible values the random variables can assume. For instance, in a random walk, S may represent possible positions the walker can assume (TOMÉ; OLIVEIRA, 2015).

Stochastic processes arise naturally in a wide variety of scientific phenomena. A classic example is Brownian motion, the erratic movement of pollen grains suspended in water, first observed by Robert Brown. This phenomenon was later rigorously explained through the work of Einstein and Langevin, who described such motion using the Fokker-Planck and stochastic differential equations.

We can also apply stochastic modeling to social sciences. In opinion dynamics, stochastic models simulate how individual beliefs and opinions evolve under the influence of social in-

teractions and how they spread information within their social networks. Similarly, stochastic epidemiological models account for randomness in individual transmission events, analyzing the competition between infection, recovery, and vaccination dynamics and leading to more realistic predictions, considering the impact of rare events such as superspreaders.

In engineering, the operation of modern electrical grids involves numerous stochastic elements, from fluctuating energy demands to variable renewable energy inputs such as wind and solar power. Stochastic models enable grid stability analysis and the design of robust control strategies to ensure continuous operation despite unpredictable fluctuations.

3.2 MARKOV PROCESSES

Stochastic processes can be categorized based on their dependency structure. A critical case is the Markov process, named after Andrey Markov, where the future state depends only on the present state and not on the past states. This property, known as the Markov property, dramatically simplifies the mathematical treatment of these processes. Non-Markovian processes, by contrast, involve memory effects, requiring information about past states to determine future evolution (TOMÉ; OLIVEIRA, 2015).

So, mathematically, the Markov property is given by

$$P(X_{t+\Delta t} = x_{t+\Delta t} \mid X_t = x_t, X_{t-1} = x_{t-1}, \ldots) = P(X_{t+\Delta t} = x_{t+\Delta t} \mid X_t = x_t).$$

The state space S of the process can be discrete or continuous, and t may represent discrete or continuous time. The transition probabilities between states are denoted by $P(x', t' \mid x, t)$, which is the probability of transitioning from state x at time t to state x' at time t'.

Hence, the joint probability distribution for a Markovian stochastic system until time t_ℓ can be written in the form:

$$\begin{aligned} P(x_0, t_0; x_1, t_1; \ldots; x_\ell, t_\ell) = P(x_\ell, t_\ell | x_{\ell-1}, t_{\ell-1}) P(x_{\ell-1}, t_{\ell-1} | x_{\ell-2}, t_{\ell-2}) \cdots \\ \cdots P(x_1, t_1 | x_0, t_0) P(x_0). \end{aligned} \tag{3.1}$$

Thus, the marginal probability at t is given by

$$P(x, t) = \sum_{x_{t-1}} P(x | x_{t-1}) P(x_{t-1}). \tag{3.2}$$

In general, these transition probabilities depend on time. However, for this work, we will consider stationary Marvok processes. In this case, we can write the probability of the random

variable x transitioning from state m to n as

$$P(n, t_n|m, t_m) = P(n|m) = T(n, m). \tag{3.3}$$

Hence,

$$P(n, t_{m+1}) = \sum_m T(n, m)P(m, t_m). \tag{3.4}$$

The transition probabilities can be conveniently expressed as a stochastic matrix $T(n, m)$, where some element defines the probability of transitioning from state m to state n. The matrix satisfies

$$\sum_n T(n, m) = 1, \quad T(n, m) \geq 0 \ \forall m, n. \tag{3.5}$$

Let P_t be a column vector whose entries are given by $P(n, t)$. Then, we can write the marginal probability in matrix form

$$P_t = TP_{t-1}. \tag{3.6}$$

We can extend it until the initial probability vector

$$P_t = T^t P_0 = \sum_m T^t(n, m)P_0(m), \tag{3.7}$$

where $T^t(n, m)$ is the transition probability from state m to state n after t time units.

3.3 THE MASTER EQUATION

One question of great interest is how we can describe the evolution in continuous time of a Markovian stochastic system probability distribution with time-independent transition rates. For this purpose, let us consider that the transitions in the process occur within a tiny time window τ so that the elements of the stochastic matrix are

$$T(n, m) = \tau W(n, m), \tag{3.8}$$

for $n \neq m$. Here, $W(n, m)$ is the transition rate between states m and n. In other words, it is the probability per unit time of a transition from state m to state n. Therefore, note that for the special case $m = n$, we must have

$$T(n, n) = 1 - \tau \sum_{m, m \neq n} W(m, n). \tag{3.9}$$

We can write the probability that the system will be in state n at time $t + \tau$ is

$$P(n, t + \tau) = \sum_m T(n, m)P(m, t) = T(n, n)P(n, t) + \sum_{m, m \neq n} T(n, m)P(m, t). \tag{3.10}$$

But, using Eqs. (3.8) and (3.9) , we can rewrite it as

$$P(n,t+\tau) = [1 - \tau \sum_{m \neq n} W(m,n)]P(n,t) + \tau \sum_{m,m \neq n} W(n,m)P(m,t). \tag{3.11}$$

Hence, we can organize to find the time derivative definition of the probability distribution:

$$\frac{P(n,t+\tau) - P(n,t)}{\tau} = \sum_{m,m \neq n} [W(n,m)P(m,t) - W(m,n)P(n,t)]. \tag{3.12}$$

Taking the limit $\tau \to 0$, we obtain a differential equation for the probability distribution $P(n,t)$

$$\frac{d}{dt}P(n,t) = \sum_{m,m \neq n} [W(n,m)P(m,t) - W(m,n)P(n,t)], \tag{3.13}$$

which is the master equation. That equation shows us how the stochastic transition rates govern the evolution of the probability distribution of the states. That equation is fundamental when analyzing Markovian stochastic systems with time-independent transition probabilities. The master equation bridges the microscopic dynamics of individual components and the macroscopic observables of the system as a whole.

3.3.1 Intuitive derivation of the master equation

Considering the assumptions of a Markovian stochastic system, it is also possible to get a more intuitive and interpretable derivation of the master equation. Indeed, the rate of change of $P(n,t)$ is determined by the net flow of probability into and out of state n. This is expressed as:

$$\frac{dP(n,t)}{dt} = \text{Incoming Rate} - \text{Outgoing Rate}. \tag{3.14}$$

The incoming rate is the sum of probabilities for all transitions into state n, weighted by the transition rates:

$$\text{Incoming Rate} = \sum_{m,m \neq n} W(n,m)P(n,t). \tag{3.15}$$

While the outgoing rate is the sum of probabilities for all transitions out of state n, also weighted by the transition rates:

$$\text{Outgoing Rate} = \sum_{m,m \neq n} W(m,n)P(n,t). \tag{3.16}$$

Observe that transitions from state n to itself do not affect the value of $\frac{dP(n,t)}{dt}$, as it does not impact how the distribution is changing.

Substituting the expressions for the incoming and outgoing rates into the balance equation yields the master equation:

$$\frac{dP(n,t)}{dt} = \sum_{m,m\neq n} \Big[W(n,m)P(m,t) - W(m,n)P(n,t)\Big]. \tag{3.17}$$

This equation describes the time evolution of the probability $P(n,t)$, accounting for all transitions into and out of state n.

3.3.2 Average values and observables

One of the most significant applications of the master equation is that it allows us to calculate the time evolution of the average value of a state function of the system $f(n)$. For example, the expectation value of the function $f(n)$ within an ensemble is defined as

$$\langle f(n)\rangle = \sum_n f(n)P(n,t). \tag{3.18}$$

Differentiating by time gives

$$\frac{d}{dt}\langle f(n)\rangle = \sum_n f(n)\frac{dP(n,t)}{dt}. \tag{3.19}$$

Substituting the master equation, we obtain:

$$\frac{d}{dt}\langle f(n)\rangle = \sum_{m,m\neq n} f(n)\Big[W(n,m)P(m,t) - W(m,n)P(n,t)\Big]. \tag{3.20}$$

3.4 ERGODICITY AND MONTE CARLO SIMULATIONS

Phase space is defined in statistical mechanics as a space in which every point corresponds to a particular configuration of the system, fully specified by its generalized coordinates and momenta. For tridimensional gas with N particles, it is thus $6N$-dimensional: $3N$ position coordinates and $3N$ momentum coordinates of the particles. All possible values of both momenta and positions of the particles in the system define the phase space (METROPOLIS et al., 1953).

A system is ergodic if its trajectory in phase space will pass arbitrarily closely to all phase space points consistent with its conservation laws (for example, energy or momentum). Ergodicity in maths means, for a dynamical system explained by a phase space Γ, which contains the generalized position and momentum vector $\mathbf{x}$, and a probability measure $P(\mathbf{x})$:

$$\lim_{T\to\infty} \frac{1}{T} \int_0^T f(\mathbf{x}(t))\, dt = \int_\Gamma f(\mathbf{x}) P(\mathbf{x})\, d\mathbf{x},$$

for any observable $f(\mathbf{x})$. That is the equality between the time average (left-hand side) and the ensemble average (right-hand side), which is the defining property of an ergodic system.

For a system to be ergodic, the dynamics must explore a volume in phase space consistent with conserved quantities rather than be confined to a small region. $\frac{\partial P}{\partial t} = 0$ for a time-invariant system, and the system describes over time the evolution of the probability distribution $P(\mathbf{x})$ that describes the system. Moreover, the system's dynamics must visit phase space points rapidly enough so that there is no statistically significant correlation between the initial and final states.

As long as phase-space exploration is not constrained, most equilibrium statistical mechanics systems are ergodic, from ideal gases to liquids and many spin systems (for instance, the Ising model in its usual conditions). Due to ergodicity, all phase space will ultimately be explored and equilibrated, while in non-ergodic systems like glasses or systems with energy barriers, due to being stuck in a part of phase space or long-lived correlations due to constraints.

The Monte Carlo method is a computational approach that uses pseudo-random numbers sampling to simulate stochastic phenomena and to estimate valuable properties. The technique was popularized during the 1940s by researchers working on nuclear physics and the Manhattan Project, such as Stanislaw Ulam and John von Neumann (GOULD et al, 1996). Ulam coined the term in collaboration with Nicholas Metropolis because his uncle was fond of gambling at the famous Monte Carlo casino, which also works based on random sampling. In particular, von Neumann, Ulam and Metropolis, among others, suggested that these pseudo-random numbers can be exploited to simulate the phase space trajectories of physical systems. Then, given that these trajectories are ergodic, we can use them to compute averages that describe the macroscopic state of the system.

Monte Carlo simulations are especially useful for solving problems with systems with many degrees of freedom and (or) analytically intractable. Stanislaw Ulam and John von Neumann utilized the Monte Carlo method to solve complex problems in nuclear physics, particularly regarding nuclear weapon design and analysis. They used the technique to research the random behavior of neutron scattering in fissile materials such as uranium and plutonium. The paths and interactions of millions of neutrons are complex and analytically intractable. However, by

random sampling, the Monte Carlo method enabled them to identify the probabilities of these interactions, which helped determine whether some configuration of nuclear material would achieve a sustained chain reaction to generate enough radiation power.

Algorithms based on detailed balance, which basically means that the probability of the system being in state A and going to state B is equal to the probability of the system being in state B and going back to state A, ensure the system's ergodicity so that the simulation allows access to the full range of possible micro-states, allowing these computed averages to converge to their actual values. The equivalence between the time average and the ensemble average enables using Monte Carlo simulations to sample phase space and compute averages efficiently.

Figure 9 – Monte Carlo estimation of Pi. If the dots are generated randomly, the ratio between the blue dots and the total number of dots is proportional to the ratio between the circle and the square area.

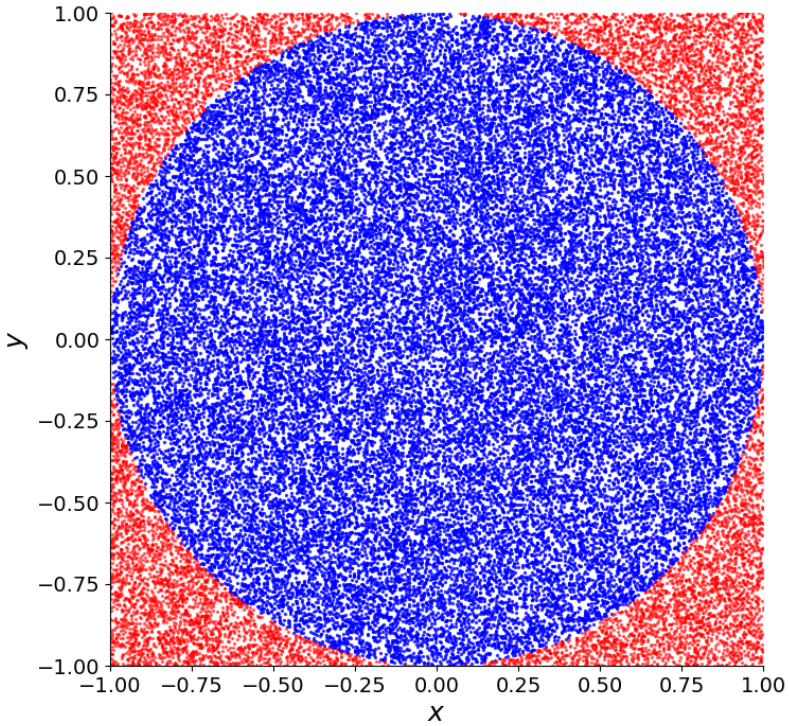

Source: Author.

One of the practical applications of the Monte Carlo method is to approximate integrals and sums over high-dimensional spaces through random sampling. Consider a function $f(\mathbf{x})$ defined over a domain Ω with a probability density $P(\mathbf{x})$. The expectation value of $f(\mathbf{x})$ is

given by:

$$\langle f(\mathbf{x})\rangle = \int_{\Omega} f(\mathbf{x})P(\mathbf{x})\,d\mathbf{x}. \tag{3.21}$$

In practice, this integral can be approximated by sampling K points $\mathbf{x}_1, \mathbf{x}_2, \ldots, \mathbf{x}_K$ from $P(\mathbf{x})$ and computing:

$$\langle f(\mathbf{x})\rangle \approx \frac{1}{K}\sum_{i=1}^{K} f(\mathbf{x}_i). \tag{3.22}$$

As $K \to \infty$, this estimate converges to the actual value of the integral, assuming the system satisfies the ergodic property. In this work, we use such properties of the Monte Carlo method to estimate numerically relevant quantities that characterize the system's dynamics and criticality.

Fig 9 shows a classic example where the coordinates of the dots are generated using pseudorandom numbers. In that way, the fraction of dots that fall inside the circle (the blue ones) is proportional to the circle area. Similarly, the total number of dots is proportional to the square area. It is possible to estimate the value of π using that proportion. In that case, since the circle has a unit radius and the square has a side equal to 2, then

$$\pi \approx 4\frac{\text{Blue dots}}{\text{Blue dots} + \text{Red dots}}. \tag{3.23}$$

Using only 50000 points, it is possible to get a reasonable estimate of $\pi \approx 3.14$.

4 THE MAJORITY-VOTE MODEL

"Life in society requires consensus as an indispensable condition.
But consensus, to be productive, requires that each individual
contribute independently out of his experience and insight."
Solomon E. Asch

This chapter explains the complex relationship between individual psychology and collective behavior, drawing from social psychology, neuroscience, and physics. With these psychological principles, we move on to the majority-vote model, a simple yet powerful Sociophysics model that adapts the Ising model of statistical mechanics for studying social dynamics. This mathematical model helps us infer how individual behaviors and group pressures lead to complex collective outcomes.

Here, we also define the cooperative majority-vote model and analyze it using mean-field calculations for the order parameter and the entropy flux. Additionally, we discuss finite-size scaling techniques and the hyper-scaling and unitary relation for the critical exponents of the system. The mean-field results closely follow the calculations from the author's published paper (OLIVEIRA et al., 2024).

4.1 SOLOMON ASCH'S AND GREGORY BERNS' EXPERIMENTS

The Solomon Asch Conformity experiment was a landmark study in social psychology conducted during the early 1950s to demonstrate how social pressure from a majority group could push a person to conform. Solomon was interested to see whether people would align with the majority opinion, even when that opinion was clearly incorrect. His experiment has since been regarded as a foundation for understanding social dynamics, peer pressure, and how group consensus may shape individual decisions (ASCH, 1955).

In the Asch experiment, the participants were told that they were in a study of visual perception (See Fig. 10). Each subject was placed in a room with several other people. They were said to be other participants, but they were actually confederates of the experimenter. The task was relatively simple: the card deck series would show each group some cards with lines. On one card was a single line, while on the other card were three lines of varying lengths, which were referred to as A, B and C, and all that a subject had to do was compare the length

of the single line on one card to the three lines on the other card and pick out which line was the same length as that on the first card. The answer was unequivocal: The lengths of the lines looked significantly different. The simplicity of the task made the correct answer clear, making this a good context for studying conformity because mistakes could be clearly due to social influence and not perceptual difficulty (ASCH, 1955).

Figure 10 – Illustration of one question in the experiment by Solomon Asch. Subjects need to decide which line on the right, A, B or C, is most similar to the line on the left. However, before deciding, they hear the answers of other potential subjects, who are actually actors, often giving the wrong answer on purpose.

Source: Series Discovering Psychology by Zimbardo (1990).

Multiple trials of this task were performed; on some trials, the confederates were asked to provide identical incorrect responses. For example, if the correct line were line A, all the confederates would deliberately pick line B or C. One participant, who was seated so that he answered after almost all the confederates had responded, was thus exposed to the unanimous but incorrect opinion of the group before he reported his answer. Based on this setup, Asch predicted that participants would be socially pressured to conform to the group's wrong answer, even if they knew it was wrong. This setup enabled him to see if people would accept the consensus opinion or hold fast to their personal judgment.

The outcome of Asch's experiment was surprising and significant. It was found that 75% of the participants conformed to the group consensus in at least one trial during the experiment (on average, $1/3$ of the incorrect answers were agreed upon by the participants). Although

the correct alternative was obvious, the influence to align with the group was so powerful that many subjects doubted or even rejected their own perceptions. Some knew the correct answer and chose the incorrect one because they did not want to create conflict or were somewhat doubtful after hearing the group's collective response. Others began to question their own judgment, illustrating the power of group dynamics over an individual's cognition and decision-making. There was also public compliance versus private acceptance, meaning that some subjects did conform publicly while privately accepting the correct answer. Others, by contrast, underwent private acceptance: they believed a group's incorrect answer was the correct answer.

One of this experiment's most striking results is that a considerable fraction of the participants consented to a clearly wrong answer. What can we expect in the real world when our questions are even more challenging, and we often can not see the correct answer? How much more susceptible to peer pressure and irrational behavior are we?

Asch's work on group behavior led to substantial research with enormous ramifications for understanding social dynamics, from adolescent peer pressure to organizational decision-making. This experiment illustrated how group thinking, the process whereby group consensus prevails over individual judgment, sometimes leads to suboptimal or even irrational conclusions. Asch's work has also illuminated research from fields as varied as economics, marketing, politics and ethics.

In 2005, Gregory Berns expanded on Asch's work by using brain imaging (functional magnetic resonance imaging or fMRI) in all participants while performing a task that tested their susceptibility to social conformity. The participants were placed inside an fMRI scanner and asked to mentally rotate and compare 3D objects to determine if they were the same or different. However, before making their decisions, participants saw the answers of a group, where, similar to Asch's conformity experiment, sometimes the group gave incorrect answers by design. The idea was to measure brain activity when participants conformed to the group's incorrect answers versus when they resisted (BERNS et al., 2005).

When participants conformed to incorrect group answers, brain activity in the occipital and parietal lobes (visual processing areas) changed, suggesting that social pressure altered their actual perception of the objects rather than just their willingness to agree with the group. On the other hand, resisting conformity triggered the amygdala (fear and emotional center of the brain), indicating that going against social norms causes stress or emotional discomfort. This study shows that social pressure actually alters the perception of reality, not just decision-

making. Group pressure is powerful enough to reshape both beliefs and perceptions, influencing people on a deep level.

4.2 CACIOPPO'S LONELINESS

"Health and well-being for a member of our species
requires, among other things, being satisfied and secure
in our bonds with other people, a condition of 'not being lonely'
that, for want of a better word, we call social connection."
John T. Cacioppo

Why are humans so susceptible to peer pressure, even when it is clear that what the majority is saying is wrong? John T. Cacioppo and William Patrick were among the pioneers in the field of social neuroscience. They became known worldwide for their studies on loneliness and the neurological bases of social processes. In their seminal book *Loneliness: Human Nature and the Need for Social Connection* (CACIOPPO; PATRICK, 2008), they explain that social contact is an essential part of human existence and evolution. Throughout a significant part of our history, humans have lived as hunters and gatherers, and being in groups was crucial to survival. Throughout generations, our brain learned these patterns, and today, in the same way, the brain creates sensations of hunger and thirst to communicate the body's needs for food and water, and the brain creates the feeling of loneliness to communicate its social and psychological needs.

Therefore, the subjective experience of social disconnection functions as a signal for adaptive behavior and survival. Similar to starving, being isolated can precipitate a cascade of negative life events or outcomes, including diminished brain power, increased susceptibility to bodily maladies and hypersensitivity to social threats. Indeed, the psychologist and neuroscientist Julianne Holt-Lunstad performed a meta-analysis of 148 studies and showed that there was a 50% increased likelihood of survival for participants with stronger social relationships, regardless of age, sex, initial health status, cause of death, and follow-up period. Chronic loneliness can lead to health problems such as increased blood pressure, inflammation, and compromised immune systems, as well as negatively affecting mental health (anxiety and depression), with an overall impact on mortality risk similar in magnitude to that of smoking 15 cigarettes a day. (HOLT-LUNSTAD; SMITH; LAYTON, 2010)

"The need to connect socially with others
is as basic as our need for food, water, and shelter."
Matthew Lieberman

These findings are strikingly congruent with the dynamics revealed by the experiments on conformity performed by Solomon Asch. The evolutionary forces require humans to conform to social groups, and loneliness can serve as a psychological engine for social affiliation. Hence, the discomfort of being the outlier persuaded individuals to consent to the group's terms even in defiance of what they think is right, giving rise to behaviors that foster group cohesion over objective veracity and ultimately changing their truth. That resembles Asch's experiment, where some of his experimental subjects began questioning their perceptual experience after a succession of group pressures, indicating a more profound layer at which social groups influence individuals' cognition.

4.3 SOCIAL INFLUENCE AND THE ISING MODEL: THE MAJORITY-VOTE MODEL

The key finding is that individuals can often exhibit irrational behavior and are evolutionarily susceptible to conforming with the group even in defiance of their personal truth and logic, which has striking parallels with some physical systems, like the Ising model. The Ising model was proposed to describe ferromagnetic materials and consists of a lattice of spins, where each spin is allowed to adopt one out of two states (e.g., $+1$ or -1). However, each spin also interacts with its neighbors, and to minimize their magnetic energy, they tend to be aligned with each other. On the other hand, thermal energy disrupts spin alignment and causes fluctuations in the system. Despite its simplicity, this powerful model exhibits a phase transition at a critical temperature, making it a realistic representation of ferromagnetic behavior.

The majority-vote model generalizes the Ising model to social systems in which spins correspond to binary individual opinions or behaviors, and the energy minimization principle corresponds to the tendency of individuals to be influenced by the social environment. For example, a spin-up (down) could represent voting in the democrats (the republicans) or buying (selling) an asset in the financial market. In this context, the temperature corresponds to a noise parameter q, representing the agent's nonconformity, and models the probability of an individual disagreeing with their social connections' majoritarian opinion. (OLIVEIRA, 1992)

Hence, we represent the agent's i opinion by a stochastic variable σ_i that may assume

the values $+1$ or -1. However, the agents' opinions, beliefs or behavior may change as they interact. Consider $S(x)$ to be the signal function given by $S(x) = -1, 0, 1$ for $x < 0, x = 0, x > 0$, respectively. Hence, if agent i agrees with the majority of his connections, that is, $\sigma_i S\left(\sum_{j\in neighbors}\sigma_j\right) = 1$, the probability $w_i(\sigma)$ of agent i changing his opinion is $w_i(\sigma) = q$, following the definition that the social temperature q is the probability of an agent disagreeing with the majority. Here, $\sigma = (\sigma_1, \cdots, \sigma_N)$ denotes the system state or the configuration of opinion of the N agents.

Similarly, if agent i disagrees with the majority of his friends and family so that we have $\sigma_i S\left(\sum_{j\in neighbors}\sigma_j\right) = -1$, the probability $w_i(\sigma)$ of agent i changing his opinion is $w_i(\sigma) = 1-q$. If there is no majority, $\sigma_i S\left(\sum_{j\in neighbors}\sigma_j\right) = 0$ and i may assume each possible opinion with equal probability, so $w_i(\sigma) = 1/2$.

Hence, $w_i(\sigma)$ is a function of $\sigma_i S\left(\sum_{j\in neighbors}\sigma_j\right)$ subject to the equations

$$\begin{cases} w_i(\sigma) = q, & \text{if } \sigma_i S\left(\sum_{j\in neighbors}\sigma_j\right) = 1, \text{ anticonformity.} \\ w_i(\sigma) = 1-q, & \text{if } \sigma_i S\left(\sum_{j\in neighbors}\sigma_j\right) = -1, \text{ conformity.} \\ w_i(\sigma) = 1/2, & \text{if } \sigma_i S\left(\sum_{j\in neighbors}\sigma_j\right) = 0, \text{ independence.} \end{cases} \tag{4.1}$$

Thus, since there are three possible cases, we can assume a general equation with three unknown coefficients of the form

$$w_i(\sigma) = a + b\sigma_i S\left(\sum_{j\in neighbors}\sigma_j\right) + c\left[\sigma_i S\left(\sum_{j\in neighbors}\sigma_j\right)\right]^2. \tag{4.2}$$

Substituting each case of Eqs. (4.1) in Eq. (4.2), we have a system of three equations and three unknown coefficients a, b and c. The solution yields the general opinion transition probability that depends on the local majority and the social noise level

$$w_i(\sigma) = \frac{1}{2}\left[1 - (1-2q)\sigma_i S\left(\sum_{j\in neighbors}\sigma_j\right)\right]. \tag{4.3}$$

Note that each individual i is affected by a different local majority, representing his social interactions, such as family, coworkers and friends, directly manifesting the social pressure represented in Asch's experiments. Furthermore, the model is symmetric under the transformation $\sigma_i \to -\sigma_i$, $\forall\ i$.

The model is deterministic at $q = 0$ as agents always adopt the local majority opinion. For increasing values of the social temperature q, the system becomes increasingly disordered, and agents increasingly act in nonconformity regarding the majority of their social contacts. The

model has physical meaning when the probability of consenting with the majority is higher than the probability of acting in nonconformity, following empirical data, such as Aschs experiment. Therefore, we may impose

$$1 - q > q > 0 \Longrightarrow 0 < q < 1/2. \tag{4.4}$$

In particular, for $q = 1/2$, every agent assumes a given opinion randomly.

4.4 OVERVIEW OF THE MAJORITY-VOTE MODEL LITERATURE

Oliveira et al. conducted the first study of the majority-vote model (OLIVEIRA, 1992; OLIVEIRA; MENDES; SANTOS, 1993), where he obtained the results for the model defined on the square lattice using Monte Carlo simulations. He shows the model has a critical noise parameter $q_c = 0.075 \pm 0.001$, where the order parameter undergoes a second-order phase transition. He estimated values for the critical exponents as $\beta/\nu = 0.125 \pm 0.005$, $\gamma/\nu = 1.73 \pm 0.05$, and $1/\nu = 1.01 \pm 0.05$, in agreement with the exact values for the two-dimensional Ising model calculated by Onsager (ONSAGER, 1944).

Therefore, the majority-vote model on a square lattice belongs to the same universality class as the two-dimensional Ising model; that is, they share the same critical behavior near phase transitions, yielding the same critical exponents, symmetries, and dimensionality despite their different microscopic mechanics. The universality classes give us predictive power because if a new model has the same symmetry and dimensionality, we can predict its critical exponents and also explain why they behave similarly. Indeed, Grinstein, Jayaparakash, and He (GRINSTEIN; JAYAPRAKASH; HE, 1985) conjectured that nonequilibrium models with inversion symmetry belong to the same universality class as the Ising model, both defined on regular lattices.

Scientists have proposed several model variations to investigate a specific problem or analyze the impact of some factors on the social dynamics of groups. There are two components defining a complex system: the network structure and the system's dynamics. In this context, Some researchers analyzed the effect of complex networks of interactions on societal polarization (CAMPOS; OLIVEIRA; MOREIRA, 2003; PEREIRA; MOREIRA, 2005; LIMA, 2007). Other scholars analyzed different opinion dynamics, such as considering heterogeneous communities, independence, and more than two possible opinions, among other variations (VILELA; MOREIRA; SOUZA, 2012; LIMA, 2013; VIEIRA; CROKIDAKIS, 2016; VILELA; STANLEY, 2018; SANTOS; TEIXEIRA, 1995; COSTA; SOUZA, 2005; MELO; PEREIRA; MOREIRA, 2010; LIMA, 2012; VILELA et

al., 2020).

The majority-vote model and other stochastic lattice models are formulated in terms of stochastic rules with no prior connection to thermodynamics. However, some scholars have been analyzing the entropy production and thermodynamics of the majority-vote model using mean-field approximation and Monte Carlo simulations. These studies explore the thermodynamics of opinion dynamics and show that entropy production exhibits a singularity at the critical point. They can also be used to study the system's phase transitions (HAWTHORNE et al., 2023; SILVA et al., 2020; CROCHIK; TOME, 2005).

4.5 COOPERATIVE MAJORITY-VOTE MODEL

One of the most important phenomena to our societies, and still also one of the most misunderstood collective phenomena, is collaborative behavior. Cooperative phenomena challenge scientists across several fields, from biology, sociology, economics, psychology, anthropology and sociophysics. Various species, from social insects to humans, create groups that altruistically work toward a common benefit. In human society, this collaborative conduct is crucial in shaping the actions and opinions of individuals and influencing decision-making in political, religious, ethnic, and socioeconomic challenges. Cooperation deeply influences how people form alliances, build institutions, and perform political and economic negotiations, enabling the formation of complex social structures (CAPRARO, 2013; PENNISI, 2005; JONG; VEIJER, 2014).

In this work, we investigate how cooperative behavior influences public opinion formation using the majority-vote model. To accomplish that, we introduce a parameter μ, named the noise sensitivity, to the standard majority-vote model to yield the distinct influence of the social temperature over the individuals of the society and consider two types of individuals, cooperative and regular. Hence, we assume a fraction f of the society as cooperative individuals under the effect of a social temperature μq, where $0 < \mu < 1$, whilst a regular individual is under the influence of the regular noise q. Adding the noise sensitivity parameter μ to the model addresses individuals more socially susceptible to agreeing with others to support them. In the opinion dynamic context, we consider that cooperation behavior acts supporting consensus and social order, promoting the ideas, opinions and beliefs from their social interactions. Thus, we

denote the flip probability of a given agent i as

$$w_i(\sigma) = \frac{1}{2}\left[1 - (1 - 2\mu_i q)\sigma_i S\left(\sum_{j \in neighbors} \sigma_j\right)\right], \tag{4.5}$$

where

$$\mu_i = \begin{cases} \mu, & \text{if } i \text{ is a cooperative agent.} \\ 1, & \text{if } i \text{ is a regular agent.} \end{cases} \tag{4.6}$$

Thus, a noise sensitivity $\mu < 1$ increases the agreement probability by attenuating the effect of the noise parameter q of the society.

Note that for $f = 0$, we recover the standard homogeneous majority-vote model with noise (OLIVEIRA, 1992; OLIVEIRA; MENDES; SANTOS, 1993). For $f = 1$, all individuals are cooperative, and the system also behaves as the standard MVM under the linear transform $q \longrightarrow q/\mu$. The case for $\mu = 0$ corresponds to a bimodal distribution of noise, where a fraction f of the individuals are noiseless, always agreeing with their nearest interacting neighbors (VILELA; MOREIRA; SOUZA, 2012; VILELA; SOUZA, 2017). However, the system's behavior is nontrivial for $0 < f < 1$ and $0 < \mu < 1$, the focus of our work.

On the topological aspect, we investigate how Affinity-Based Scale-Free Networks, which provide a better approximation for the degree distribution of real social media networks such as X, introduced in Section 2.3, affect the opinion dynamics of the majority-vote model.

4.6 REVERSIBILITY OF THE MAJORITY-VOTE DYNAMICS

Stochastic models, like the majority-vote Model, have an initial system's state and then evolve until a stationary state, where the probability distribution of finding the system at a given state is independent of time. These statistical models can have reversible or irreversible time evolutions. In reversible models, the dynamics is governed by a Hamiltonian that models the interaction between the system's components so that the transition between two states depends on the system's energy and the energy involved in the transition. On the other hand, we cannot describe an irreversible model using a Hamiltonian. The transition probability between the possible states of the system solely controls the dynamics.

For reversible systems, the stationary states correspond to states of thermodynamic equilibrium: the probability of the system going through a given sequence of microscopic states in direct order is equal to the likelihood of the system going through the same sequence in reverse order, a property known as Kolmogorov's criterion. In other words, reversible systems

have detailed balance:

$$P(A)W(A \to B) = P(B)W(B \to A), \forall A, B \in S. \tag{4.7}$$

That is, the probability of the system being in state A and transitioning to state B is equal to the likelihood of the system being in state B and transitioning to state A, for all states A, B in the state space S.

However, irreversible systems lack detailed balance, and their stationary states are out of thermodynamic equilibrium: the probability that the system follows a particular trajectory in phase space from its initial state to a final state, in general, differs from the probability that the system will follow the same trajectory in reverse.

We can prove by contradiction that the majority-vote model fails Kolmogorov's criterion and has irreversible dynamics. Let us consider the majority-vote Model on a two-dimensional square lattice with periodic boundary conditions with side $L = 4$, hence $N = 16$ individuals. We shall represent the system's state using a matrix, where each element in the matrix represents its respective site in the lattice along with its state $(\sigma_{ij} = \pm 1, \sigma_{ij} = \sigma_{11}, \sigma_{12}, \ldots, \sigma_{LL})$. Let A, B, C and D be four matrices corresponding to four different microstates of this system, each of them occurring in the stationary regime with probability $P(A)$, $P(B)$, $P(C)$ and $P(D)$, respectively. If the majority-vote model is reversible, it obeys Kolmogorov's criterion, and we must have that

$$\begin{aligned} &P(A)W(A \to B)W(B \to C)W(C \to D)W(D \to A) = \\ &P(A)W(A \to D)W(D \to C)W(C \to B)W(B \to A). \end{aligned} \tag{4.8}$$

We consider now the probability of the left trajectory $A \to B \to C \to D$. So, initially, the system is in state A, defined as:

$$A = \begin{pmatrix} +1 & +1 & +1 & +1 \\ +1 & -1 & +1 & +1 \\ +1 & +1 & +1 & +1 \\ +1 & +1 & +1 & +1 \end{pmatrix}.$$

It then transitions to state B ($\sigma_{23} \to -1$), represented by:

$$B = \begin{pmatrix} +1 & +1 & +1 & +1 \\ +1 & -1 & -1 & +1 \\ +1 & +1 & +1 & +1 \\ +1 & +1 & +1 & +1 \end{pmatrix},$$

with a transition probability q. Hence, $P(B) = P(A)q$. Then it evolves to state C ($\sigma_{24} \to -1$), represented by:

$$C = \begin{pmatrix} +1 & +1 & +1 & +1 \\ +1 & -1 & -1 & -1 \\ +1 & +1 & +1 & +1 \\ +1 & +1 & +1 & +1 \end{pmatrix},$$

also with a transition probability of q. Thus, $P(C) = P(B)q = P(A)q^2$. Now, it transitions to state D ($\sigma_{23} \to 1$), given by:

$$D = \begin{pmatrix} +1 & +1 & +1 & +1 \\ +1 & -1 & +1 & -1 \\ +1 & +1 & +1 & +1 \\ +1 & +1 & +1 & +1 \end{pmatrix},$$

with a transition probability $1/2$. Hence, $P(D) = P(C)1/2 = P(A)q^2/2$. Then it evolves back to state A ($\sigma_{24} \to 1$) with probability $1 - q$. Hence, the whole trajectory $A \to B \to C \to D \to A$ has probability $P(A)q^2(1-q)/2$.

On the other hand, the reverse trajectory has probability

$$\begin{aligned} &P(A)W(A \to D)W(D \to C)W(C \to B)W(B \to A) = \\ &P(A) \times q \times \frac{1}{2} \times (1-q) \times (1-q) = P(A)\frac{q}{2}(1-q)^2. \end{aligned} \tag{4.9}$$

Therefore,

$$\begin{aligned} &P(A)W(A \to B)W(B \to C)W(C \to D)W(D \to A) \neq \\ &P(A)W(A \to D)W(D \to C)W(C \to B)W(B \to A). \end{aligned} \tag{4.10}$$

and the majority-vote model fails Kolmogorov's criterion and hence has irreversible dynamics and lacks detailed balance.

4.7 ENTROPY PRODUCTION

Irreversible systems continuously produce entropy even in the stationary state, as they are still out of thermodynamic equilibrium. However, the entropy production of reversible systems vanishes at the equilibrium state. Even though the microstate of a stochastic reversible system continues to change even in the steady state and the entropy of several parts of the system varies, the net change is zero. That is because reversible systems satisfy detailed balance. While some individual transitions might still increase entropy, these increases are counterbalanced by equally probable transitions that decrease entropy by the same amount. Hence, the production of entropy of stochastic reversible systems vanishes at the steady state. Therefore, non-zero stationary entropy production is a signature of irreversibility.

To investigate the irreversibility of the majority-vote model, we consider the Boltzmann-Gibbs entropy, which states that the entropy $S(t)$ of a system at time t is given by

$$S(t) = -\sum_{\sigma} P(\sigma,t)\ln P(\sigma,t). \tag{4.11}$$

A given society configuration can be denoted by $\sigma = (\sigma_1, \sigma_2, ..., \sigma_i, ..., \sigma_N)$, meaning the first agent has opinion σ_1, the second σ_2, and so on. Hence, the majority-vote model master equation that expresses the time evolution of the probability $P(\sigma,t)$ of finding the system in the state σ at a time t is

$$\frac{d}{dt}P(\sigma,t) = \sum_{i=1}^{N}\left[w_i(\sigma^i)P(\sigma^i,t) - w_i(\sigma)P(\sigma,t)\right], \tag{4.12}$$

where the state σ^i can be obtained from the state σ flipping the i-th agent's opinion, i.e., $\sigma^i = (\sigma_1, \sigma_2, ..., -\sigma_i, ..., \sigma_N)$.

Therefore, differentiating Eq. (4.11) with respect to time and using the master equation, we can express the time derivative of the entropy as

$$\frac{dS(t)}{dt} = -\sum_{\sigma}\left[\frac{dP(\sigma,t)}{dt}\ln P(\sigma,t) + P(\sigma,t)\frac{1}{P(\sigma,t)}\frac{dP(\sigma,t)}{dt}\right]. \tag{4.13}$$

$$\frac{dS(t)}{dt} = -\sum_{\sigma}\frac{dP(\sigma,t)}{dt}\ln P(\sigma,t) - \frac{d}{dt}\sum_{\sigma}P(\sigma,t), \tag{4.14}$$

where $\sum_\sigma P(\sigma,t) = 1$, so $\frac{d}{dt}\sum_\sigma P(\sigma,t) = 0$. Thus,

$$\Rightarrow \frac{dS(t)}{dt} = -\sum_{\sigma}\frac{dP(\sigma,t)}{dt}\ln P(\sigma,t). \tag{4.15}$$

Now, we plug the master equation and get

$$\frac{dS(t)}{dt} = -\sum_{\sigma}\sum_{i}\ln P(\sigma,t)\left[w_i(\sigma^i)P(\sigma^i,t) - w_i(\sigma)P(\sigma,t)\right]. \tag{4.16}$$

On the other hand, if we do the transformation $\sigma \to \sigma^i$, we have

$$\begin{aligned}\frac{dS(t)}{dt} &= -\sum_{\sigma}\sum_{i} \ln P(\sigma^i,t)\Big[w_i(\sigma)P(\sigma,t) - w_i(\sigma^i)P(\sigma^i,t)\Big] \\ &= \sum_{\sigma}\sum_{i} \ln P(\sigma^i,t)\Big[w_i(\sigma^i)P(\sigma^i,t) - w_i(\sigma)P(\sigma,t)\Big].\end{aligned} \tag{4.17}$$

Summing Eqs. (4.16) and (4.17) , we get

$$\frac{dS(t)}{dt} = \frac{1}{2}\sum_{\sigma}\sum_{i} \ln \frac{P(\sigma^i,t)}{P(\sigma,t)}\Big[w_i(\sigma^i)P(\sigma^i,t) - w_i(\sigma)P(\sigma,t)\Big]. \tag{4.18}$$

The rate of change of entropy has two main components:

$$\frac{dS(t)}{dt} = \Pi - \Phi, \tag{4.19}$$

where Π is the system's entropy production due to irreversible processes and Φ is the entropy flux from the system to the environment. Following the second law of thermodynamics, the entropy production Π is positive definite. On the other hand, the entropy flux can be positive or negative. Entropy production will still exist when a non-equilibrium or irreversible system achieves the stationary state. Still, the system's entropy remains constant, so entropy production is counterbalanced by the entropy flux $\Pi = \Phi > 0$.

We don't have enough equations to determine both the entropy production and the entropy flux now, but we can find a proper definition for the entropy production. In non-equilibrium thermodynamics, a natural approach is to consider a space-time description where current values determine the "action functional" governing the path space measure. The key idea is that equilibrium states have time-reversal dynamics in space-time, and currents allow this time-reversal invariance to be broken. Hence, we shall see the entropy production as a measure of the distance between the original space-time trajectory and the time-reversed one. Thus, we may define the (average) entropy production of a system as the Kullback-Leibler (KL) divergence between the forward and reversed trajectory distributions (MAES; REDIG, 2000; KULLBACK; LEIBLER, 1951)

$$\Pi = D_{\mathsf{KL}}(P^j(\omega) \parallel P^j(\theta\omega)) = \left\langle \ln \frac{P^j(\omega)}{P^j(\theta\omega)} \right\rangle_{P^j(\omega)} = \sum_{\omega} P^j(\omega) \ln \frac{P^j(\omega)}{P^j(\theta\omega)}, \tag{4.20}$$

where $P^j(\omega)$ is the probability of a trajectory ω in phase space, θ is the time-reversal operator, and the average is calculated over the original trajectories' distribution $P^j(\omega)$. Note that the relative trajectory weight must be well defined; that is, time-reversed trajectories must be possible, even though with a much smaller probability, a property known as dynamical reversibility.

Therefore, entropy production arises from breaking detailed balance in non-equilibrium processes, quantifying irreversibility.

Note that the Kullback-Leibler divergence, unlike standard metrics like Euclidean distance, is not symmetric in general: $D_{\mathsf{KL}}(P||Q) \neq D_{\mathsf{KL}}(Q||P)$, not satisfying the triangle inequality. That is because $D_{\mathsf{KL}}(P||Q)$ measures how much information is lost when using the distribution Q to approximate P, quantifying the expected number of extra bits required to code samples from a true distribution P when using a code based on an approximate distribution Q, but $D_{\mathsf{KL}}(Q||P)$ describes the opposite. Thus, the KL divergence quantifies the "distance" between distributions in terms of the inefficiency of assuming Q when the true distribution is P. That asymmetry of the Kullback-Leibler divergence is essential to measure the irreversibility between the forward and time-reversed trajectory distributions.

Additionally, from analyzing the entropy production from a single trajectory ω, the ratio of forward and reverse probabilities satisfies:

$$\Pi(\omega) = \ln \frac{P^j(\omega)}{P^j(\theta\omega)} \Rightarrow \frac{P^j(\omega)}{P^j(\theta\omega)} = e^{\Pi(\omega)}, \tag{4.21}$$

which is the Fluctuation Theorem (FT). Here, $\Pi(\omega)$ is the stochastic entropy production for a specific trajectory ω. That result implies that entropy-decreasing fluctuations (time-reversed trajectories) are exponentially suppressed compared to entropy-increasing fluctuations (forward trajectories). Therefore, even though negative entropy fluctuations can temporarily occur at the microscopic scale, entropy always tends to increase in the long run, in agreement with the Second Law of Thermodynamics. For a formal derivation of the fluctuation theorem, please see (EVANS; COHEN; MORRISS, 1993).

We remark that the entropy production definition given by Eq. (4.20) agrees with the second law of thermodynamics because Π is always non-negative. Indeed, note that $-\log(x)$ is a convex function since its second derivative is always positive. Thus, Jensen's Inequality is valid (check the appendix for a proof of Jensen's Inequality), and we have

$$\Pi = -\left\langle \ln \frac{P^j(\theta\omega)}{P^j(\omega)} \right\rangle_{P^j(\omega)} \geq -\ln \left\langle \frac{P^j(\theta\omega)}{P^j(\omega)} \right\rangle_{P^j(\omega)}, \tag{4.22}$$

where we calculate the expectation over the probability distribution $P^j(\omega)$ as

$$\left\langle \frac{P^j(\theta\omega)}{P^j(\omega)} \right\rangle_{P^j(\omega)} = \sum_{\omega} P^j(\omega) \frac{P^j(\theta\omega)}{P^j(\omega)} = \sum_{\omega} P^j(\theta\omega) = 1. \tag{4.23}$$

Therefore, it follows that $\Pi \geq 0$, under the second law of thermodynamics. Additionally, for a system in equilibrium, $P^j(\omega) = P^j(\theta\omega), \forall\omega$, so the entropy production vanishes for systems in equilibrium, as it should be.

Note that we can rewrite Eq. (4.20) in terms of transition rates between states:

$$\Pi = \sum_{i,j} P_i W_{i\to j} \ln \frac{P_i W_{i\to j}}{P_j W_{j\to i}}, \tag{4.24}$$

where P_i is the probability of the system occupying state i and $W_{i\to j}$ are transition probabilities from microscopic state i to j. Note that $P_i W_{i\to j}$ is the probability of the trajectory $i \to j$.

Hence, applying Eq. (4.24) to the majority-vote model, considering that one individual opinion can change per transition (or equivalently, one spin can flip per transition, with the parallel that spins represent opinions), the possible trajectories in phase space are from a given configuration σ to a state σ^i, with $i \in [1, N]$. Therefore, we can calculate the entropy production as

$$\Pi = \sum_{\sigma} \sum_{i} P(\sigma, t) w_i(\sigma) \ln \frac{P(\sigma, t) w_i(\sigma)}{P(\sigma^i, t) w_i(\sigma^i)}. \tag{4.25}$$

Where the sum over σ and i enables us to compute the reversibility between all possible trajectories from the configuration σ to configuration σ^i, and $P(\sigma, t)w_i(\sigma)$ is the probability of the trajectory $\sigma \to \sigma^i$. Note that the reverse trajectory $\sigma^i \to \sigma$ always exists and is possible, therefore, all time reversed trajectories are well defined.

On the other hand, if we rewrite Eq. (4.25) by doing $\sigma \to \sigma^i$, we have

$$\Pi = \sum_{\sigma} \sum_{i} P(\sigma^i, t) w_i(\sigma^i) \ln \frac{P(\sigma^i, t) w_i(\sigma^i)}{P(\sigma, t) w_i(\sigma)} = -\sum_{\sigma} \sum_{i} P(\sigma^i, t) w_i(\sigma^i) \ln \frac{P(\sigma, t) w_i(\sigma)}{P(\sigma^i, t) w_i(\sigma^i)}. \tag{4.26}$$

Thus, if we sum the Eqs. (4.25) and (4.26), we get

$$\Pi = \frac{1}{2} \sum_{\sigma} \sum_{i} \ln \frac{w_i(\sigma^i) P(\sigma^i, t)}{w_i(\sigma) P(\sigma, t)} \left[w_i(\sigma^i) P(\sigma^i, t) - w_i(\sigma) P(\sigma, t) \right]. \tag{4.27}$$

Note that this function is also nonnegative because it has the form $f(x, y) = (x - y) \ln \frac{x}{y} \geq 0, \forall x, y$ and it vanishes in the equilibrium when we have detailed balance: $w_i(\sigma^i) P(\sigma^i, t) = w_i(\sigma) P(\sigma, t)$. Combining the Equations (4.18) and (4.27), we can calculate the entropy flux:

$$\begin{aligned}
\Phi =& \frac{1}{2} \sum_{\sigma} \sum_{i} \ln \frac{w_i(\sigma^i) P(\sigma^i, t)}{w_i(\sigma) P(\sigma, t)} \left[w_i(\sigma^i) P(\sigma^i, t) - w_i(\sigma) P(\sigma, t) \right] \\
& - \frac{1}{2} \sum_{\sigma} \sum_{i} \ln \frac{P(\sigma^i, t)}{P(\sigma, t)} \left[w_i(\sigma^i) P(\sigma^i, t) - w_i(\sigma) P(\sigma, t) \right] \\
=& \frac{1}{2} \sum_{\sigma} \sum_{i} \ln \frac{w_i(\sigma^i)}{w_i(\sigma)} \left[w_i(\sigma^i) P(\sigma^i, t) - w_i(\sigma) P(\sigma, t) \right] \\
=& \frac{1}{2} \sum_{\sigma} \sum_{i} w_i(\sigma^i) P(\sigma^i, t) \ln \frac{w_i(\sigma^i)}{w_i(\sigma)} + \frac{1}{2} \sum_{\sigma} \sum_{i} w_i(\sigma) P(\sigma, t) \ln \frac{w_i(\sigma)}{w_i(\sigma^i)}.
\end{aligned} \tag{4.28}$$

We do the transformation $\sigma \to \sigma^i$ just in the left sum and get

$$\begin{aligned}\Phi &= \frac{1}{2}\sum_{\sigma}\sum_{i} w_i(\sigma)P(\sigma,t)\ln\frac{w_i(\sigma)}{w_i(\sigma^i)} + \frac{1}{2}\sum_{\sigma}\sum_{i} w_i(\sigma)P(\sigma,t)\ln\frac{w_i(\sigma)}{w_i(\sigma^i)}. \\ &= \sum_{\sigma}\sum_{i} w_i(\sigma)P(\sigma,t)\ln\frac{w_i(\sigma)}{w_i(\sigma^i)} \Longrightarrow \Phi = \left\langle \sum_{i} w_i(\sigma)\ln\frac{w_i(\sigma)}{w_i(\sigma^i)} \right\rangle .\end{aligned} \tag{4.29}$$

Therefore, we conclude that the entropy flux can be written as an average. Thus, it is possible to use Monte Carlo simulations to estimate the system's entropy flux. While, in general, it is not possible to calculate the entropy production by Monte Carlo simulations (because the expression for Π cannot be written as an average), it is possible to estimate the entropy production using such simulations for the stationary regime, because in these states $\Pi = \Phi$.

4.8 THE ORDER PARAMETER AND FINITE SIZE EFFECTS

To quantify the agreement level between individuals in a social system, we calculate the system order parameter, or magnetization M, to characterize transitions from dissent ($M = 0$) to consensus ($M = 1$). Thus, magnetization is a measure of the order of society, initially used in the context of models of magnetic spin materials, and is calculated through the equation:

$$M_L(q,\mu,f) = \left\langle \left\langle \frac{1}{N}\left|\sum_{i=1}^{N}\sigma_i\right| \right\rangle_t \right\rangle_c \equiv \langle\langle m\rangle_t\rangle_c , \tag{4.30}$$

where N is the number of individuals in the network, $\langle ...\rangle_t$ represents temporal averages made in the regime stationary and $\langle ...\rangle_c$ represents averages over different configurations of society.

Note that as this order parameter measures the agreement between individuals, the magnetization is invariant through the transformation $\sigma_i \longrightarrow -\sigma_i$. In other words, magnetization is symmetrical in terms of the inversion of the state of opinion of all sites in the network. As individuals interact with each other, the magnetization of the system changes over time until it oscillates around an equilibrium value $M_L(q)$ reached after a thermalization or relaxation time τ.

In an analogy to a magnetic system, the noise parameter q plays the role of the system temperature. The lower the social temperature q, the more ordered the system of social interactions. Hence, one can anticipate that:

1. For a zero social temperature $q = 0$, all agents will be in the same state, that is, $\sigma_i = 1$ (or -1) for all i, exhibiting an absolute consensus, where the magnetization is maximum.

2. For non-zero noise, but smaller than a given pseudo-critical value, $0 < q < q_c(N)$, the majority part of individuals will be in one of two possible states, with no total consensus, but a predominance of a given opinion. This state characterizes the ferromagnetic phase of the system. The pseudo-critical temperature $q_c(N)$ is analogous to the critical Curie temperature of a ferromagnetic material at which the system is entirely disordered.

3. Finally, for $q \geq q_c(N)$, the system exhibits the paramagnetic phase, where $M \longrightarrow 0$ in the thermodynamic limit $N \longrightarrow \infty$. On average, half of the individuals present an opinion, and the other half present an opposite opinion.

In short, with the increase in the noise value, the community evolves from an ordered state of low entropy to a disordered state of high entropy, characterizing a phase transition of the system around the pseudo critical noise $q_c(N)$, where the production of social entropy is maximum.

On the other hand, measuring the magnitude of consensus oscillations is interesting as the balance of agreement of opinions that society achieves is dynamic (since people continue to change their opinions over time). This property is investigated by the magnetization variance, called magnetic susceptibility and is given by:

$$\chi(q, \mu, f) = N \left[\langle \langle m^2 \rangle_t \rangle_c - \langle \langle m \rangle_t \rangle_c^2 \right]. \tag{4.31}$$

The susceptibility reaches its maximum value at the pseudo-critical social temperature of the system q_c. In this way, the magnetic susceptibility can be used to estimate the critical temperature of the investigated system.

Another quantity of interest is the fourth-order Binder cumulant:

$$U(q, \mu, f) = 1 - \frac{\langle \langle m^4 \rangle_t \rangle_c}{3 \langle \langle m^2 \rangle_t \rangle_c^2}. \tag{4.32}$$

The cumulant can be explored to find the phase transition point $q_c(N \to \infty) \equiv q_c$, which is independent of the system size (valid at the thermodynamic limit $N \longrightarrow \infty$), as will be explained in more detail below. Such a noise value is denoted by the only point where the different U_N curves intersect.

The magnetization and magnetic susceptibility behavior vary with the system size. In this context, it is possible to obtain a set of critical exponents that characterize the unique behavior of thermodynamic functions in the order-disorder phase transition around the critical point q_c and tell us how the system size affects these functions. In particular, when two or more distinct

systems have the same set of critical exponents, they are said to belong to the same universality class, uniting systems that are apparently very different from each other into the same group (STANLEY, 1971; YEOMANS, 1992).

Given the parameter, $\varepsilon = q - q_c$, which measures the distance to the critical point, the critical exponent λ associated with a given thermodynamic function $f(\varepsilon)$ can be defined as:

$$\lambda = \lim_{\varepsilon \to 0} \left\{ \frac{\ln |f(\varepsilon)|}{\ln |\varepsilon|} \right\}, \tag{4.33}$$

if the limit exists. In this case, the function will be:

$$f(\varepsilon) \sim |\varepsilon|^{\lambda}, \tag{4.34}$$

valid only in the limit $|\varepsilon| \to 0$, when the system is close to critical noise q_c. From the relation (4.34), it is possible to obtain scaling relations of finite size when the network is a hyperlattice of side L :

$$M_L(q) = L^{-\frac{\beta}{\nu}} \tilde{M} \left(\varepsilon L^{\frac{1}{\nu}} \right), \tag{4.35}$$

$$\chi_L(q) = L^{\frac{\gamma}{\nu}} \tilde{\chi} \left(\varepsilon L^{\frac{1}{\nu}} \right), \tag{4.36}$$

$$U_L(q) = \tilde{U} \left(\varepsilon L^{\frac{1}{\nu}} \right), \tag{4.37}$$

$$c(L) = q_c + b L^{-\frac{1}{\nu}}. \tag{4.38}$$

On the one hand, magnetization and susceptibility depend on the size of the lattice L for finite-dimensional systems. On the other hand, based on the Equations (4.35) and (4.36), when calculating M and χ in $q = q_c$ for systems of different sizes, it is possible to estimate the critical exponents β/ν and γ/ν and obtain their universal scaled forms, $\tilde{M}(\varepsilon L^{\frac{1}{\nu}})$, $\tilde{\chi}(\varepsilon L^{\frac{1}{\nu}})$ and $\tilde{U}(\varepsilon L^{\frac{1}{\nu}})$ which are independent of the size of the simulated network. However, the critical exponent associated with the fourth-order Binder cumulant is zero. Therefore, for $|\varepsilon| = 0$, we have that:

$$U_L(q = q_c) = U(q = q_c) = \tilde{U}(0). \tag{4.39}$$

This property makes it possible to find the universal critical noise in the thermodynamic limit at the intersection of several U_L curves. That yields more accurate estimates of the critical point q_c than simply identifying the pseudo-critical noise of a very large system that can be reasonably numerically simulated, given the constraints of finite resources and time.

By deriving Eq. (4.37) under the condition that $|\varepsilon| = 0$ produces an equation that can be exploited to investigate the third critical exponent $1/\nu$

$$U'_L(q = q_c) = L^{\frac{1}{\nu}} \tilde{U}(0). \tag{4.40}$$

Also, using the Equations (4.35), (4.36) and (4.37), we can obtain a relationship between the critical exponents and the hyperlattice's dimension:

$$\frac{2\beta + \gamma}{\nu} = d, \tag{4.41}$$

known as the hyperscaling relation. The majority-vote model does not have second-order phase transitions for dimensions below the lower critical dimension. For example, the model does not exhibit a phase transition in one dimension. There is also an upper critical dimension, where the system's behavior is known to be indistinguishable from the results predicted by mean-field theory (which we will explore in detail below). Hence, the hyperscaling relation is valid only for critical systems with dimensions between the lower and the upper critical dimension (HONG; HA; PARK, 2007).

However, for systems with complex interaction structures, the concept of network dimension is unclear. After all, these non-trivial topologies do not have a clear definition of linear size L. Thus, a volumetric scaling with the number of individuals/spins/nodes of the correlation length near criticality is often assumed, instead of the linear correlation we used above $\xi \sim L$ (HONG; HA; PARK, 2007; VILELA et al., 2020)

$$\xi \sim N. \tag{4.42}$$

Under this assumption, the finite-size scaling equations now have the following form:

$$M_L(q) = N^{-\beta/\bar{\nu}} \tilde{M}(\varepsilon N^{1/\bar{\nu}}), \tag{4.43}$$

$$\chi_N(q) = N^{\gamma/\bar{\nu}} \tilde{\chi}(\varepsilon N^{1/\bar{\nu}}), \tag{4.44}$$

$$U_L(q) = \tilde{U}(\varepsilon N^{1/\bar{\nu}}), \tag{4.45}$$

$$q_c(N) = q_c + bN^{-1/\bar{\nu}}. \tag{4.46}$$

In which we use $\bar{\nu}$ instead of ν since we now assume a volumetric scaling for the correlation length. That emphasizes that the values of these critical exponents are different than the ones following a linear scaling.

Note that for a regular lattice in d dimensions, $N = L^d$. Then, the finite-size scaling relations for the magnetization and magnetic susceptibility are given by:

$$M_L(q) = L^{-d\beta/\bar{\nu}} \tilde{M}(\varepsilon N^{1/\bar{\nu}}), \tag{4.47}$$

$$\chi_N(q) = L^{d\gamma/\bar{\nu}} \tilde{\chi}(\varepsilon N^{1/\bar{\nu}}). \tag{4.48}$$

Therefore, the hyper-scaling relation becomes:

$$2d\frac{\beta}{\bar{\nu}} + d\frac{\gamma}{\bar{\nu}} = d, \tag{4.49}$$

or

$$2\frac{\beta}{\bar{\nu}} + \frac{\gamma}{\bar{\nu}} \equiv \upsilon = 1, \tag{4.50}$$

known as the unitary relation for critical exponents. Therefore, using the volumetric hyper-scaling relation for regular lattices cannot estimate the network's dimension. The unitary conjecture states that under the volumetric scaling $\xi \sim N$, the exponent $\upsilon = 1$ is valid for any network. This conjecture has already been verified for several regular and complex networks, and we also verify the validity of this conjecture for the affinity-based scale-free networks in this work. Although the unitary relation cannot be used to estimate the network dimension, the unitary relation can serve as a test of the criticality of systems with regular and complex interaction topologies to verify the values of the estimated critical exponents (VILELA et al., 2020).

4.9 MEAN-FIELD APPROACH

4.9.1 Order Parameter

We can obtain an approximate analytical solution for the order parameter and the entropy flux (which is also the entropy production in the stationary state) as a function of social noise for the majority-vote model using a mean-field approximation. In this approximation, we consider that each individual interacts with all the other agents of the society, corresponding to a mean-field limit.

We denote a given configuration of the society as $\sigma = (\sigma_1, \sigma_2, ..., \sigma_i, ..., \sigma_N)$, where the first agent has opinion σ_1, the second σ_2, and so on. Let us derive the behavior of the stationary magnetization m:

$$\frac{dm}{dt} = \frac{d}{dt}\left(\frac{1}{N}\sum_{i=1}^{N}\sigma_i\right) = \frac{d}{dt}\langle\sigma_i\rangle = \frac{d}{dt}\left[\sigma_i P(\sigma_i, t) + (-\sigma_i)P(-\sigma_i, t)\right], \tag{4.51}$$

where $P(\sigma_i, t)$ is the probability of finding a single agent i with opinion σ_i. Hence,

$$\frac{dm}{dt} = \sigma_i\frac{d}{dt}P(\sigma_i, t) - \sigma_i\frac{d}{dt}P(-\sigma_i, t). \tag{4.52}$$

Consider $w_i(\sigma)$ to be the transition probability from an agent i with opinion σ_i. Therefore, using the master equation for $P(\sigma_i, t)$ and $P(-\sigma_i, t)$, we get

$$\begin{aligned}\frac{dm}{dt} &= \sigma_i \left[P(-\sigma_i, t)w_i(-\sigma_i) - P(\sigma_i, t)w_i(\sigma)\right] - \sigma_i \left[P(\sigma_i, t)w_i(\sigma) - P(-\sigma_i, t)w_i(-\sigma_i)\right] \\ &= -2\left[\sigma_i P(\sigma_i, t)w_i(\sigma) - \sigma_i P(-\sigma_i, t)w_i(-\sigma_i)\right].\end{aligned} \tag{4.53}$$

Thus,

$$\frac{dm}{dt} = \frac{d\langle\sigma_i\rangle}{dt} = -2\left\langle\sigma_i w_i(\sigma)\right\rangle. \tag{4.54}$$

That is the general equation governing the time evolution of the order parameter. Using the transition probability of the cooperative majority-vote model, where a fraction f of the agents are cooperative (the solution to the standard majority-vote dynamics can be obtained by considering $\mu_i = 1$, $\forall i$, or $f = 0$):

$$w_i(\sigma) = \frac{1}{2}\left[1 - (1 - 2\mu_i q)\sigma_i S\left(\sum_\delta \sigma_{j+\delta}\right)\right], \tag{4.55}$$

it follows that, for all Nf cooperative individuals with $\mu_j = \mu$, we get the following set of equations

$$\frac{d}{dt}\left\langle\sigma_j\right\rangle = -\left\langle\sigma_j\right\rangle + \Theta_\mu \left\langle S\left(\sum_\delta \sigma_{j+\delta}\right)\right\rangle, \tag{4.56}$$

for $j = 1, 2, ..., Nf$, where we used $\sigma_j^2 = 1$, $\forall j$, and we define $\Theta_\mu = 1 - 2\mu q$. Similarly, for the remaining $N(1-f)$ agents with $\mu_k = 1$, we have

$$\frac{d}{dt}\left\langle\sigma_k\right\rangle = -\left\langle\sigma_k\right\rangle + \Theta \left\langle S\left(\sum_\delta \sigma_{k+\delta}\right)\right\rangle, \tag{4.57}$$

where $\Theta = 1 - 2q$ and $k = Nf + 1, Nf + 2, ..., N$. Adding Equations (4.56) and (4.57) for all agents, we obtain an equation describing the entire system

$$\sum_{i=1}^{N} \frac{d}{dt}\left\langle\sigma_i\right\rangle = -\sum_{i=1}^{N}\left\langle\sigma_i\right\rangle + N\left[f\Theta_\mu + (1-f)\Theta\right]\left\langle S\left(\sum_\delta \sigma_{i+\delta}\right)\right\rangle. \tag{4.58}$$

We can write the signal function $S\left(\sum_\delta \sigma_\delta\right)$ as an expansion in terms of products of σ_δ in the following form:

$$S(\sigma_1 + \cdots + \sigma_g) = a_1(\sigma_1 + \cdots + \sigma_g) + a_2(\sigma_1\sigma_2 + \cdots + \sigma_{g-1}\sigma_g) + \ldots a_g(\sigma_1\sigma_2 \ldots \sigma_g), \tag{4.59}$$

where g is the number of neighbors of the central node i being considered. That is a cumulant series, a common method in statistical mechanics to capture correlations between variables at different orders. In this context, the first cumulant (a_1) represents linear contributions,

equivalent to the mean interaction across the neighbors. The second cumulant (a_2) captures non-linear correlations between pairs of individuals, and higher-order cumulants measure higher-order correlations.

By choosing values for each of the spins $\sigma_1 = \pm 1, \ldots, \sigma_g = \pm 1$, and calculating $S(\sigma_1 + \cdots + \sigma_g)$, we get a set of linear equations that we can solve to find the value of the cumulants $a_1, \ldots, a_g$. In particular, by exploiting a given configuration $\sigma_1 = \pm 1, \ldots, \sigma_g = \pm 1$ and applying the transformation $\sigma_i \to -\sigma_i, \forall i$, we conclude that all even cumulants are zero. Hence, the expansion reduces to

$$S(\sigma_1 + \cdots + \sigma_g) = a_1(\sigma_1 + \cdots + \sigma_g) + a_3(\sigma_1\sigma_2\sigma_3 + \cdots + \sigma_{g-2}\sigma_{g-1}\sigma_g) + \ldots \tag{4.60}$$

As we simulate the cooperative majority-vote model on the square lattice, in the mean-field approach, this corresponds to considering that each agent i interacts with four randomly selected neighbors that we label as a, b, c and d. In that case,

$$S\left(\sum_{\delta} \sigma_{i+\delta}\right) = S(\sigma_a + \sigma_b + \sigma_c + \sigma_d) =$$
$$a_1(\sigma_a + \sigma_b + \sigma_c + \sigma_d) + a_3(\sigma_a\sigma_b\sigma_c + \sigma_a\sigma_b\sigma_d + \sigma_a\sigma_c\sigma_d + \sigma_b\sigma_c\sigma_d).$$

Consider the case $\sigma_a = \sigma_b = \sigma_c = \sigma_d = 1$, so the cumulants must satisfy

$$4(a_1 + a_3) = 1. \tag{4.61}$$

Now, if $\sigma_a = \sigma_b = \sigma_c = 1$ but $\sigma_d = -1$, we have

$$2(a_1 - a_3) = 1. \tag{4.62}$$

Hence, $a_1 = 3/8$ and $a_3 = -1/8$. That is,

$$S(\sigma_a + \sigma_b + \sigma_c + \sigma_d) = \frac{3}{8}(\sigma_a + \sigma_b + \sigma_c + \sigma_d) - \frac{1}{8}(\sigma_a\sigma_b\sigma_c + \sigma_a\sigma_b\sigma_d + \sigma_a\sigma_c\sigma_d + \sigma_b\sigma_c\sigma_d).$$

In the mean-field approximation, we consider $\langle \sigma_l\sigma_u\sigma_v \rangle \approx \langle \sigma_l \rangle \langle \sigma_u \rangle \langle \sigma_v \rangle \approx m^3$. Thus, we write

$$\left\langle S\left(\sum_{\delta} \sigma_{i+\delta}\right)\right\rangle = \frac{m}{2}(3 - m^2). \tag{4.63}$$

By using this result in Eq. (4.58), we obtain a differential equation for the order parameter

$$\frac{d}{dt}m = -\epsilon m + \zeta m^3, \tag{4.64}$$

where

$$\epsilon = 1 - \frac{3}{2}\left[f\Theta_\mu + (1-f)\Theta\right], \; \zeta = -\frac{1}{2}\left[f\Theta_\mu + (1-f)\Theta\right]. \tag{4.65}$$

Multiplying both sides of the equation by m

$$\frac{1}{2}\frac{d}{dt}m^2 = -\epsilon m^2 + \zeta m^4, \tag{4.66}$$

which is a first-order separable differential equation for the variable $\eta = m^2$. Therefore, by separating variables:

$$\frac{1}{2\eta(\epsilon - \eta\zeta)}\, d\eta = -dt. \tag{4.67}$$

Integrating both sides of the equation and considering the initial condition $t = 0$ and $\eta(0) = m^2(0) = m_0^2$, we obtain

$$\ln\left[\frac{\eta/\eta_0}{(\epsilon - \zeta\eta)/(\epsilon - \zeta\eta_0)}\right] = -2\epsilon t. \tag{4.68}$$

Thus, substituting back $\eta = m^2$, $\eta_0 = m_0^2$ and solving the quadratic equation, we get

$$m(t) = \pm m_0\sqrt{\frac{\epsilon}{(\epsilon - \zeta m_0^2)e^{2\epsilon t} + m_0^2\zeta}}. \tag{4.69}$$

The Eq. (4.69) provides the temporal value of the system's order parameter. We are particularly interested in the stationary solution, which we can obtain by taking the limit $t \to \infty$. Then, if $\epsilon > 0$, we obtain the paramagnetic or disordered solution:

$$m = 0. \tag{4.70}$$

On the other hand, for $\epsilon < 0$, we obtain the ferromagnetic state (ordered) solution:

$$m = \pm\sqrt{\frac{\epsilon}{\zeta}} = \pm\sqrt{\frac{2\,|\epsilon|}{f\Theta_\mu + (1-f)\Theta}}, \tag{4.71}$$

where we used Eq. (4.65). Substituting ϵ, $\Theta_\mu = 1 - 2\mu q$, and $\Theta = 1 - 2q$, we obtain the stationary ordered solution as a function of the main model parameters:

$$m = \pm\sqrt{\frac{1 - 6q\left[1 - f\left(1-\mu\right)\right]}{1 - 2q\left[1 - f\left(1-\mu\right)\right]}} \equiv \pm\sqrt{\frac{1-6\bar{q}}{1-2\bar{q}}}, \tag{4.72}$$

with $\bar{q} = \bar{\mu}q = q[(1 - f(1-\mu)]$ is the average social noise value. Imposing $m = 0$, we obtain the critical social noise:

$$q_c(\mu, f) = \frac{1}{6\left[1 - f\left(1-\mu\right)\right]}. \tag{4.73}$$

In this case, note that $\epsilon > 0$ corresponds to $q > q_c$ and $\epsilon > 0$ to $q < q_c$ so that Eqs. (4.70) and (4.72) are valid for $q > q_c$ and $q < q_c$, respectively.

Note that when $f = 0$, Eq. (4.72) yields the standard mean-field result for m

$$m = \pm\sqrt{\frac{1-6q}{1-2q}}, \tag{4.74}$$

with $q_c = 1/6$ for the critical noise in the mean-field limit (CROKIDAKIS; OLIVEIRA, 2012; CROCHIK; TOMÉ, 2005). For $f = 1$, $q_c = 1/6\mu$ as expected because everyone is cooperative, the system is the standard model with $q \to q/\mu$.

Figure 11 – Mean-field solution of the order parameter as a function of the average social noise. Here, full lines correspond to stable solutions, and dashed lines correspond to unstable stationary solutions. The black dot where the blue and red curves meet highlights the critical social noise point.

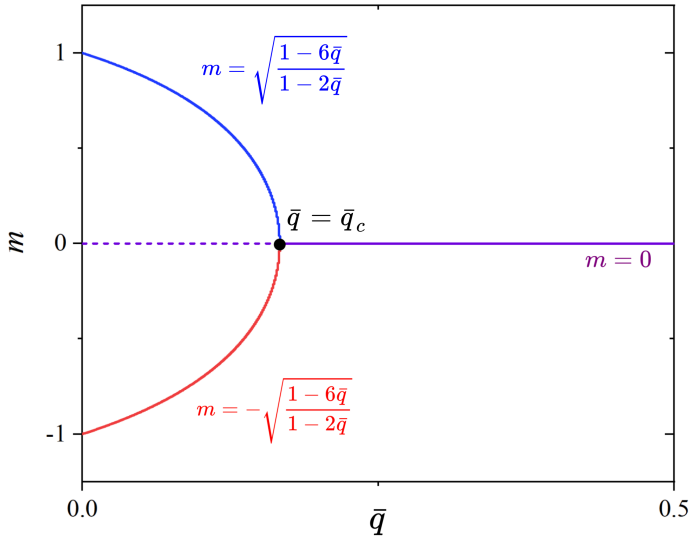

Source: Author.

Near the phase transition where $q = q_c + \Delta q$ we know that $m \sim (|q - q_c|)^\beta$. in this case, expanding Eq. (4.72) in a Taylor series around $\Delta q = 0$, we find:

$$m \approx \pm 3\sqrt{\Delta q}\sqrt{f(1-\mu) - 1} + \mathcal{O}(\Delta q^{3/2}). \tag{4.75}$$

Thus, we have the mean-field exponent $\beta = 1/2$, indicating that the model belongs to the mean-field Ising universality class.

For confirmation, note that the three stationary solutions given by Eqs. (4.72) and (4.70) can also be obtained by imposing $dm/dt = 0$ in Eq.(4.64). Note, however, that for $q < q_c$, the $m = 0$ solution is unstable, while the ordered solutions given by Eq. (4.72) are imaginary to $q > q_c$. That is, we can represent the order parameter solutions in a bifurcation diagram as shown in Fig. 11. For $\bar{q} > \bar{q}_c$, we have a horizontal purple stable solution at $m = 0$, indicating a symmetric state where the order parameter is zero. Then, at $\bar{q} = \bar{q}_c$, marked by the black dot, a bifurcation/phase transition occurs, where the system exhibits symmetry breaking, displaying either an excess of $+1$ opinions (blue solution) or -1 opinions (red curve). These two symmetric branches became stable for $\bar{q} < \bar{q}_c$, and the purple solution became unstable

(represented in dashed lines). That characterizes a Supercritical Pitchfork Bifurcation because, at the critical point, the system undergoes a transition where the single symmetric solution loses stability, and symmetry breaking occurs (STROGATZ, 2018).

4.9.2 Entropy Production

In this section, we use the mean-field formulation to develop an analytical expression for the entropy flux in the stationary regime. The idea is to develop Eq. (4.29). To do that, we use Eq. (4.55) to calculate

$$\ln\frac{w_i(\sigma)}{w_i(\sigma^i)} = \ln\left[\frac{1-\sigma_i S\left(\sum_\delta \sigma_{i+\delta}\right)+2\mu_i q\sigma_i S\left(\sum_\delta \sigma_{i+\delta}\right)}{1+\sigma_i S\left(\sum_\delta \sigma_{i+\delta}\right)-2\mu_i q\sigma_i S\left(\sum_\delta \sigma_{i+\delta}\right)}\right]. \tag{4.76}$$

Note that the product $\sigma_i S\left(\sum_\delta \sigma_{i+\delta}\right)$ may assume only three possible values: $-1, 0$ and 1. Therefore,

$$\ln\frac{w_i(\sigma)}{w_i(\sigma^i)} = \begin{cases} \ln\left(\frac{\mu_i q}{1-\mu_i q}\right)\times 1, & \text{if } \sigma_i S\left(\sum_\delta \sigma_{i+\delta}\right)=1, \\ \ln\left(\frac{\mu_i q}{1-\mu_i q}\right)\times 0, & \text{if } \sigma_i S\left(\sum_\delta \sigma_{i+\delta}\right)=0, \\ \ln\left(\frac{\mu_i q}{1-\mu_i q}\right)\times -1, & \text{if } \sigma_i S\left(\sum_\delta \sigma_{i+\delta}\right)=-1. \end{cases} \tag{4.77}$$

Hence, one can write that

$$\ln\frac{w_i(\sigma)}{w_i(\sigma^i)} = \ln\left[\frac{\mu_i q}{1-\mu_i q}\right]\sigma_i S\left(\sum_\delta \sigma_{i+\delta}\right). \tag{4.78}$$

Thus, we can apply that to the entropy flux equation (Eq. (4.29)):

$$\Phi = \left\langle \sum_i w_i(\sigma)\ln\frac{w_i(\sigma)}{w_i(\sigma^i)}\right\rangle. \tag{4.79}$$

Separating the sum between cooperative and regular agents, we get

$$\Phi = \sum_{j=1}^{Nf}\left\langle \ln\left[\frac{\mu q}{1-\mu q}\right]\sigma_j S\left(\sum_\delta \sigma_{j+\delta}\right)w_j(\sigma)\right\rangle + \sum_{k=Nf+1}^{N}\left\langle \ln\left[\frac{q}{1-q}\right]\sigma_k S\left(\sum_\delta \sigma_{k+\delta}\right)w_k(\sigma)\right\rangle.$$

Thus, substituting the equation for the transition probability, we get

$$\begin{aligned}\Phi = &\frac{Nf}{2}\ln\left[\frac{\mu q}{1-\mu q}\right]\left[\langle\sigma_i\rangle\langle S\left(\sum_\delta \sigma_{j+\delta}\right)\rangle - \Theta_\mu\langle S^2\left(\sum_\delta \sigma_{j+\delta}\right)\rangle\right] + \\ &\frac{N(1-f)}{2}\ln\left[\frac{q}{1-q}\right]\left[\langle\sigma_i\rangle\langle S\left(\sum_\delta \sigma_{j+\delta}\right)\rangle - \Theta\langle S^2\left(\sum_\delta \sigma_{j+\delta}\right)\rangle\right].\end{aligned} \tag{4.80}$$

Squaring Eq.(4.63) and using the property $\sigma_a^2 = \sigma_b^2 = \sigma_c^2 = \sigma_d^2 = 1$, we get

$$\begin{aligned}\left[S\left(\sum_{\delta}\sigma_{j+\delta}\right)\right]^2 =& \frac{1}{32}\left(\sigma_b\sigma_c + \sigma_b\sigma_d + \sigma_c\sigma_d + \sigma_a\sigma_b + \sigma_a\sigma_c + \sigma_a\sigma_d\right) - \frac{3}{8}\sigma_a\sigma_b\sigma_c\sigma_d \\ &- \frac{3}{16}\left(\sigma_b\sigma_c + \sigma_a\sigma_b + \sigma_a\sigma_c + \sigma_b\sigma_d + \sigma_c\sigma_d + \sigma_a\sigma_d\right) + \frac{5}{8} \\ &+ \frac{9}{32}\left(\sigma_a\sigma_b + \sigma_a\sigma_d + \sigma_a\sigma_c + \sigma_c\sigma_d + \sigma_c\sigma_d + \sigma_b\sigma_d\right).\end{aligned}$$

Thus, we use the approximation $\langle\sigma_u\sigma_v\rangle \approx \langle\sigma_u\rangle\langle\sigma_v\rangle \approx m^2$ and calculate the average value of the square of the signal function of the social interactions:

$$\left\langle\left[S\left(\sum_{\delta}\sigma_{j+\delta}\right)\right]^2\right\rangle = \frac{1}{8}\left(5 + 6m^2 - 3m^4\right). \tag{4.81}$$

Now we divide Eq. (4.80) by the total number N of agents and combine it with equations (4.63) and (4.81) and derive an expression for the entropy flux per site φ:

$$\begin{aligned}\varphi \equiv \Phi/N = f\ \ln\left(\frac{\mu q}{1-\mu q}\right) \times \left[\frac{1}{4}(3m^2 - m^4) - \frac{\Theta_\mu}{16}(5 + 6m^2 - 3m^4)\right] + \\ +(1-f)\ \ln\left(\frac{q}{1-q}\right) \times \left[\frac{1}{4}(3m^2 - m^4) - \frac{\Theta}{16}(5 + 6m^2 - 3m^4)\right].\end{aligned} \tag{4.82}$$

That is the general equation for the entropy flux as a function of the order parameter. We get the temporal value of the entropy flux by substituting the temporal value of the magnetization given by Eq. (4.69). Thus, we obtain

$$\begin{aligned}\varphi(t) = f\ln\left(\frac{\mu q}{1-\mu q}\right)\left[\frac{1}{\xi(t)}\left(\frac{3m_0^2\epsilon}{4} - \frac{6m_0^2\epsilon\Theta_\mu}{16}\right) - \frac{1}{\xi^2(t)}\left(\frac{m_0^4\epsilon^2}{4} - \frac{3m_0^4\epsilon^2\Theta_\mu}{16}\right) - \frac{\Theta_\mu}{16}5\right] \\ + (1-f)\ln\left(\frac{q}{1-q}\right)\left[\frac{1}{\xi(t)}\left(\frac{3m_0^2\epsilon}{4} - \frac{6m_0^2\epsilon\Theta}{16}\right) - \frac{1}{\xi^2(t)}\left(\frac{m_0^4\epsilon^2}{4} - \frac{3m_0^4\epsilon^2\Theta}{16}\right) - \frac{\Theta}{16}5\right],\end{aligned} \tag{4.83}$$

where $\xi(t) = (\epsilon - \zeta m_0^2)e^{2\epsilon t} + m_0^2\zeta$. Therefore, to obtain the stationary entropy flux, we can either take the limit $t \to \infty$ in Eq. (4.83), where the disordered (ordered) solution is given by $\epsilon > 0$ ($\epsilon < 0$), or just set $m = 0$ (use Eq. (4.72)). Thus, the stationary disordered solution of the entropy flux, valid for $q > q_c(\mu, f)$ is given by:

$$\varphi = \frac{5}{16}f\Theta_\mu\ \ln\left(\frac{1-\mu q}{\mu q}\right) + \frac{5}{16}(1-f)\Theta\ \ln\left(\frac{1-q}{q}\right). \tag{4.84}$$

For $q < q_c(\mu, f)$ (or $\epsilon < 0$), we get the entropy flux for the ordered/ferromagnetic state of the system:

$$\begin{aligned}\varphi = \frac{f}{(1-2\bar{q})^2}\ \ln\left(\frac{1-\mu q}{\mu q}\right)\left\{\bar{q}\left[3 - \Theta_\mu(2+\bar{q})\right] - \mu q\right\} \\ + \frac{1-f}{(1-2\bar{q})^2}\ \ln\left(\frac{1-q}{q}\right)\left\{\bar{q}\left[3 - \Theta(2+\bar{q})\right] - q\right\}.\end{aligned} \tag{4.85}$$

We remark that in the stationary state, the entropy flux is equal to the entropy production. Hence, these equations also enable us to calculate the entropy production per particle.

In particular, for the special case of $f = 0.0$, we combine Equations (4.84) and (4.85) to obtain the expression of the entropy production of the standard majority-vote model:

$$\varphi(q) = \left(\frac{q}{1-2q}\right)^2 (3+2q)\ \ln\left(\frac{1-q}{q}\right) H(q_c - q) + \frac{5}{16}(1-2q)\ \ln\left(\frac{1-q}{q}\right) H(q-q_c), \quad (4.86)$$

where $H(t)$ is the Heaviside function and $q_c(\mu, f = 0.0) \equiv q_c = 0.075$ is the critical noise of the isotropic majority-vote model.

4.10 MAJORITY-VOTE MONTE CARLO ALGORITHM

We display in the Algorithm 1 the computational steps to simulate the majority-vote model using the Monte Carlo Method. Note that the numerical quantities still vary in the stationary regime. Hence, we average over time and over different initial configurations and networks to obtain a statistically consistent physical result. As we are simulating finite-size systems over different temperatures, these constraints may drive the system to non-stationary configurations under the time window analyzed, leading to the possibility of non-ergodic behavior, where the system gets trapped in specific configurations for long periods. For example, in critical slowing down phenomena, the correlation length diverges as the system approaches the critical point so that the transition of a single agent impacts a larger region due to the increased correlation length, and the system takes longer to explore the whole configuration space and reach equilibrium after a single perturbation.

In this way, Monte Carlo simulations of the majority-vote model and similar ones like the Ising model rely on averaging over a finite time and different initial configurations to reduce the effects and the possibility of trapped realizations, thus enhancing ergodicity. If the simulation happens on a regular network, such as the square lattice, generating and sampling over several networks is unnecessary. However, it is still possible to simulate different samples and average them. As the system is stochastic, even simulating the same system with the same initial condition on the same network several times can lead to different results.

Algorithm 1 Monte Carlo Simulation for the majority-vote model

1: Initialize the system:
   - Create a network with N nodes.
   - Assign spins $\sigma_i \in \{-1, +1\}$ based on M_0.
2: Define parameters: q, τ, N_{steps}, t_{skip}, N_{samples} and N_{networks}.
3: Initialize accumulators: $m \leftarrow 0$, $m_2 \leftarrow 0$, $m_4 \leftarrow 0$ and $s \leftarrow 0$.
4: **for** Network $= 1$ to N_{networks} **do**
5: **for** Sample $= 1$ to N_{samples} **do**
6: **for** $t = 1$ to τ **do** ▷ Relaxation (thermalization)
7: **for** $i \in$ network nodes **do**
8: Compute majority opinion:

$$S_{\text{majority}} = \text{sign}\left(\sum_{\text{neighbors } j} \sigma_j\right)$$

9: Compute flip probability:

$$w = \frac{1}{2}\left[1 - (1 - 2q)\sigma_i S_{\text{majority}}\right]$$

10: Generate random $r \in [0, 1)$.
11: **if** $r < w$ **then**
12: Flip spin: $\sigma_i \leftarrow -\sigma_i$.
13: **end if**
14: **end for**
15: **end for**
16: **for** $t = 1$ to N_{steps} **do** ▷ Monte Carlo steps
17: **for** $i \in$ network nodes **do**
18: Compute w and generate r.
19: **if** $r < w$ **then**
20: Flip spin: $\sigma_i \leftarrow -\sigma_i$.
21: **end if**
22: **end for**
23: **if** $t \mod t_{\text{skip}} = 0$ **then**
24: Compute magnetization and entropy flux:

$$m(t) = \frac{1}{N}\left|\sum_{i=1}^{N} \sigma_i\right|, \quad s(t) = \frac{1}{N}\sum_{i=1}^{N} \ln\frac{q_i}{1 - q_i}\sigma_i S_{\text{majority}} w_i$$

25: Accumulate moments:

$$m \leftarrow m + m(t), \quad m_2 \leftarrow m_2 + m(t)^2, \quad m_4 \leftarrow m_4 + m(t)^4, \quad s \leftarrow s + s(t)$$

26: **end if**
27: **end for**
28: **end for**
29: **end for**
30: Compute averages:

$$m \leftarrow \frac{m}{N_{measurements}}, \quad m_2 \leftarrow \frac{m_2}{N_{measurements}}, \quad m_4 \leftarrow \frac{m_4}{N_{measurements}}, \quad s \leftarrow \frac{s}{N_{measurements}}$$

where

$$N_{measurements} = N_{\text{steps}}/t_{\text{skip}}/N_{networks}/N_{samples}.$$

31: Compute thermodynamical functions:

$$M = m, \quad X = N \cdot [m_2 - m^2], \quad U = 1 - \frac{m_4}{3 \cdot m_2^2}, \quad S = s$$

5 COOPERATIVE MAJORITY-VOTE MODEL RESULTS

This chapter explores the effects of collaborative dynamics on the majority-vote model in regular square lattice networks for the order parameter and the entropy flux. We also discuss the results using mean-field simulations and compare them to the mean-field analytical solutions.

5.1 SQUARE LATTICE SOCIAL NETWORKS

We employ Monte Carlo simulations on square lattices with side L ranging from 40 to 200, so the total number of agents is $N = L^2$. Note that a Monte Carlo step (MCS) corresponds to the trial of updating N individuals randomly chosen accordingly to Eq. 4.55 (hence, the same agent may be selected more than one time). Next, we wait 2×10^4 MCS to allow the system to reach the steady state, and we take the time averages of the thermodynamical functions over the next 10^5 MCS. We repeat the process up to 100 independent samples to calculate configurational averages. The procedure is described in detail in the algorithm 1. In this system, a fraction f of the agents are cooperative, and we select a random subset of the society to be collaborative individuals.

Figure 12 – Cooperative majority-vote model in the square lattice with $L = 200$, $\mu = 0.5$ and several values of the fraction of cooperative agents f. Here we exhibit the social temperature dependence of (a) the order parameter $M_L(q, \mu, f)$, (b) the susceptibility $\chi_L(q, \mu, f)$ and (c) Binder cumulant $U_L(q, \mu, f)$. From left to right, we vary f from 0.0 to 1.0 with an increment of $\Delta f = 0.1$. The lines are just guides to the eyes.

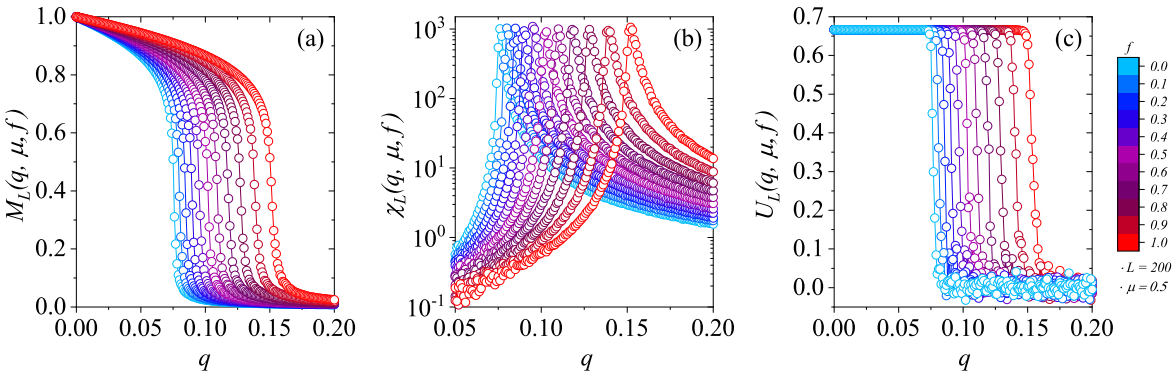

Source: Author.

Figure 12 shows how the fraction f of cooperative individuals with noise attenuation $\mu = 0.5$ affects the society. In this case, the collaborative agents have a 50% increased chance of

agreeing with most of their social connections. We plot (a) the magnetization/order parameter $M_L(q, \mu, f)$, (b) the variance of the order parameter/magnetic susceptibility $\chi_L(q, \mu, f)$, and (c) the Binder cumulant $U_L(q, \mu, f)$ versus the social temperature q, for $L = 200$ and several values of the cooperative fraction. Note that for small noise parameter values q, $M(q, \mu, f) = O(1)$ indicates the ordered phase of the social system, where one opinion is dominant in society.

Figure 13 – Snapshots of the simulation on a square network of size $L = 150$ with social temperature fixed at $q = 0.075$ and noise tolerance $\mu = 0.5$. In this result, the white (black) dots stand for $+1$ (-1). We vary the cooperative fraction from (a) $f = 0.00$, (b) $f = 0.20$, (c) $f = 0.50$, and (d) $f = 1.00$. Here, we observe that f promotes consensus of the social system.

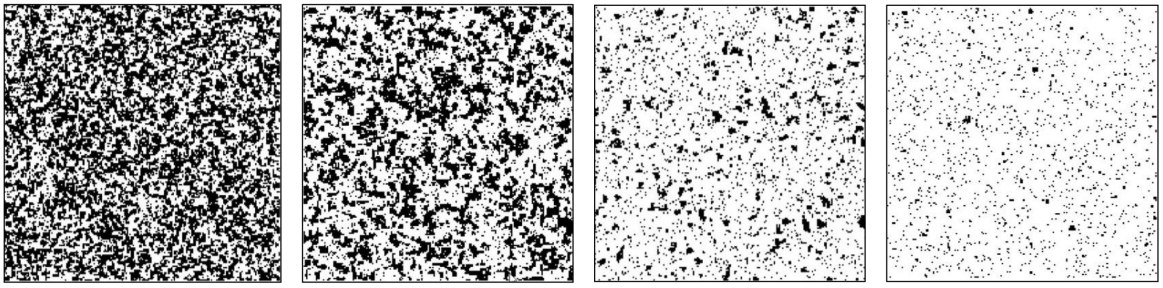

Source: Author.

By increasing the social temperature q, $M_L(q, \mu, f)$ continuously decreases to zero for all values of the cooperative fraction f. However, systems with more cooperative agents display higher robustness to the social noise, requiring higher values of q so that the order parameter vanishes. Additionally, the order parameter does not decay regularly with q. Still, the system undergoes a second-order phase transition near a critical temperature $q_c(\mu, f)$, where the magnetization goes to zero continuously, the magnetic susceptibility $\chi_L(q, \mu, f)$ exhibits a maximum and the Binder cumulant $U_L(q, \mu, f)$ decreases swiftly. When $M_L(q, \mu, f) \sim 0$, the two different opinions are found with the same probability on average, characterizing a dissent.

We can visually analyze the same process represented in Figure 12 in Figure 13 where we show the snapshots of simulations for the model with noise fixed at $q = 0.075$ and $\mu = 0.5$. White (black) represents $+1$ (-1) opinion. Note that the giant white cluster contains a large portion of individuals with opinion $+1$, and it grows with f, indicating how f promotes the social order when there is a cooperative influence on the society, i.e., $\mu < 1$.

We can also see that in Figure 14, where we continuously vary the cooperative fraction f to improve the order for a square lattice with $L = 200$ and $q = 0.08, 0.09, 0.10, 0.11, 0.12$ and

Figure 14 – Disorder-order transitions as a function of the cooperative fraction f for fixed q, with system size $L = 200$ and $\mu = 0.5$. In this figure, (a), (b), and (c) represent the magnetization, susceptibility, and Binder cumulant, respectively. From left to right, $q = 0.08, 0.09, 0.10, 0.11, 0.12$, and 0.14. In (a), we also plot $q = 0.0$ (pink) and $q = 0.3$ (wine). The lines are guides to the eyes.

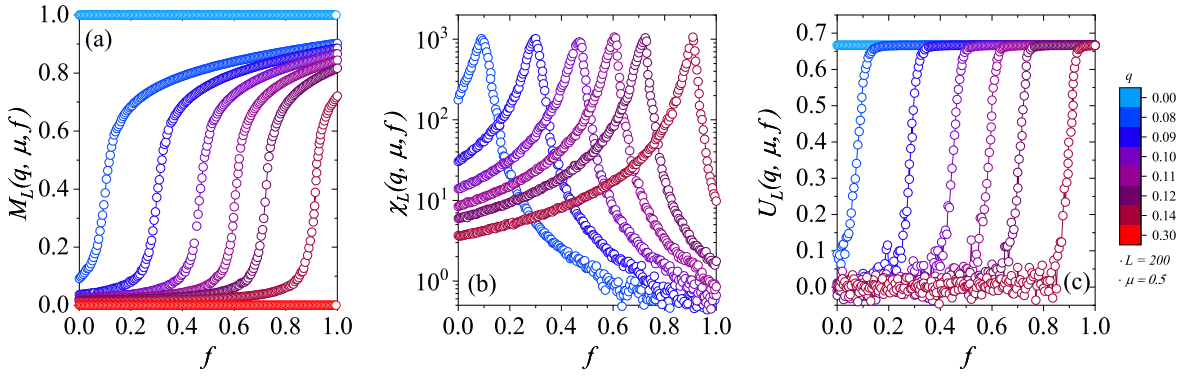

Source: Author.

0.14 (from left to right). Note the system undergoes a disorder-order transition for intermediate values of q with the collaborative fraction. However, sufficiently low (high) social temperatures suppress the phase transitions, and the community is ordered (disordered) regardless of the cooperative fraction f value. We highlight this effect in Fig. 14(a), where we use $q = 0$ (blue) and $q = 0.3$ (red symbols).

Similarly, in Figure 15, we analyze how different intensities of the cooperative behavior phenomena μ affect the society's consensus when half of the community is collaborative $f = 0.5$. We investigate the behavior of (a) the magnetization $M_L(q, \mu, f)$, (b) the susceptibility $\chi_L(q, \mu, f)$, and (c) the Binder cumulant $U_L(q, \mu, f)$ as a function of the social noise q, for $L = 200$ and diverse values of the noise sensitivity μ. The decrease in the μ value stimulates the individuals to cooperate, thus reinforcing society's robustness to disorder, even if the number of cooperative agents does not change. Indeed, cooperative agents impact their social contacts, which also influence their social contacts and so on, in a chain effect. Therefore, the influence of the collaborative agents can propagate over the entire network. We conclude that $q_c(\mu, f)$ is a monotonically decreasing function of the noise attenuation μ and a monotonically increasing function of f, as expected.

We obtain a precise estimate of the critical social temperature in the thermodynamic limit $q_c(\mu, f)$ by calculating the Binder cumulant U for different system sizes for each pair of the social noise sensitivity and cooperative fraction (μ, f). In Figure 16, we exhibit the Binder

Figure 15 – Effects of the intensity of cooperative behavior μ on the model for (a) the magnetization $M(q, c, f)$, (b) the magnetic susceptibility $\chi(q, c, f)$, and (c) the Binder fourth-order cumulant $U(q, c, f)$. From right to left, we vary μ from 0.0 to 1.0 in steps of $\Delta\mu = 0.1$ for a cooperative fraction of $f = 0.5$. The lines are guides to the eye.

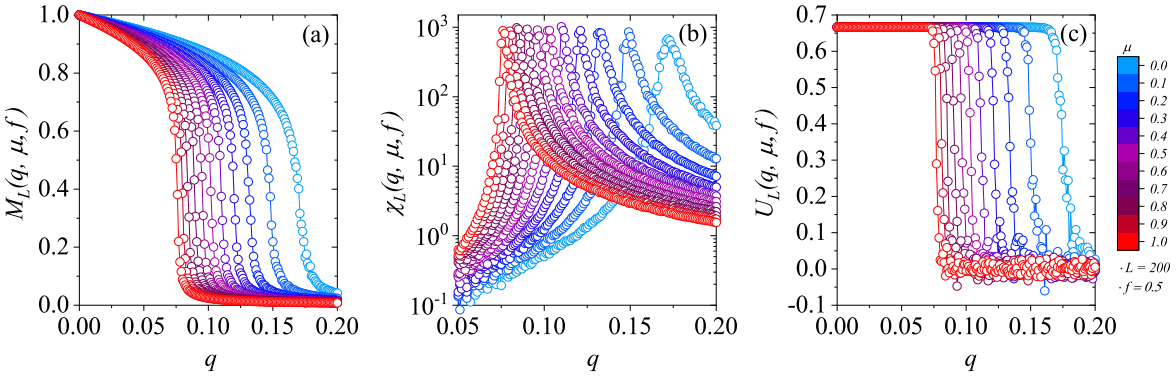

Source: Author.

cumulant for the $\mu = 0.5$ and $f = 0.3$ case. Following Eq. (4.39), we use the fact that the critical exponent of U is zero at the critical point, and we estimate the critical social noise value $q_c(\mu, f)$ from the intersection point of Binder curves for different sizes L. In this case, we estimate $q_c(\mu, f) = 0.0891(2)$ for $\mu = 0.5$ and $f = 0.3$. Note that, numerically, the curves will intersect at several points. The estimate 0.0891 is the average between the rightmost and the leftmost intersections, and the uncertainty 0.0002 is the distance from the central estimate to the further intersection. We repeat the same process to other pairs of parameters μ and f to get the set of critical points $q_c(\mu, f)$.

We summarize the critical noises for several values of f and μ in Table 1, yielding the phase diagram shown in Fig. 17. The interpolation of the critical dots $q_c(\mu, f)$ describes the phase boundary of the system that separates the ordered and disordered phases for each value of the noise sensitivity μ. Observe that the critical noise grows linearly with f when f is small but has considerable nonlinear effects with f as f increases, amplified as the collaborative intensity μ is higher. From the data and mean-field calculations (Recall Eq. (4.73)), we propose the phase boundary lines to obey an equation of type:

$$q_c(\mu, f) = \frac{1}{a - bf}, \tag{5.1}$$

where a and b are parameters that depend on μ. By executing a non-linear curve-fitting on the data points, we estimate $[a, b] = [12.8(5), 9.4(5)], [13.2(1), 6.5(1)], [13.2(1), 3.3(1)]$, respectively for $\mu = 0.25, 0.50$ and 0.75. Note that we obtain $q_c(\mu, 0) = 1/a \approx 0.075$,

Figure 16 – Binder fourth-order cumulant $U_L(q, \mu, f)$ for $\mu = 0.5$ and cooperative fraction $f = 0.3$. The intersection of curves for societies of different sizes L provides an estimate for the critical social temperature $q_c(\mu, f)$ in the thermodynamic limit $L \to \infty$. The dashed lines represent cubic fits of the data points near the critical region $q \approx q_c$, while the continuous lines are guides to the eye.

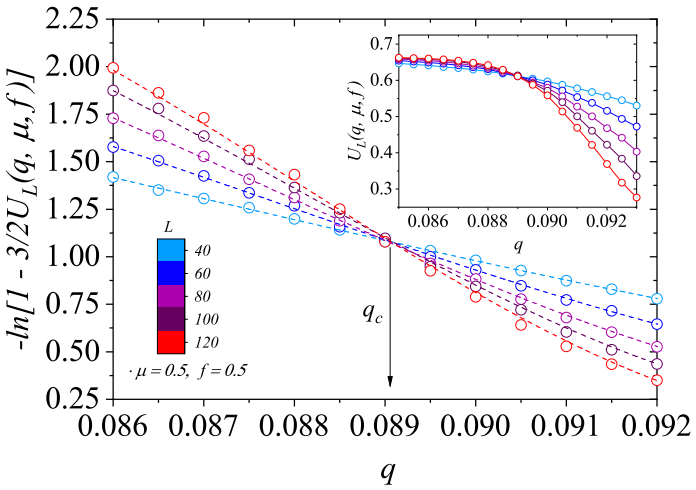

Source: Author.

Table 1 – Phase transition points $q_c(\mu, f)$ as a function of f and μ for the model on the square lattice. The critical temperatures were estimated using the Binder cumulant crossing method.

f	$q_c(\mu = 0.25)$	$q_c(\mu = 0.50)$	$q_c(\mu = 0.75)$
0.0	0.0750(1)	0.0750(3)	0.0750(1)
0.1	0.0816(2)	0.0791(2)	0.0771(1)
0.2	0.0894(1)	0.0839(1)	0.0792(1)
0.3	0.0986(1)	0.0891(2)	0.0814(1)
0.4	0.1101(2)	0.0947(2)	0.0837(1)
0.5	0.1243(1)	0.1011(1)	0.0861(2)
0.6	0.1420(3)	0.1085(2)	0.0886(2)
0.7	0.1626(3)	0.1167(2)	0.0912(2)
0.8	0.1963(3)	0.1264(2)	0.0941(2)
0.9	0.2418(3)	0.1374(1)	0.0970(1)
1.0	0.3002(1)	0.1503(2)	0.1000(1)

Source: Author.

Figure 17 – Phase diagram of the model in the parameter space q versus f. The curves depict the phase boundary separating ordered and disordered phases for different noise sensitivity values μ. The circles represent numerical estimates of the critical points $q_c(\mu, f)$, obtained from the intersection of the Binder cumulant curves for different system sizes. The lines are non-linear fits based on Eq. (5.1).

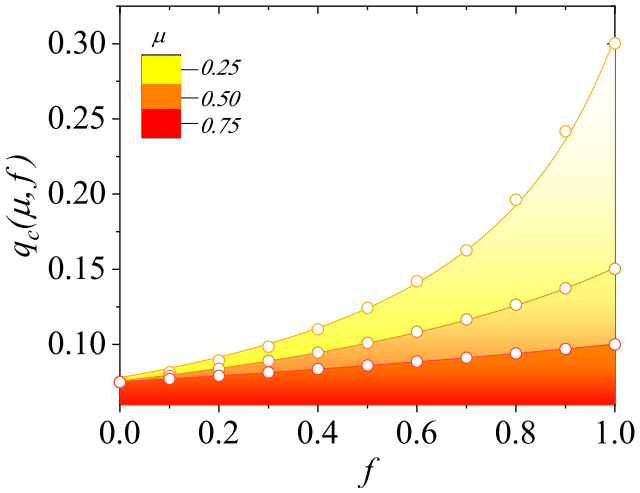

Source: Author.

in agreement with the result of the isotropic majority-vote model, which we also verify for $f = 0.0$ in table 1 (OLIVEIRA, 1992). Additionally, $q_c(\mu, 1) = 1/(a-b) \approx 0.075/\mu$ as expected the fact that if all agents are cooperative $f = 1$, the system is equivalent to the isotropic case with $q \to q/\mu$.

We investigate the finite size effects on the social dynamics of the cooperative majority-vote model in Figure 18, where we show the magnetization, susceptibility and Binder cumulant for $f = 0.8$ and $\mu = 0.5$, with $L = 40, 60, 80, 100$ and 120. Note that at the critical point $q_c(\mu, f) \approx 0.13$ (see Table 1), $M \to 0$ as $L \to \infty$, remaining non-zero for noise values below $q_c(\mu, f)$. Also, the larger L, the more intense the magnetization fluctuations, yielding the highest peaks observed for the magnetic susceptibilities near $q_c(\mu, f)$. That is because the correlation length increases with the system size so that, near the phase transition, a single opinion flip of one agent can cascade through the social network of interactions, affecting several other people in a domino effect.

We explore the behavior of M, χ and U near the critical point by estimating the critical exponents β/ν, γ/ν, and $1/\nu$ that characterize the phase transition of the model following Eqs. (4.35), (4.36) and (4.37). With these equations, we obtain the critical exponents of the phase transitions and capture the universal behavior of the magnetization, magnetic susceptibility,

Figure 18 – System size dependence of the model for (a) the order parameter M, (b) the variance χ, and (c) the Binder cumulant U, for different system sizes $L = 40, 60, 80, 100$, and 120. Here, we fix $f = 0.8$ and $\mu = 0.5$. The lines are guides to the eyes.

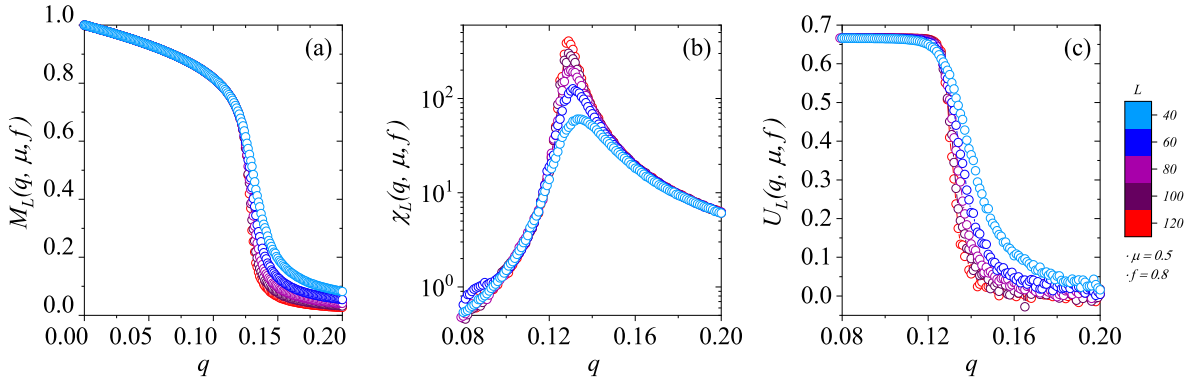

Source: Author.

and Binder cumulant given by the universal scaling functions $\widetilde{M}$, $\widetilde{\chi}$ and $\widetilde{U}$ that depend only on the scaling variable $x = \varepsilon L^{\frac{1}{\nu}}$.

In Figure 19, we illustrate the numerical results for $\mu = 0.5$ and several values of f. By measuring the linear coefficient of each line in Fig. 19(a), Fig. 19(b) and Fig. 19(c), we estimate $\beta/\nu \approx 0.125$, $\gamma/\nu \approx 1.75$ and $1/\nu \approx 1$ considering the error bars. We have f from 0.0 to 1.0 with $\Delta f = 0.2$ from the bottom to the top. We confirm our results by performing the data collapse of the rescaled versions of (d) $M(q,\mu,f)$, (e) $\chi(q,\mu,f)$ and (f) $U(q,\mu,f)$ over the rescaled social noise using $\beta/\nu = 0.125$, $\gamma/\nu = 1.75$ and $1/\nu = 1$. We shift all plots in this figure to avoid overlapping. We remark that despite the different behaviors observed in Fig. 12, Figs. 19(d), (e), and (f) yield only one universal curve independently on f. We repeat the same procedure for other μ values, as $\mu = 0.25$ and $\mu = 0.75$ also supplying the same set of critical exponents.

Note that the $\mu = 1$ case is the isotropic majority-vote model (OLIVEIRA, 1992; OLIVEIRA; MENDES; SANTOS, 1993), while $\mu = 0$ corresponds to a bimodal distribution of noiseless agents (VILELA; MOREIRA; SOUZA, 2012). We conclude that the critical exponents of the cooperative majority-vote model are the same as those in an equilibrium two-dimensional Ising model, regardless of μ and f. This follows Grinsteins criterion, which states that nonequilibrium stochastic spin-like systems with up-down symmetry in regular lattices fall into the same universality class of the equilibrium Ising model (OLIVEIRA, 1992; GRINSTEIN; JAYAPRAKASH; HE, 1985; BAXTER, 1982).

Figure 19 – Finite-size scaling analysis of the model on the square lattice. (a) The magnetization, (b) the magnetic susceptibility, and (c) the Binder fourth-order cumulant as functions of system size L in log-log scale for several values of the cooperative fraction f evaluated at the critical point $q = q_c(\mu, f)$ for $\mu = 0.5$. The solid lines represent linear fits to the data, yielding the standard Ising model critical exponents for square lattices. Using the critical exponents $\beta/\nu = 0.125$, $\gamma/\nu = 1.75$, and $1/\nu = 1$, we rescale (d) the order parameter, (e) its variance, and (f) the Binder cumulant versus the rescaled noise parameter, yielding a universal collapse for each graph. The curves are vertically shifted for better visualization. We consider $f \in [0.0, 1.0]$ with increments of $\Delta f = 0.2$ from bottom to top.

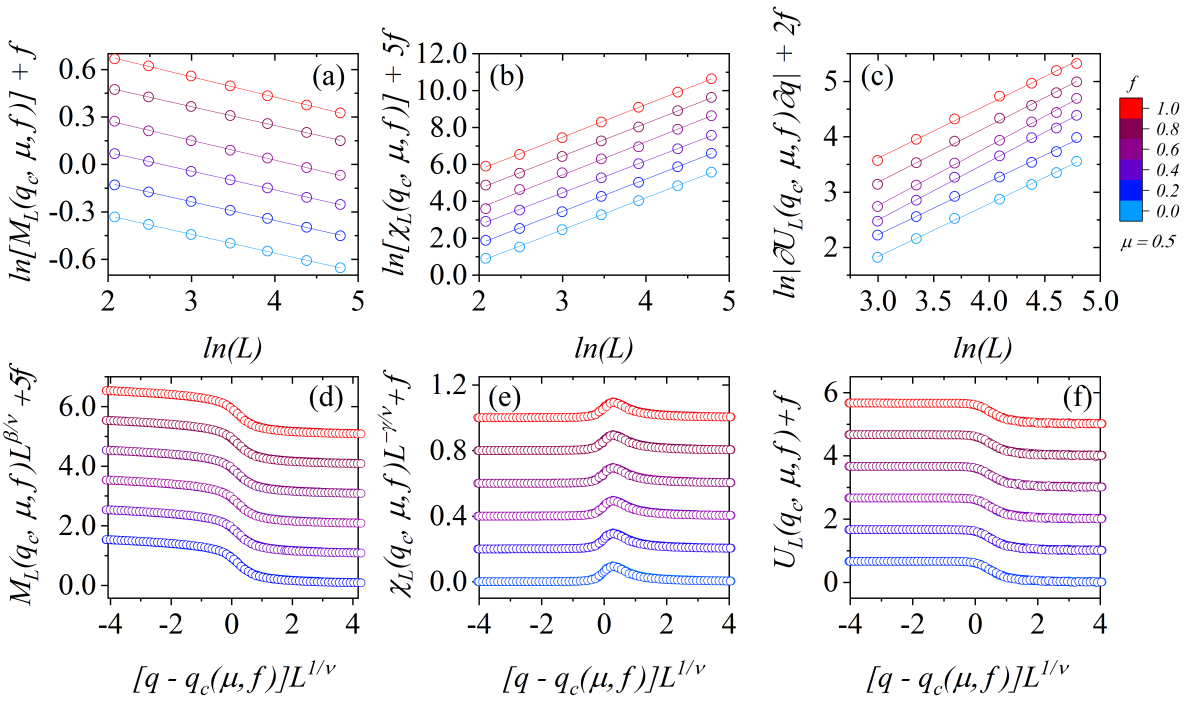

Source: Author.

5.2 MEAN-FIELD INVESTIGATION

We verify the mean-field calculations by performing Monte Carlo simulations using the mean-field approach. Following the mean-field assumptions, we randomly select an agent whose four neighbors are also randomly chosen. Here we considered systems with N spins, for $N = 1600, 3600, 6400, 10000$ and 40000. We skip the thermalization time of 10^4 MCS and evaluate the time averages over the next 10^5 MCS with up to 100 different samples.

In Figure 20, we show (a) the order parameter $M_L(q, \mu, f)$, (b) its variance $\chi_L(q, \mu, f)$ and (c) the Binder cumulant $U_L(q, \mu, f)$ as functions of the fraction of collaborative individuals f for several values of the noise q. We estimate the magnetization numerically from Eq. (4.30) (circles) and compare it with the analytical solution (4.72) (full lines), thus validating

Figure 20 – Behavior of the order parameter as a function of the cooperative fraction f for several values of the noise parameter q at fixed $\mu = 0.5$. (a) Magnetization, (b) magnetic susceptibility, and (c) Binder cumulant. The dashed lines in (a) correspond to the analytical predictions from Eq. (4.72), while the symbols represent the numerical results averaged over 20 independent samples for a system size of $L = 200$.

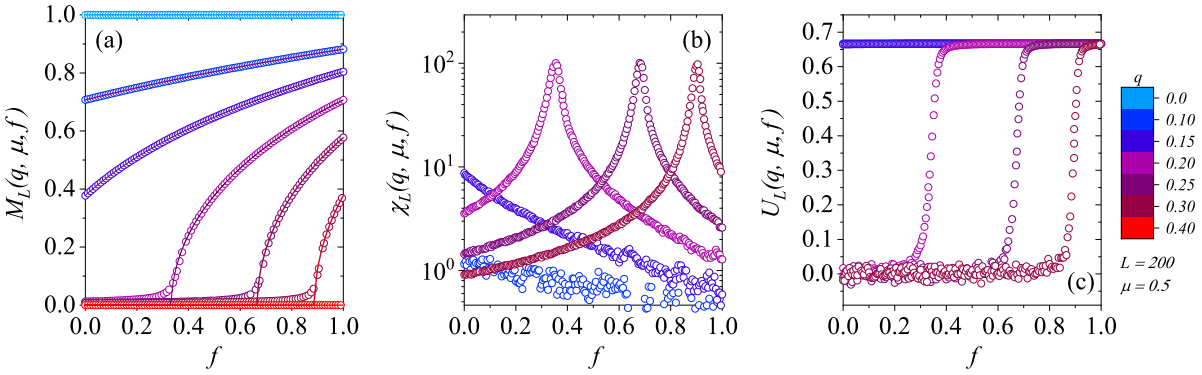

Source: Author.

the analytical solution of the mean-field calculations. The small divergences near the phase transition point result from the limited nature of the simulated network with $L = 200$, whereas the analytical solution assumes the thermodynamic limit $N \longrightarrow \infty$.

Figure 20(a) shows that increasing societal collaborative agents promote social ordering. Extreme temperatures, $q \to 0$ or $q \to 0.5$, suppress the disorder-order phase transitions, causing the system to remain ordered or disordered regardless of the presence of cooperative agents. The maximum of each susceptibility curve in Fig. 20(b) denotes the critical values of f that yield an order-disorder phase transition on the system. Additionally, as f increases, the critical temperature necessary to vanish the order consensus increases, improving social robustness. This system's behavior agrees with Eq. (4.73), where $q_c(\mu, f)$ is a monotonically increasing function of f.

In Figure 21, we obtain the mean-field phase diagram in the $q \times f$ parameter space, expressing how the boundary separating society's ordered and disordered phases behaves as a function of f and μ. The lines stand for the analytical solutions given by Eq. (4.73), and the open circles represent the numerical data estimates, agreeing with the mean-field results. These results also agree qualitatively with the Monte Carlo simulation data we obtained for the model on square lattices.

In Fig. 22, we show how cooperative behavior changes the Supercritical Pitchfork Bifurcation of the order parameter. In general, it increases the cooperative phenomena (either

Figure 21 – Mean-field phase diagram in the parameter space q versus f. The solid lines represent the analytical phase boundaries obtained from Eq. (4.73), which separate the ordered and disordered phases of the system for different values of the noise sensitivity parameter μ. The open circles correspond to numerical estimates of the critical points $q_c(\mu, f)$, determined by the crossing points of the Binder cumulant curves. Here, we use $f \in [0.0, 1.0]$ with increments of $\Delta f = 0.1$.

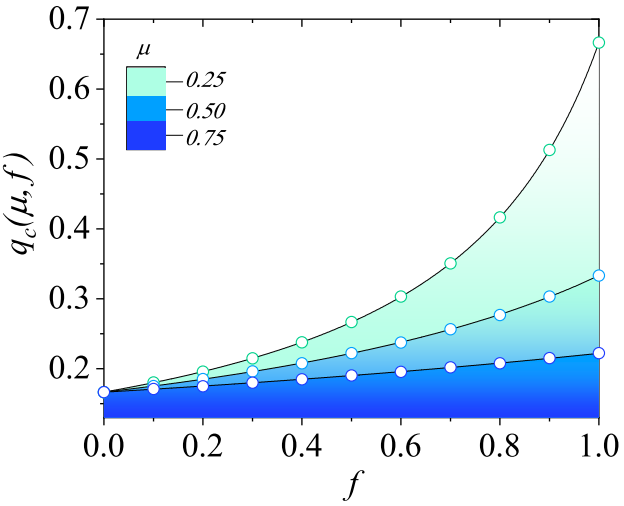

Source: Author.

by increasing the collaborative fraction f or decreasing the noise sensitivity μ), attenuates the bifurcation, and can even suppress it. The collaborative agents boost symmetry breaking and increase the distance between the two stable symmetric branches. Therefore, cooperative phenomena incentivize the system's strong preference for one of the two possible opinions.

Since we have an equation describing the mean-field critical social temperature (Eq. (4.73)), we can generate a density plot to see how the whole spectrum of collaborative parameters f and μ affects the critical social noise. Fig. 23 reveals the density plot and shows visually that the critical temperature has symmetry around the line $\mu = 1 - f$. Indeed, from Eq. (4.73), we can see that the critical noise is invariant due to the transformation $\mu \to 1 - f$ and $f \to 1 - \mu$, which is the symmetry around the line $\mu = 1 - f$. Therefore, a society with a fraction of f cooperative agents with cooperative intensity μ is equivalent to a society with a fraction of $1 - \mu$ collaborative agents with cooperative intensity $1 - f$. Additionally, for $0 < \mu < 1/6$, there is a critical value of the cooperative agents $f_c = 5/6(1 - \mu)$ above which the critical noise is higher than one, corresponding to the white region. In this region, society is always ordered no matter the value of the social temperature.

Finally, using the finite-size scaling relations given by the equations (4.35), (4.36) and (4.37), we plot in Figure 24 (a) the magnetization, (b) the magnetic susceptibility, and (c) the

Figure 22 – Mean-field solution of the order parameter as a function of the social noise in the Cooperative majority-Vote Model. The full lines represent stable solutions, while the dashed lines indicate unstable stationary solutions. (a) Influence of the cooperative fraction f on the bifurcation structure, showing how varying f modifies the stability of solutions. (b) Effects of the noise attenuation parameter μ, highlighting cases where bifurcations are suppressed and there is no phase transition.

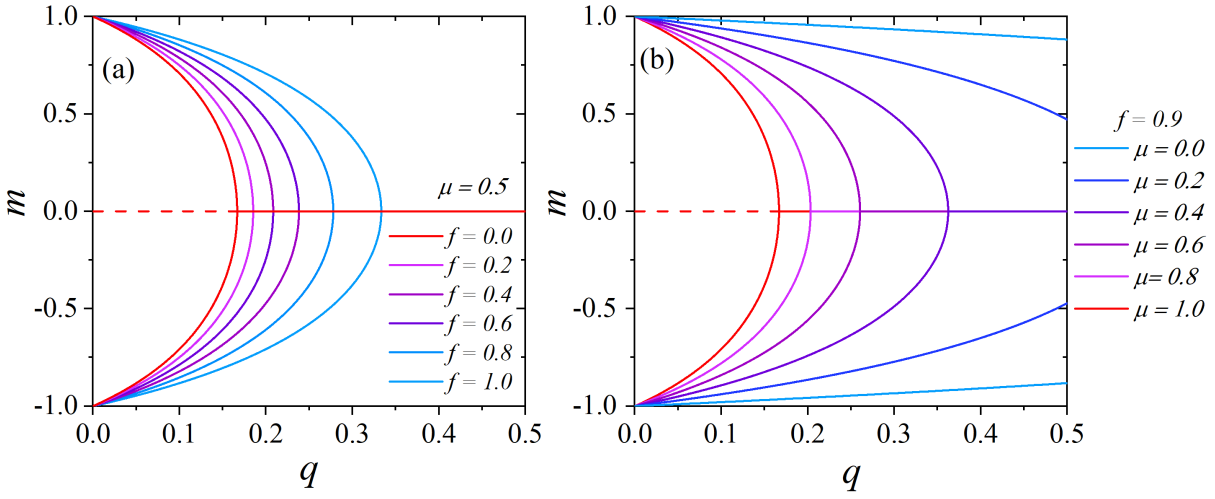

Source: Author.

absolute value of the derivative of the Binder cumulant at the critical temperature $q = q_c(\mu, f)$ versus the system size for $\mu = 0.5$. The line slopes estimate the critical exponents $\beta \approx 1/2$, $\gamma \approx 1$ and $\nu \approx 1/2$ for all values of the f and μ investigated. These results confirm that the majority-vote model with cooperative agents belongs to the mean-field Ising universality class.

Table 2 – Numerical estimates of the critical noise $q_c(\mu, f)$ as a function of μ and f for the mean-field approach. The values in parentheses indicate numerical errors in the last digit.

f	$q_c(\mu = 0.25)$	$q_c(\mu = 0.50)$	$q_c(\mu = 0.75)$
0.0	0.1665(1)	0.1665(1)	0.1664(3)
0.1	0.1802(1)	0.1753(1)	0.1711(2)
0.2	0.1957(3)	0.1851(1)	0.1750(1)
0.3	0.2149(1)	0.1961(1)	0.1799(2)
0.4	0.2376(4)	0.2077(3)	0.1848(1)
0.5	0.2667(1)	0.2224(2)	0.1904(1)
0.6	0.3031(3)	0.2373(1)	0.1955(1)
0.7	0.3507(1)	0.2566(2)	0.2018(2)
0.8	0.4163(4)	0.2768(2)	0.2076(1)
0.9	0.5128(1)	0.3033(3)	0.2152(1)
1.0	0.6664(1)	0.3332(2)	0.2221(1)

Source: Author.

Figure 23 – Density plot of the social critical noise following the mean-field prediction from Eq. (4.73), spanning the full spectrum of the cooperative parameters μ and f.

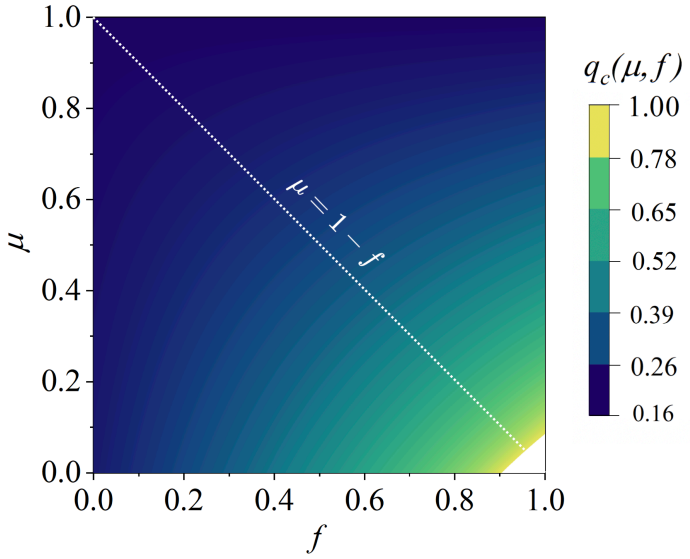

Source: Author.

Figure 24 – Log-log plots for (a) the magnetization $M(q,\mu,f)$, (b) the susceptibility $\chi(q,\mu,f)$, and (c) the Binder cumulant $U(q,\mu,f)$, evaluated at the critical noise $q = q_c(\mu,f)$ versus the system size L for $\mu = 0.5$. The solid lines are obtained from linear regression, and their slopes correspond to the respective critical exponents in the mean-field limit. The curves are vertically shifted for better visualization. We consider $f \in [0.0, 1.0]$ with increments of $\Delta f = 0.2$ from bottom to top.

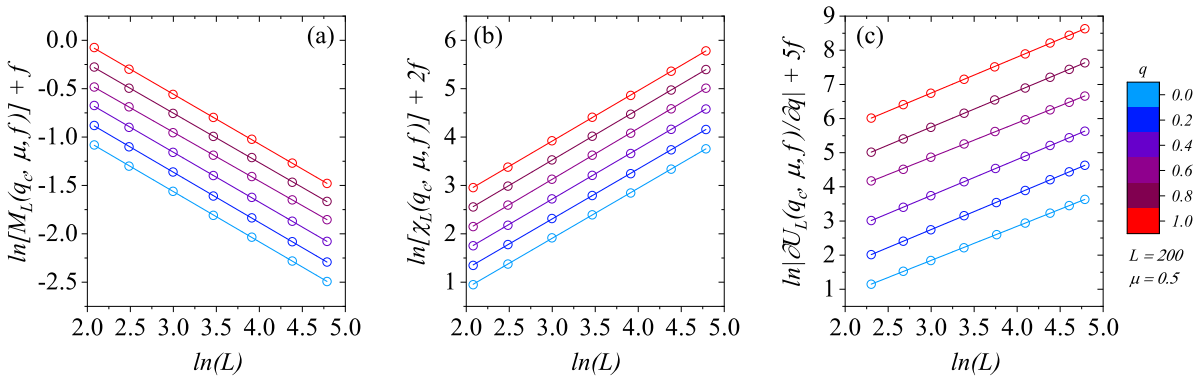

Source: Author.

Figure 25 – Stationary social entropy flux $\varphi_L(q,\mu,f)$ for the collaborative majority-Vote model as a function of the social temperature q for different parameters obtained via Monte Carlo simulations on the square lattice. (a) Fixing $\mu = 0.5$ and $f = 0.5$ while varying the system size L. (b) Fixing $L = 180$ and $\mu = 0.5$ while varying the cooperative fraction f. (c) Fixing $L = 180$ and $f = 0.5$ while varying the noise attenuation μ. The solid lines serve as visual guides.

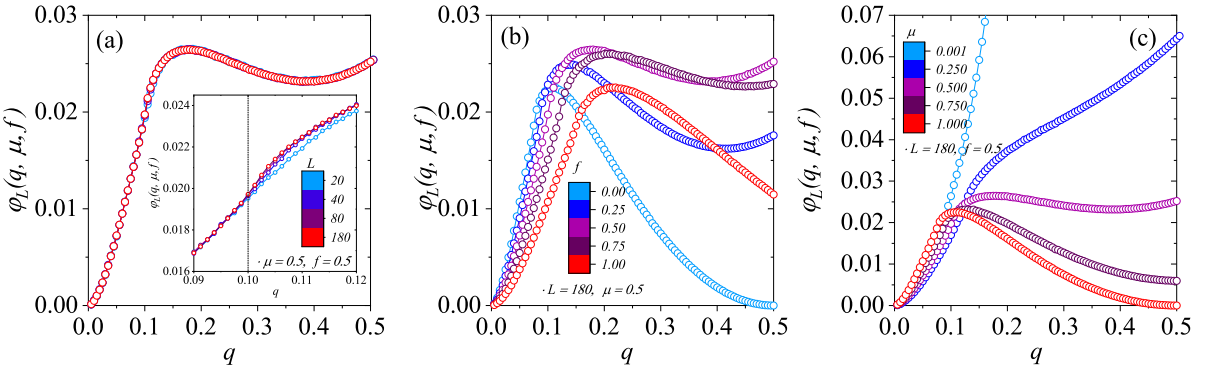

Source: Author.

5.3 COOPERATIVE MAJORITY-VOTE ENTROPY PRODUCTION

In Figure 25, we plot the numerical results on the square lattice of the social entropy production per agent $\varphi_L(q,\mu,f)$ in the stationary regime for several values of (a) the system size L, (b) the collaborative fraction f and (c) the noise attenuation μ as a function of the society temperature q. We observe in (a) that the entropy flux per agent has a weak sensitivity to variations in the population size (therefore, the entropy flux is proportional to the number of agents, which means the entropy flux is extensive, as expected. Recall that we defined $\varphi \equiv \Phi/N$ in Eq. (4.82)) but a strong dependence on (b) the fraction of collaborative agents present in society and (c) noise attenuation in a log-linear scale.

The curves for $f = 0.0$ and $\mu = 1.0$ in Figures 25(b) and (c), respectively, display the flux of entropy of the standard majority-vote model. This flux has a maximum that occurs after the critical noise $q_c(\mu, f = 0.0) = 0.075$ and vanishes for $q \to 0$ or $q \to 1/2$.

Figure 25(b) displays that, when $f = 1.00$ and $\mu = 0.5$, the entropy flux curve follows the isotropic flux case under the linear transform $q \to q/\mu$. Thus, this flux vanishes for $q \to 0$ and $q \to 1/2\mu$. For $0 < f < 1$, we model a nonhomogeneous society with two different types of agents with distinct noise sensibilities. Hence, after the maximum, instead of approaching zero, the entropy flux of nonhomogeneous societies increases again, supported by the discrepancy between the collaborative and regular agents, as depicted in Figure 25(b). Indeed, Figure 25(c) reveals that this phenomenon intensifies as μ becomes smaller because the social temperature disparity among the agents increases.

Note that as a general pattern, the critical temperature $q_c(\mu, f)$ does not coincide with the maximum of $\varphi_L(q,\mu,f)$. Actually, the critical noise is an inflection point for the entropy flux that occurs before the maximum point, as we can see in the detail of Figure 25(a). Therefore, similarly to the Ising model, the entropy flux yields a finite singularity at the critical point of the form

$$\varphi_L(q,\mu,f) = \varphi_L(q_c(\mu,f),\mu,f) + A_{\pm} \mid q - q_c(\mu,f) \mid^{(1-\alpha)}, \tag{5.2}$$

where $A_{\pm}$ are the amplitudes of the regimes before and after the critical social temperature point $q_c(\mu, f)$. Thus, instead of a maximum in the entropy flux, the second-order phase transition that occurs on the critical noise maximizes the derivative of the entropy flux concerning the social temperature, as we can see in Fig. 26(a) for $\mu = 0.5$ and $f = 0.5$ when

Figure 26 – (a) System size dependence of the partial derivative of the entropy flux with respect to the social temperature for $\mu = 0.5$ and $f = 0.5$. (b) Maximum value of the entropy derivative at the critical point as a function of the natural logarithm of the system size. The solid lines serve as visual guides.

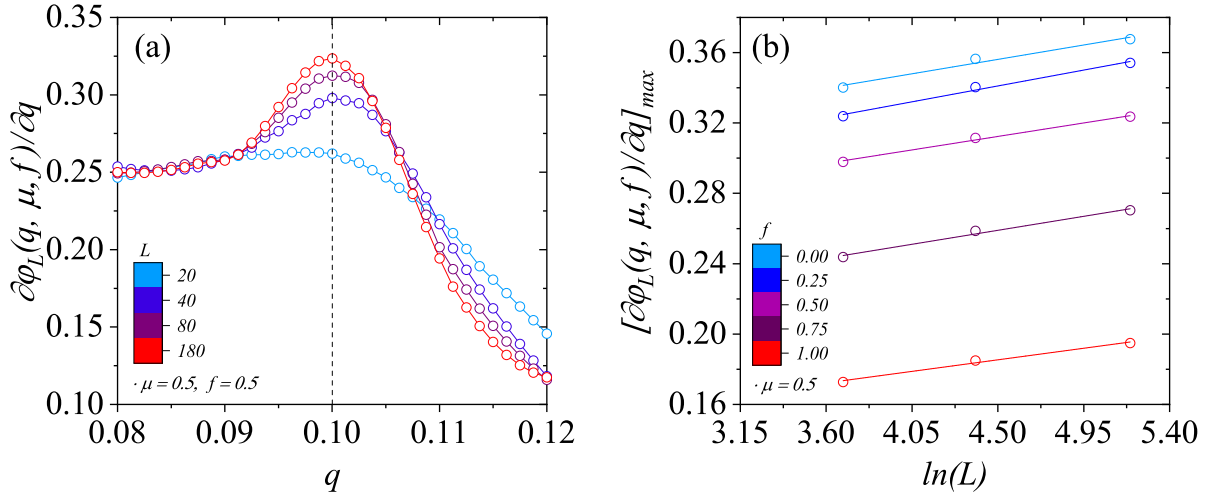

Source: Author.

Figure 27 – Mean-field stationary social entropy flux production $\varphi_L(q,\mu,f)$ as a function of the social temperature q. (a) Dependence of $\varphi_L(q,\mu,f)$ on the cooperative fraction f for $\mu = 0.5$. (b) Dependence of $\varphi_L(q,\mu,f)$ on the noise sensitivity μ for $f = 0.5$. The open circles represent numerical data obtained from Monte Carlo simulations for $N = 32400$ individuals in the mean-field regime, while the solid lines correspond to the analytical results given by Eqs. (4.84) and (4.85).

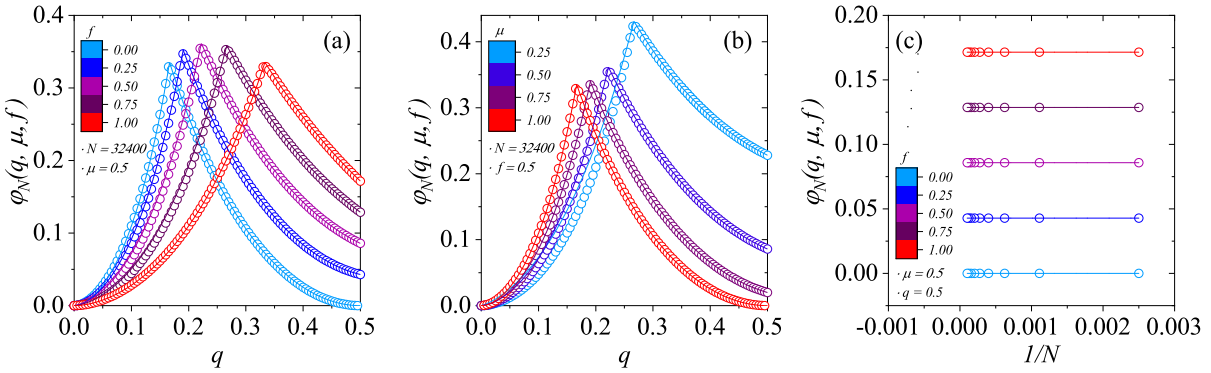

Source: Author.

$q_c(\mu = 0.5, f = 0.5) = 0.1011$ (Table 1). Indeed, from Eq. (5.2), we can write

$$\frac{\partial\varphi_L(q,\mu,f)}{\partial q} \sim \mid q - q_c(\mu,f) \mid^{-\alpha}, \tag{5.3}$$

where the exponent α corresponds to the same exponent associated with the specific heat of

the Ising model in the square lattice, $\alpha = 0$, which yields a singularity of the logarithm type. Hence, in analogy, we obtain

$$\frac{\partial \varphi_L(q,\mu,f)}{\partial q} \sim \ln \mid q - q_c(\mu,f) \mid . \tag{5.4}$$

We use the Savitzky-Golay Smooth algorithm with cubic polynomials to numerically estimate the derivate of the entropy production regarding the social noise $\partial\varphi_L(q,\mu,f)/\partial q$ for several systems of different sizes L in Fig. 26(a). By finite-size scaling theory on Eq.(5.4), the maximum value of the partial derivative of the entropy flux concerning the social temperature q must diverge at the critical point as

$$\left(\frac{\partial \varphi_L(q,\mu,f)}{\partial q}\right)_{max} \sim \ln\, L. \tag{5.5}$$

Indeed, the Fig. 26(b) confirms our conjecture given by Eq.(5.4) for $\mu = 0.5$ and several values of the cooperative fraction f. We observed the same behavior for other values of the noise sensitivity μ and f. Therefore, we proved our premise for the cooperative majority-vote model on square lattices is correct.

Figure 27 shows and confirms the mean-field stationary social entropy flux production $\varphi_L(q,\mu,f)$ as a function of the noise q for several values of the cooperative fraction f noise sensitivity μ. In Figure 27(a) we set $\mu = 0.5$ and $f = 0.00, 0.25, 0.50, 0.75$ and 1.00 while in Figure 27(b) we use $f = 0.5$ and $\mu = 0.25, 0.50, 0.75$ and 1.00. The open circles are numerical data obtained by Monte Carlo simulations for $N = 32400$ individuals in the mean-field limit, and the lines represent the analytical results given by Equations (4.84) and (4.85). There are slight deviations between the mean-field solutions and the Monte Carlo data in the ferromagnetic phase of the entropy flux due to the finite nature of the simulated systems, amplified as $\mu \to 0$.

We highlight that for nonhomogeneous societies ($0 < f < 1$), where a social temperature contrast exists between the regular and cooperative individuals, $\varphi_L(q,\mu,f)$ does not approach zero when $q = 0.5$, but remain finite independently of system size L (Figure 27(c)). However, for any isotropic case, as $f = 0$ or $\mu = 1.0$, $\varphi_L(q,\mu,f)$ tends to zero for $q = 0.5$, as expected. Differently from the square lattice network, in the mean-field framework, besides the inflection point, the critical temperature $q_c(\mu,f)$ also corresponds to the point of maximum entropy flux.

An exciting result is that, for non-equilibrium systems, such as the cooperative majority-vote model, the Maximum Entropy Production Principle proposes that among all possible non-equilibrium steady states (NESS) that satisfy the systems constraints, the one with the highest

entropy production rate is the most likely. Therefore, if real-world societies follow this principle, the heterogeneity between cooperative and non-cooperative individuals could be explained as a potential natural manifestation of the achieved NESS since combining cooperative and regular agents maximizes entropy production (MARTYUSHEV; SELEZNEV, 2006; DYKE; KLEIDON, 2010). Observe that the NESS with higher entropy production does not necessarily have more disorder, but actually, it yields a dynamic state that maximizes entropy production.

6 AFFINITY-BASED SCALE-FREE NETWORK AND SOCIAL DYNAMICS

In this chapter, we investigate the properties of the proposed scale-free network with affinity effects, defined in Sec. 2.3. Then, we explore how this network affects the majority-vote dynamics using Monte Carlo simulations to approximate opinion dynamics in real social networks.

6.1 NETWORK CHARACTERIZATION

Aligning with actual data from social networks like X, Facebook and Instagram, our network model generates scale-free networks with different curvatures as we vary ξ or α in Figures 28 and 29. That result contrasts with the original Barabasi-Albert (BA) model's distribution, which is equivalent to the $\xi = 1$ case in Fig. 28 (a), that always features $\gamma \approx 3$ with no curvature.

Figure 28 – Log-log plots of (a) the degree distribution and (b) the cumulative degree distribution of the Affinity-Based Scale-Free Network for several values of the average globalization parameter ξ.

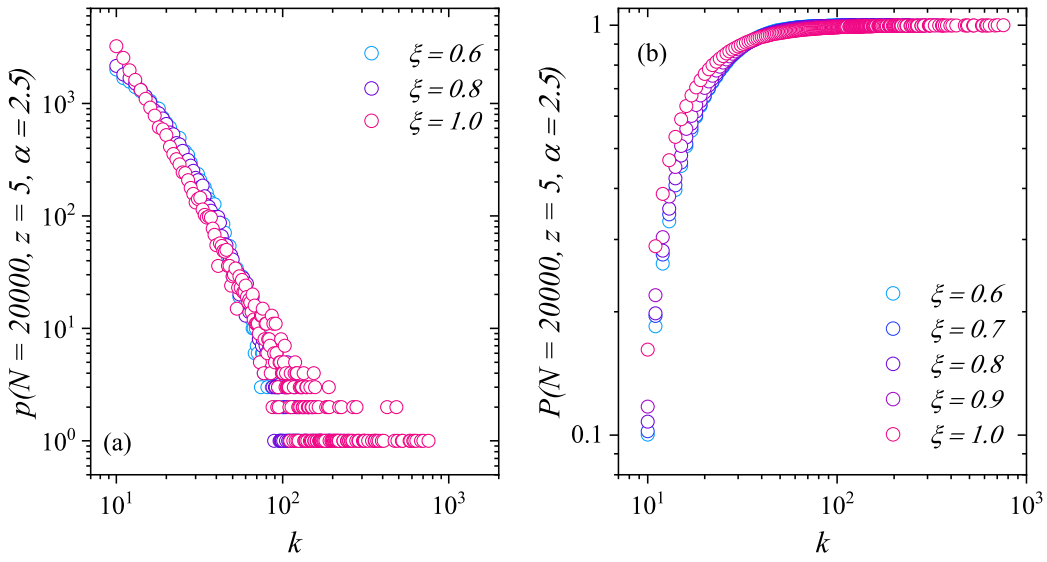

Source: Author.

The curvature in the degree distribution happens because of the homophilic effects generated by the affinity parameter, which increases the chance of local connections. Consequently, some purely preferential attachment connections are rewired to close individuals, causing an

excess of less connected individuals compared to the original BA model.

On the other hand, the cumulative degree distribution of the Affinity-Based Scale-Free Network follows the same pattern as the original BA model, converging slowly due to the scale-free property of the degree distribution. Increasing the globalization parameter ξ generates networks with higher social connectivity inequality with more prominent hubs, causing the distribution to converge slowly.

Figure 29 – Log-log plots of (a) the degree distribution and (b) the cumulative degree distribution of the Affinity-Based Scale-Free Network for several values of the average affinity parameter α.

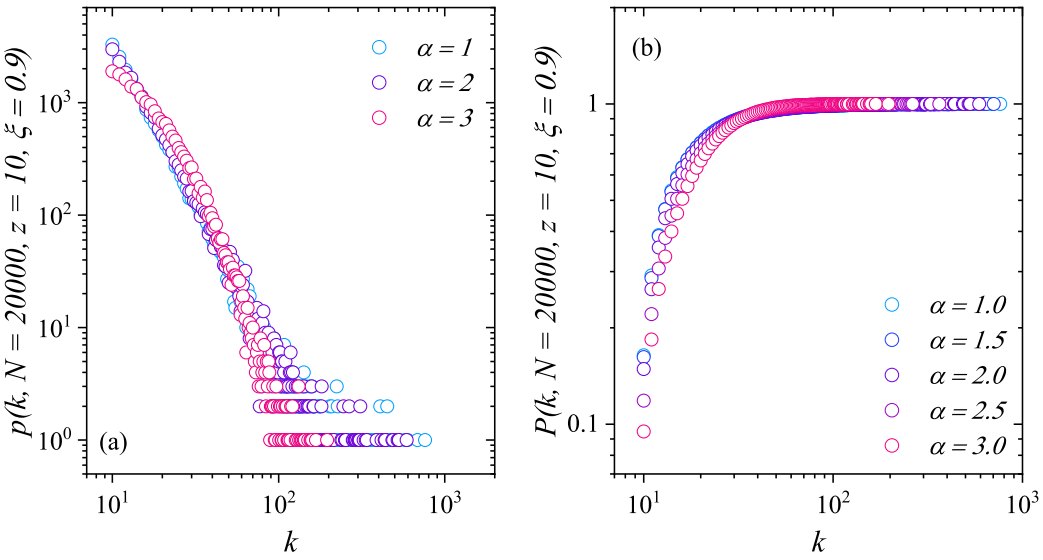

Source: Author.

In Fig. 30, we estimate the network degree distribution exponent γ for several values of the globalization parameter ξ and the local affinity α. For $\xi = 1$, the exponent is $\gamma \approx 3$, independently of α, as expected. By decreasing ξ and/or increasing α, there is a natural trend to increase γ. However, for several combinations of ξ and α, the network still yields a degree exponent close to 3, yielding scale-free behavior. Note that networks with $3 < \gamma < 3.5$ are considered weaker scale-free because they still follow a power law, but hubs become less dominant. Many real-world networks, such as biological, technological, and social networks, often exhibit γ values slightly greater than 3. In this regime, the degree variance $\langle k^2 \rangle$ converges, opposite to the divergence of the second moment for $\gamma < 3$ (NEWMAN, 2005). Observe that, for $\xi = 0$; we have a gravitational network with exponent α, and the degree exponent γ is independent of α and is given by $\gamma \approx 4$.

Figure 30 – Impact of the globalization parameter ξ and the local affinity α on the degree distribution exponent γ for a network of size $N = 20000$. The lines are guides to the eye.

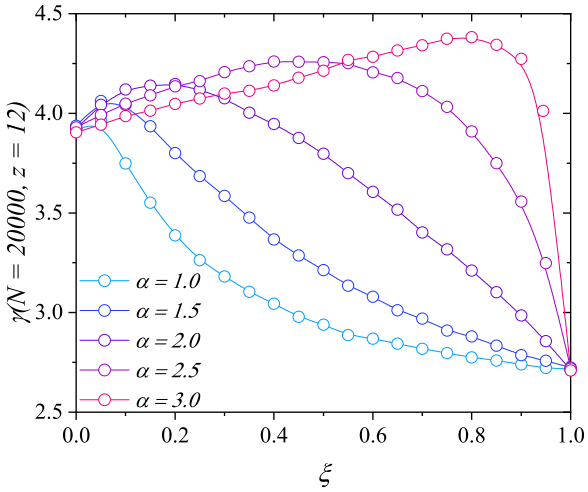

Source: Author.

Figure 31 – Temporal degree dynamics of the first network node for several values of (a) the globalization parameter ξ and (b) the affinity parameter α.

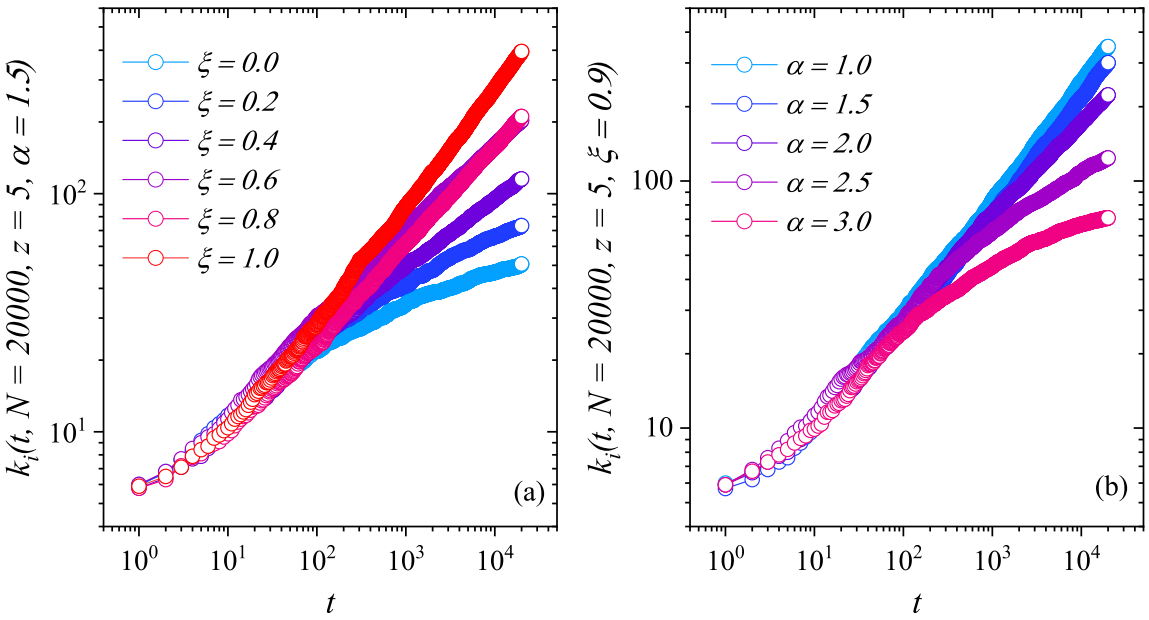

Source: Author.

Indeed, In Fig. 31, we show that the temporal degree dynamics of the first network node over time evolve in the same pattern of the BA model, still reproducing the first mover

Figure 32 – Clustering coefficient of the Affinity-Based Scale-Free Network for a network with $N = 20000$ and various values of the globalization parameter ξ and the local affinity α.

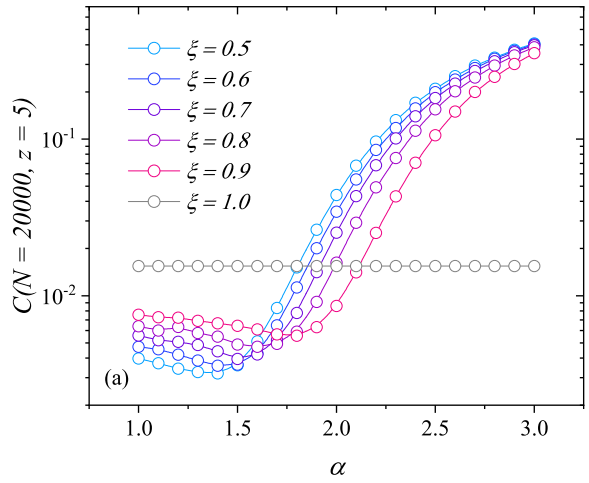

Source: Author.

Figure 33 – Average shortest path length of the Affinity-Based Scale-Free Network for a network with $N = 20000$ and various values of the globalization parameter ξ and the local affinity α.

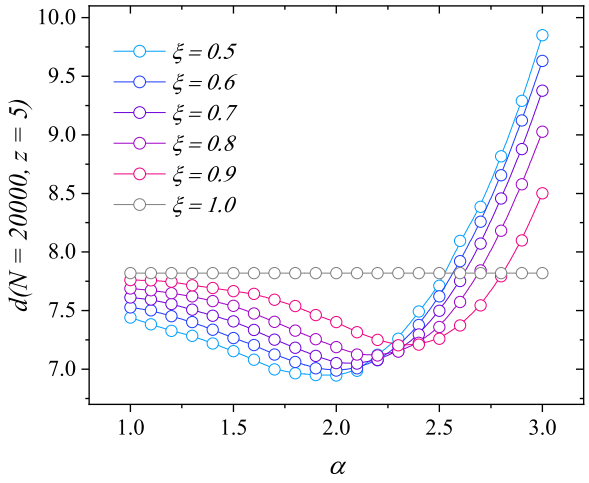

Source: Author.

advantage and the rich get richer phenomena. Note, however, that this effect is weakened because of the increased local affinity effects in the network. For the gravitational network $\xi = 0$, the network behaves like a random graph, and the degree of the initial node doesn't grow in a power law. However, globalization values such as $\xi = 0.8$ and $\xi = 0.6$ reproduce the first mover advantage phenomena similarly to the original BA model ($\xi = 1.0$).

Figure 34 – Robustness of the Affinity-Based Scale-Free Network under the random removal of a fraction of nodes for several values of the globalization parameter ξ and the local affinity α.

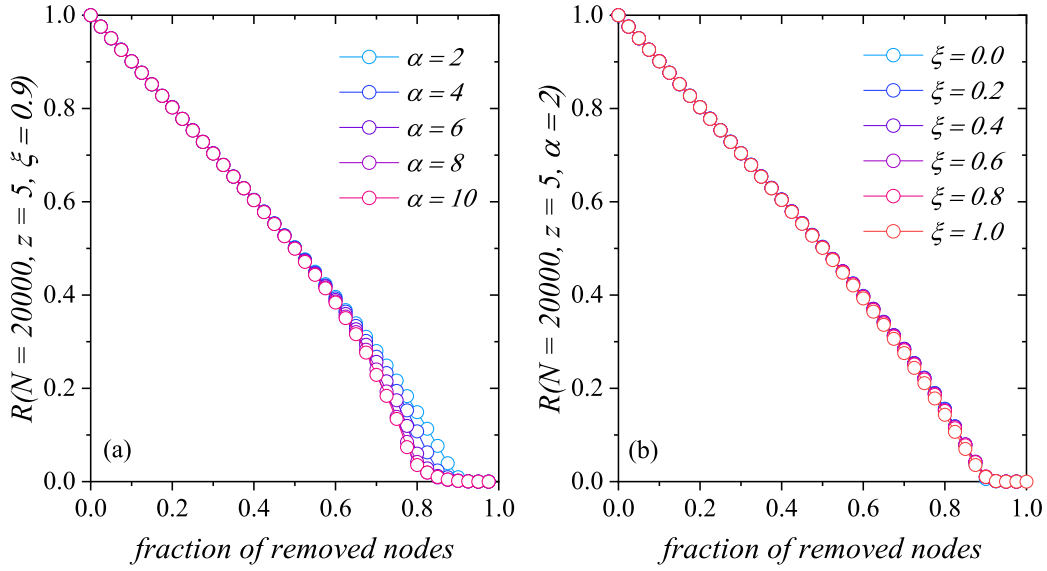

Source: Author.

Figure 32 shows how the affinity structure affects the network clustering coefficient. For small values of the local affinity α, the global clustering decreased over the original BA network, but the clustering surpassed the original clustering as α increased. Thus, for small values of α, the network decentralization level increases because some links to central hubs are rewired to individuals nearby. However, low intermediate values of α, such as 1.7 to 2.0, already create networks with higher clustering coefficients than the original BA model as the local connections start to group and create locally connected communities. The higher clustering follows the sociological "friend of my friend is also my friend" principle, as it measures the level of triadic closure in the network, aligning with real-world network properties (SIMMEL, 2013).

In Fig. 33, we show that even vast networks with $N = 20000$ nodes feature very low mean distance. Additionally, the Affinity-Based Scale-Free Network displays a lower mean distance than the original BA network, only surpassing it with higher affinity parameter values of 2.5 to 2.7. That shows improvement in efficient communication as information, news, signals, or social influence spreads faster across the network.

In Figs. 34 and 35, we explore the robustness of the Affinity-Based Scale-Free Network. While the Random Graph is highly vulnerable to random attacks and can be destroyed in a

Figure 35 – Robustness of the Affinity-Based Scale-Free Network under targeted attacks on a fraction of nodes for several values of the globalization parameter ξ and the local affinity α.

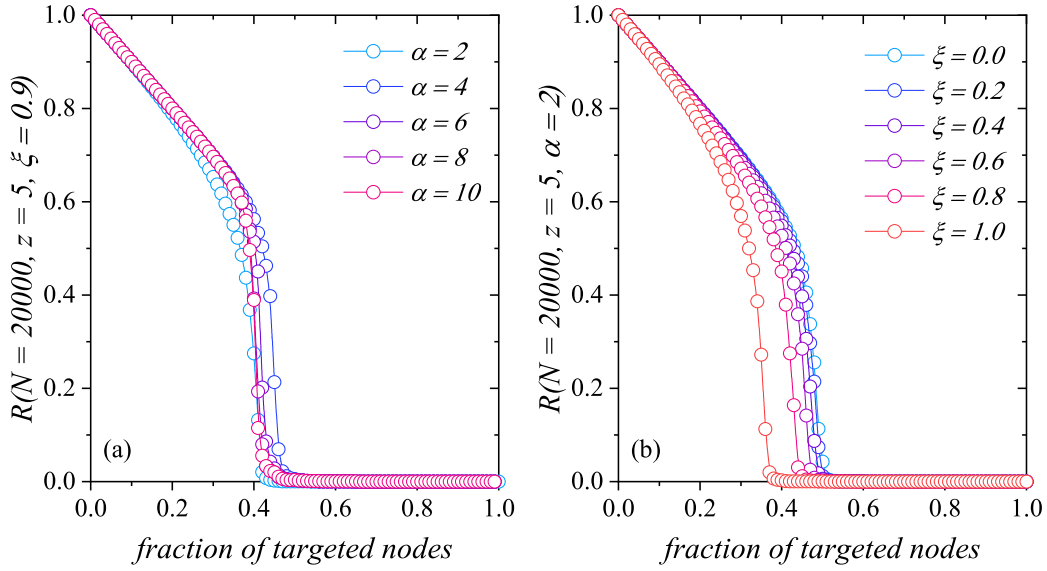

Source: Author.

relatively small value of the fraction of removed nodes, the original BA network is extremely robust to random failures, with the giant component being destroyed only when the fraction of random nodes removed is close to one. In Fig. 34, we show that the Affinity-Based Scale-Free Network, similarly to the BA model, is also very robust to random failures. In particular, the network robustness is practically independent of the globalization parameter ξ. That is, if some users leave randomly, the network giant component is not severely affected. This shows the network is robust, and information and influence can still propagate through the network via alternative paths.

On the other hand, the original BA model is highly vulnerable to targeted attacks, where hubs and popular nodes are removed first instead of random removal of nodes. Indeed, hubs (influencers, journalists, or community leaders) are central nodes, and when removed (like banning a high-profile user or because a user executed disinformation, illegal behavior or spam), the network can collapse much faster, fragmenting into small components and disrupting information flow. However, Fig. 35 shows that the Affinity-Based Scale-Free Network significantly displays higher robustness to targeted hubs attacks as the global parameter ξ decreases. This happens because local connections improve the global network clustering, generating alternate paths for information flow to maintain the network.

6.2 MAJORITY-VOTE ON AFFINITY-BASED SCALE-FREE NETWORKS

Here, we simulate the standard dynamics of the majority-vote model but on a nontrivial topology designed to capture the behavior of real social networks such as X and Facebook. In Fig. 36, we show how this network structure affects social dynamics. Note that while the local affinity modeled by the α parameter between individuals is a natural phenomenon, it decreases the community's robustness to disorder, which can promote social polarization in social networks. Still, there is an upper-limit effect: the impact of α on the order parameter saturates and approaches a natural limit. For instance, there is no virtual difference between the curves with $\alpha = 9$ and $\alpha = 10$.

Figure 36 – Effects of the intensity of local affinity α on the model for (a) the magnetization, (b) the magnetic susceptibility, and (c) the Binder fourth-order cumulant as functions of the social noise q. Here, we use $N = 10000$, $\xi = 0.9$, and $z = 5$. The lines serve as visual guides.

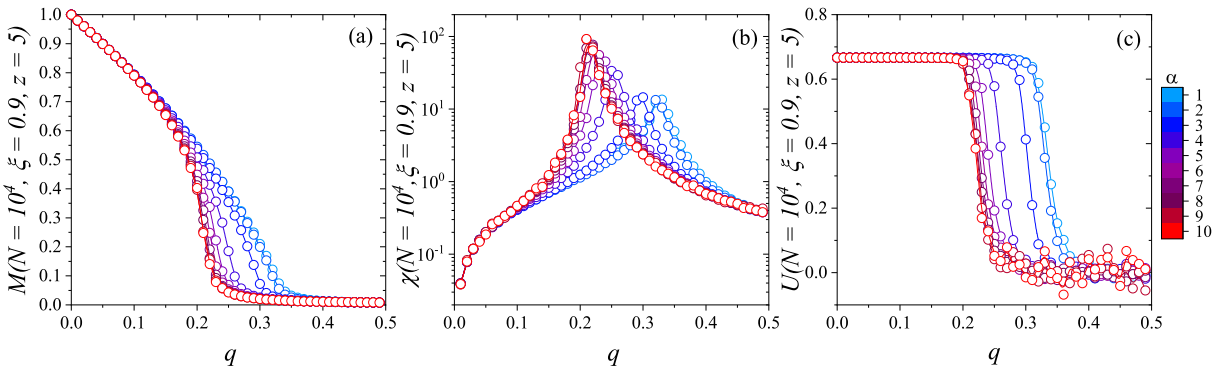

Source: Author.

Another way to look into these results is using a heat map in Fig. 37. Here, we have the advantage of extrapolating the numerical results and see at a glance the behavior of the thermodynamical functions in a spectrum of the model parameters. In particular, the vertical boundary separating the white region in Fig. 37(a) enables us to estimate the phase boundary between the ordered and disordered phases of the system. The exact boundary is highlighted by the magnetic susceptibility in Fig. 37(b) and by the orange curve on the Binder cumulant in subfigure (c).

To verify that, we estimate the critical social noise in the thermodynamic limit using the properties of the Binder cumulant, as shown in Fig. 38. Indeed, from Eq. (4.39), the binder cumulant is invariant to the system size at the critical point, and we estimate the critical

Figure 37 – Heat map of the effects of local affinity intensity α on the model for (a) the magnetization, (b) the magnetic susceptibility, and (c) the Binder fourth-order cumulant as functions of the social noise q. Here, we use $N = 10000$, $\xi = 0.9$, and $z = 5$.

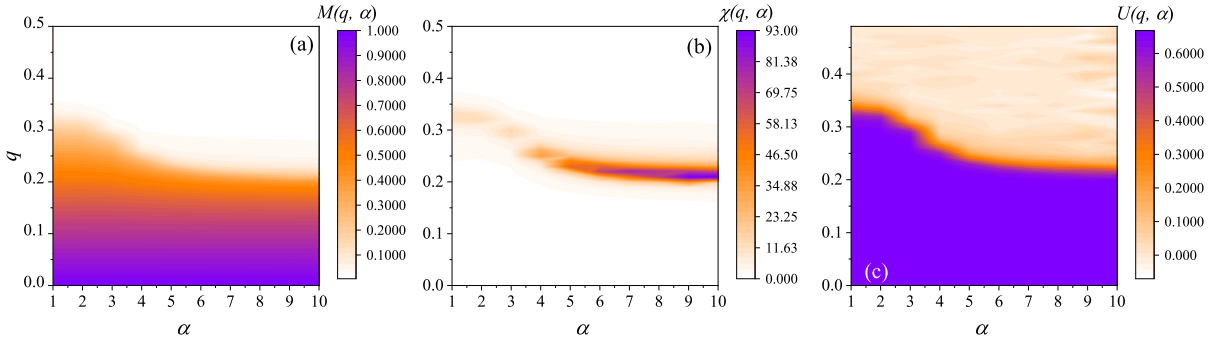

Source: Author.

Figure 38 – Binder cumulant for $\alpha = 4$, $\xi = 0.9$, and $z = 5$. The point where the curves for societies of different sizes N intersect is the estimate for the critical social temperature in the thermodynamic limit $N \to \infty$. To estimate the intersection, the lines are cubic fits of the data points near the critical region $q \approx q_c$.

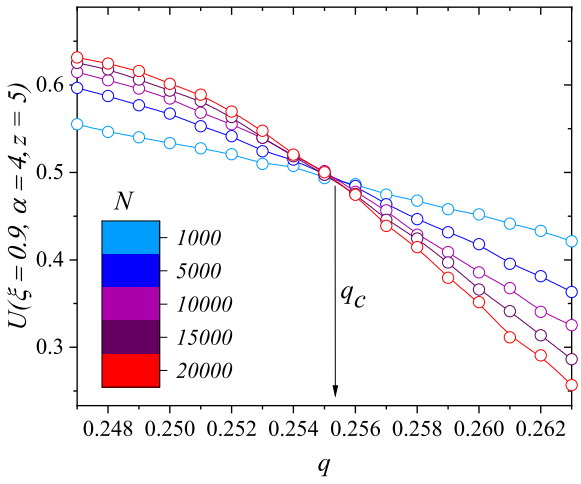

Source: Author.

social noise value $q_c(\mu, f)$ from the intersection point of Binder curves for different sizes N. We repeat the same process to other values of the social affinity pairs to obtain the set of critical points.

We obtain the phase diagram in Fig.39 using the critical social noises data. We remark that the interpolation of the critical points resembles the boundaries observed in the contour plot in Fig. 37. In particular, the phase boundary for this system suffers a phase transition:

Figure 39 – Phase diagram in the parameter space q versus α. The line denotes the phase boundary interpolation of numerical data that separates the system's ordered and disordered phases. The open circles represent the numerical results of the critical social noise, estimated by the intersection points of the Binder cumulant curves. The phase boundary undergoes a second-order phase transition at the critical value of the local affinity parameter α.

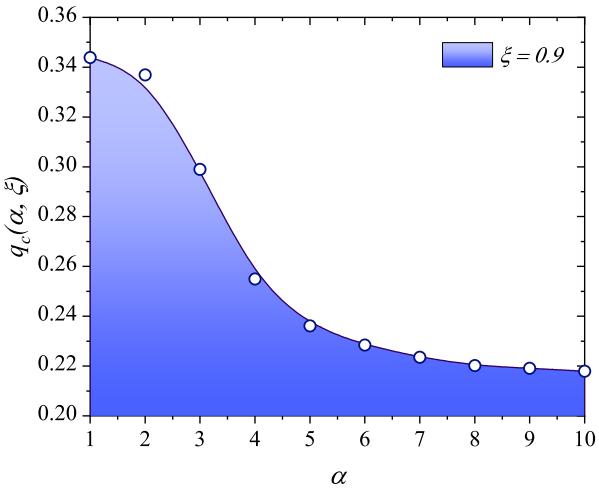

Source: Author.

Figure 40 – Log-log plots of (a) the order parameter and (b) the order parameter variance over the system size for several values of the affinity parameter α for $\xi = 0.9$. The linear fits enable us to estimate the critical exponents β/ν and γ/ν.

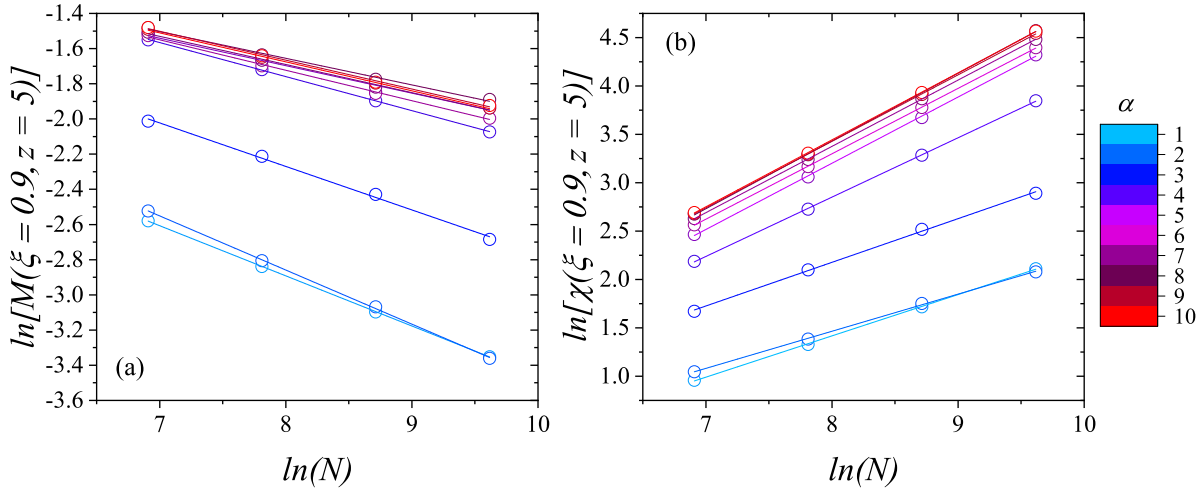

Source: Author.

the critical noise value decays abruptly at a critical value of the local affinity parameter α_c. Therefore, the system behavior changes dramatically as α increases: for low α, long-range

Figure 41 – Plot of the characteristic unitary line $y + 1.05(2)x = 1.03(1)$ estimated by the linear fit of the relation between the critical exponents $\beta/\bar{\nu}$ and $\gamma/\bar{\nu}$ for several values of the affinity parameter α and $\xi = 0.9$.

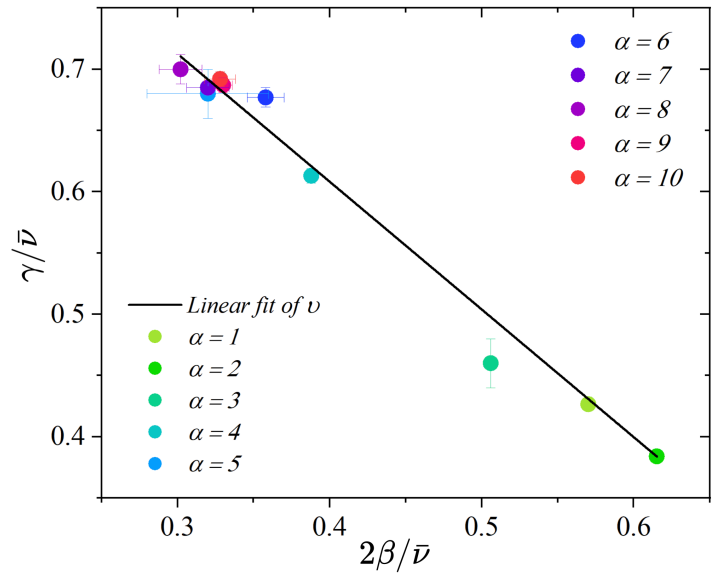

Source: Author.

Table 3 – Critical values of $\beta/\bar{\nu}$, $\gamma/\bar{\nu}$ for $z = 5$, $\xi = 0.9$, and the unitary relation in the unitary relation $\upsilon = 2\beta/\bar{\nu} + \gamma/\bar{\nu}$.

α	$\beta/\bar{\nu}$	$\gamma/\bar{\nu}$	$\upsilon = 2\beta/\bar{\nu} + \gamma/\bar{\nu}$
1	0.2851(1)	0.4265(1)	0.9967(2)
2	0.3076(1)	0.384(1)	0.9992(1)
3	0.253(1)	0.46(1)	0.966(2)
4	0.194(1)	0.613(3)	1.001(4)
5	0.16(2)	0.68(1)	1.000(4)
6	0.179(6)	0.677(4)	1.035(8)
7	0.160(7)	0.685(2)	1.005(10)
8	0.151(7)	0.700(6)	1.002(13)
9	0.165(3)	0.687(3)	1.017(6)
10	0.164(5)	0.692(3)	1.020(8)

Source: Author.

connections predominate following mainly the preferential attachment mechanism, but as α increases, the local affinity effects increase, changing the community structure, which becomes more susceptible to social polarization. However, note that for $\alpha > 7$, these affinity effects

saturate and do not significantly impact the system robustness to disorder.

We use the finite-size scaling relations given by the equations (4.35), (4.36) and (4.37) and plot in Figure 40(a) the magnetization and (b) the magnetic susceptibility at the critical temperature versus the system size for several values of the local affinity α. The slopes estimate the critical exponents $\beta/\bar{\nu}$ and $\gamma/\bar{\nu}$ for all values of the α investigated. We remark that we found a new universality class as the set of critical exponents differs from previous systems and the majority-vote model on standard Barabási networks. We display the critical exponent values in table 3, also verifying that the unitary relation is followed for each value of α, as expected (VILELA et al., 2020). We also relate the critical exponents in Fig. 41, where we obtain the characteristic unitary line of the model. Here, the linear fit over the critical exponents $2\beta/\bar{\nu}$ and $\gamma/\bar{\nu}$ shows an averaged unitary exponent $\upsilon = 1.03(1)$.

7 CONCLUSION AND FINAL REMARKS

In this work, we explore two novel, groundbreaking interdisciplinary research fields that use tools from physics, mathematics, and computer science to investigate social and economic phenomena – *Sociophysics and Econophysics*. In particular, building on empirical evidence from the experiments of Solomon Asch and Gregory Berns that showed how social pressure shapes human behavior and perception of reality, we investigate the majority-vote model, a simple and powerful model to explore opinion formation dynamics.

A critical component in modeling social and economic systems is the complex network behind human connections. Based on the Barabási-Albert (BA) Model for scale-free networks, we propose a modification to include homophily effects and define the Affinity-Based model for Scale-Free Networks, which can more closely reflect the concave degree distribution of real social networks such as X and Facebook. We also show that Affinity-Based Scale-Free Networks can generate concave degree distributions, lower mean distances, higher clusterings and improved robustness than the original Barabasi-Albert scale-free networks.

In this study, we explored the dynamical and topological effects on the majority-vote model. On the dynamic side, we investigated the impact of collaborative behavior on opinion dynamics and the production of social entropy in communities. On the topological side, we analyzed how Affinity-Based Scale-Free Networks affect society's social dynamics.

We employ Monte Carlo simulations for both the cooperative majority-vote model on a square lattice and the majority-vote model defined on affinity-based scale-free networks and found a second-order consensus-dissensus phase transition. While the cooperative majority-vote model yields the same universality class as the 2D equilibrium Ising model, we discovered a new one for the majority-vote model on affinity-based scale-free networks. We show that improving the cooperative fraction f promotes the formation of a giant cluster of consenting individuals, suppressing the phase transition. The collaborative behavior enhance the social robustness of society to opinion disorder. On the other hand, the local affinity α decreases the community robustness and can lead to social polarization in social networks. This result shows how algorithms that increase the affinity in users can lead to platforms and virtual communities with high social polarization.

Using a mean-field approach, we validate the cooperative majority-vote model numerical results with analytical calculations. We use the master equation to obtain the expressions for

the order parameter and the critical social noise of the system, exhibiting qualitative agreement with the Monte Carlo results on the square lattice. We also confirm the analytical equations by comparing them with mean-field Monte Carlo simulations. We remark that, in the mean-field limit, the analytical solution is similar to the isotropic majority-vote model expression, where the noise q is replaced by the average noise of the system $\bar{q} = \bar{\mu}q = q[(1 - f(1 - \mu)]$.

We study the cooperative model entropy production by combining the Gibbs entropy with the master equation, and we find the analytical expression of the entropy production via the mean-field formulation. Our results for the entropy flux of the isotropic majority-vote model ($f = 0.0$) rectify previous results about the entropy production in the majority-vote model (CROCHIK; TOMÉ, 2005; TOMÉ; OLIVEIRA, 2015). We verify our calculations using the mean-field Monte Carlo simulation results.

Additionally, we conjecture that the coexistence of cooperative and non-cooperative individuals could be a potential natural manifestation of the Maximum Entropy Production Principle, where the most probable non-equilibrium steady states have the highest entropy production rate. Indeed, our simulations show that systems with a combination of collaborative and regular individuals maximize the system's stationary entropy production.

As an extension of this work, it would be essential to investigate the effects of cooperative behavior in the majority-vote model in complex networks. Additionally, the presence of non-compliance agents with $1 < \mu \leq 2$, with the opposite behavior of the collaborative agents, can be explored. A study of the impact of these dissent agents on opinion dynamics can deepen our understanding of society and the effects of collective noncooperative behavior on consensus dynamics.

REFERENCES

ALBERT, R.; JEONG, H.; BARABÁSI, A.-L. Diameter of the world-wide web. *nature*, Nature Publishing Group UK London, v. 401, n. 6749, p. 130–131, 1999.

ASCH, S. E. Opinions and social pressure. *Scientific American*, JSTOR, v. 193, n. 5, p. 31–35, 1955.

BALL, P. The physical modelling of society: a historical perspective. *Physica A: Statistical Mechanics and its Applications*, Elsevier, v. 314, n. 1-4, p. 1–14, 2002.

BARABÁSI, A.-L. Network science. *Philosophical Transactions of the Royal Society A: Mathematical, Physical and Engineering Sciences*, The Royal Society Publishing, v. 371, n. 1987, p. 20120375, 2013.

BAXTER, R. J. The inversion relation method for some two-dimensional exactly solved models in lattice statistics. *Journal of Statistical Physics*, Springer, v. 28, n. 1, p. 1–41, 1982.

BERNS, G. S.; CHAPPELOW, J.; ZINK, C. F.; PAGNONI, G.; MARTIN-SKURSKI, M. E.; RICHARDS, J. Neurobiological correlates of social conformity and independence during mental rotation. *Biological psychiatry*, Elsevier, v. 58, n. 3, p. 245–253, 2005.

BOGUNÁ, M.; PASTOR-SATORRAS, R.; DÍAZ-GUILERA, A.; ARENAS, A. Models of social networks based on social distance attachment. *Physical Review EStatistical, Nonlinear, and Soft Matter Physics*, APS, v. 70, n. 5, p. 056122, 2004.

CACIOPPO, J. T.; PATRICK, W. *Loneliness: Human nature and the need for social connection*. [S.l.]: WW Norton & Company, 2008.

CAMPOS, P. R. A.; OLIVEIRA, V. M. de; MOREIRA, F. G. B. Small-world effects in the majority-vote model. *Physical Review E*, APS, v. 67, n. 2, p. 026104, 2003.

CAPRARO, V. A model of human cooperation in social dilemmas. *PloS one*, Public Library of Science, v. 8, n. 8, p. e72427, 2013.

COSTA, L. S. A.; SOUZA, A. J. F. de. Continuous majority-vote model. *Physical Review E*, APS, v. 71, n. 5, p. 056124, 2005.

CROCHIK, L.; TOMÉ, T. Entropy production in the majority-vote model. *Physical Review E*, APS, v. 72, n. 5, p. 057103, 2005.

CROKIDAKIS, N.; OLIVEIRA, P. M. C. de. Impact of site dilution and agent diffusion on the critical behavior of the majority-vote model. *Physical Review E*, APS, v. 85, n. 4, p. 041147, 2012.

DYKE, J.; KLEIDON, A. The maximum entropy production principle: Its theoretical foundations and applications to the earth system. *Entropy*, Molecular Diversity Preservation International, v. 12, n. 3, p. 613–630, 2010.

EVANS, D. J.; COHEN, E. G. D.; MORRISS, G. P. Probability of second law violations in shearing steady states. *Physical review letters*, APS, v. 71, n. 15, p. 2401, 1993.

FARZAM, A.; SAMAL, A.; JOST, J. Degree difference: a simple measure to characterize structural heterogeneity in complex networks. *Scientific reports*, Nature Publishing Group UK London, v. 10, n. 1, p. 21348, 2020.

GALAM, S. Sociophysics: A review of galam models. *International Journal of Modern Physics C*, World Scientific, v. 19, n. 03, p. 409–440, 2008.

GALAM, S.; MOSCOVICI, S. Towards a theory of collective phenomena: Consensus and attitude changes in groups. *European Journal of Social Psychology*, Wiley Online Library, v. 21, n. 1, p. 49–74, 1991.

GELL-MANN, M. *The Quark and The Jaguar: Adventures in the Simple and Complex*. [S.l.]: Owl Books, 1995.

GOULD, H.; TOBOCHNIK, J.; MEREDITH, D. C.; KOONIN, S. E.; MCKAY, S. R.; CHRISTIAN, W. An introduction to computer simulation methods: applications to physical systems. *Computers in Physics*, American Institute of Physics, v. 10, n. 4, p. 349–349, 1996.

GRINSTEIN, G.; JAYAPRAKASH, C.; HE, Y. Statistical mechanics of probabilistic cellular automata. *Physical review letters*, APS, v. 55, n. 23, p. 2527, 1985.

HAWTHORNE, F.; HARUNARI, P. E.; OLIVEIRA, M. J. de; FIORE, C. E. Nonequilibrium thermodynamics of the majority vote model. *Entropy*, MDPI, v. 25, n. 8, p. 1230, 2023.

HOLT-LUNSTAD, J.; SMITH, T. B.; LAYTON, J. B. Social relationships and mortality risk: a meta-analytic review. *PLoS medicine*, Public Library of Science, v. 7, n. 7, p. e1000316, 2010.

HONG, H.; HA, M.; PARK, H. Finite-size scaling in complex networks. *Physical review letters*, APS, v. 98, n. 25, p. 258701, 2007.

JONG, G. J. A. L. T. de; VEIJER, J. Cooperative behavior in strategic decision making: Human capital and personality traits. *Behavioral strategy: Emerging perspectives*, p. 55–78, 2014.

KULLBACK, S.; LEIBLER, R. A. On information and sufficiency. *The annals of mathematical statistics*, JSTOR, v. 22, n. 1, p. 79–86, 1951.

LADYMAN, J.; LAMBERT, J.; WIESNER, K. What is a complex system? *European Journal for Philosophy of Science*, Springer, v. 3, p. 33–67, 2013.

LIMA, F. W. S. Majority-vote on undirected barabási-albert networks. *Communications in Computational Physics*, v. 2, n. 2, p. 358–366, 2007.

LIMA, F. W. S. Three-state majority-vote model on square lattice. *Physica A: Statistical Mechanics and its Applications*, Elsevier, v. 391, n. 4, p. 1753–1758, 2012.

LIMA, F. W. S. Majority-vote model with heterogeneous agents on square lattice. *International Journal of Modern Physics C*, World Scientific, v. 24, n. 11, p. 1350083, 2013.

MAES, C.; REDIG, F. Positivity of entropy production. *Journal of statistical physics*, Springer, v. 101, p. 3–15, 2000.

MARTYUSHEV, L. M.; SELEZNEV, V. D. Maximum entropy production principle in physics, chemistry and biology. *Physics reports*, Elsevier, v. 426, n. 1, p. 1–45, 2006.

MCAULEY, J.; LESKOVEC, J. *Social circles: Facebook*. 2012. Accessed: Jun 9, 2024. Available at: <https://snap.stanford.edu/data/egonets-Facebook.html>.

MCAULEY, J.; LESKOVEC, J. *Social circles: Twitter*. 2012. Accessed: Jun 9, 2024. Available at: <https://snap.stanford.edu/data/ego-Twitter.html>.

MELO, D. F. F.; PEREIRA, L. F. C.; MOREIRA, F. G. B. The phase diagram and critical behavior of the three-state majority-vote model. *Journal of Statistical Mechanics: Theory and Experiment*, IOP Publishing, v. 2010, n. 11, p. P11032, 2010.

METROPOLIS, N.; ROSENBLUTH, A. W.; ROSENBLUTH, M. N.; TELLER, A. H.; TELLER, E. Equation of state calculations by fast computing machines. *The journal of chemical physics*, American Institute of Physics, v. 21, n. 6, p. 1087–1092, 1953.

NEWMAN, M. E. Power laws, pareto distributions and zipf's law. *Contemporary physics*, Taylor & Francis, v. 46, n. 5, p. 323–351, 2005.

OLIVEIRA, I. V.; WANG, C.; DONG, G.; DU, R.; FIORE, C. E.; VILELA, A. L.; STANLEY, H. E. Entropy production on cooperative opinion dynamics. *Chaos, Solitons & Fractals*, Elsevier, v. 181, p. 114694, 2024.

OLIVEIRA, M. J. de. Isotropic majority-vote model on a square lattice. *Journal of Statistical Physics*, v. 66, n. 1, p. 273, 1992.

OLIVEIRA, M. J. de; MENDES, J. F. F.; SANTOS, M. A. Nonequilibrium spin models with ising universal behavior. *J. Phys. A: Math. Gen.*, v. 26, p. 2317, 1993.

ONNELA, J.-P.; SARAMÄKI, J.; HYVÖNEN, J.; SZABÓ, G.; LAZER, D.; KASKI, K.; KERTÉSZ, J.; BARABÁSI, A.-L. Structure and tie strengths in mobile communication networks. *Proceedings of the national academy of sciences*, National Acad Sciences, v. 104, n. 18, p. 7332–7336, 2007.

ONSAGER, L. Crystal statistics. i. a two-dimensional model with an order-disorder transition. *Physical Review*, APS, v. 65, n. 3-4, p. 117, 1944.

PENNISI, E. How did cooperative behavior evolve? *Science*, American Association for the Advancement of Science, v. 309, n. 5731, p. 93–93, 2005.

PEREIRA, L. F. C.; MOREIRA, F. G. B. Majority-vote model on random graphs. *Physical Review E*, APS, v. 71, n. 1, p. 016123, 2005.

PINCHAK, N. P.; BROWNING, C. R.; CALDER, C. A.; BOETTNER, B. Activity locations, residential segregation and the significance of residential neighbourhood boundary perceptions. *Urban Studies*, SAGE Publications Sage UK: London, England, v. 58, n. 13, p. 2758–2781, 2021.

PORCIÚNCULA, G. G.; JÚNIOR, M. I. S.; PEREIRA, L. F. C.; VILELA, A. L. Consensus effects of social media synthetic influence groups on scale-free networks. *arXiv preprint arXiv:2409.10830*, 2024.

SANTOS, M. A.; TEIXEIRA, S. Anisotropic voter model. *Journal of statistical physics*, Springer, v. 78, n. 3-4, p. 963–970, 1995.

SAVOIU, G.; SIMAN, I. I. Sociophysics: A new science or a new domain for physicists in a modern university. *Econophysics: Background and applications in economics, finance, and sociophysics*, Academic Press, p. 149–168, 2012.

SILVA, R. da; OLIVEIRA, M. J. de; TOMÉ, T.; FELÍCIO, J. Drugowich de. Analysis of earlier times and flux of entropy on the majority voter model with diffusion. *Physical Review E*, APS, v. 101, n. 1, p. 012130, 2020.

SIMMEL, G. Soziologie.: Untersuchungen über die formen der vergesellschaftung. Duncker & Humblot, 2013.

STANLEY, H. E. *Phase transitions and critical phenomena. Clarendon*. [S.l.]: Oxford, 1971.

STAUFFER, D.; OLIVEIRA, S. M. M. de; OLIVEIRA, P. M. C. de; MARTINS, J. S. de S. *Biology, sociology, geology by computational physicists*. [S.l.]: Elsevier, 2006.

STROGATZ, S. H. *Nonlinear dynamics and chaos: with applications to physics, biology, chemistry, and engineering*. [S.l.]: CRC press, 2018.

THOMAS, R. J. Sources of friendship and structurally induced homophily across the life course. *Sociological Perspectives*, SAGE Publications Sage CA: Los Angeles, CA, v. 62, n. 6, p. 822–843, 2019.

TIZZONI, M.; BAJARDI, P.; POLETTO, C.; RAMASCO, J. J.; BALCAN, D.; GONÇALVES, B.; PERRA, N.; COLIZZA, V.; VESPIGNANI, A. Real-time numerical forecast of global epidemic spreading: case study of 2009 a/h1n1pdm. *BMC medicine*, Springer, v. 10, p. 1–31, 2012.

TOMÉ, T.; OLIVEIRA, M. J. de. *Stochastic dynamics and irreversibility*. [S.l.]: Springer, 2015.

VIEIRA, A. R.; CROKIDAKIS, N. Phase transitions in the majority-vote model with two types of noises. *Physica A: Statistical Mechanics and its Applications*, Elsevier, v. 450, p. 30–36, 2016.

VILELA, A. L. M.; MOREIRA, F. G. B.; SOUZA, A. J. F. de. Majority-vote model with a bimodal distribution of noises. *Physica A: Statistical Mechanics and its Applications*, Elsevier, v. 391, n. 24, p. 6456–6462, 2012.

VILELA, A. L. M.; SOUZA, A. J. F. de. Majority-vote model with a bimodal distribution of noises in small-world networks. *Physica A: Statistical Mechanics and its Applications*, v. 488, p. 216–223, 2017.

VILELA, A. L. M.; STANLEY, H. E. Effect of strong opinions on the dynamics of the majority-vote model. *Scientific reports*, Nature Publishing Group, v. 8, n. 1, p. 1–8, 2018.

VILELA, A. L. M.; ZUBILLAGA, B. J.; WANG, C.; WANG, M.; DU, R.; STANLEY, H. E. Three-state majority-vote model on scale-free networks and the unitary relation for critical exponents. *Scientific Reports*, v. 10, p. 8255, 2020.

YEOMANS, J. M. *Statistical mechanics of phase transitions*. [S.l.]: Clarendon Press, 1992.

Appendix: Proof of Jensen's Inequality

Jensen's inequality is a fundamental theorem of probability theory with applications in information theory and machine learning. This work uses this theorem to show that the entropy production equation is always nonnegative, in conformity with the second law of thermodynamics in Sec. 4.

Theorem (Jensen's Inequality): Let $f : \mathbb{R} \to \mathbb{R}$ be a convex function, and let $x_1, x_2, \ldots, x_n$ be real numbers. If $t_1, t_2, \ldots, t_n$ are non-negative weights such that

$$\sum_{i=1}^{n} t_i = 1, \tag{1}$$

then

$$f\left(\sum_{i=1}^{n} t_i x_i\right) \leq \sum_{i=1}^{n} t_i f(x_i). \tag{2}$$

Proof by Induction

For $n = 1$, we trivially have

$$f(x_1) \leq f(x_1). \tag{3}$$

For $n = 2$, let $t_1 + t_2 = 1$, with $t_1, t_2 \geq 0$. Geometrically, the convexity condition means that the function f lies below the secant line connecting any two points on its graph. Therefore,

$$f(t_1 x_1 + t_2 x_2) \leq t_1 f(x_1) + t_2 f(x_2). \tag{4}$$

That is, the function evaluated at a weighted average of two points is less than or equal to the same weighted average of function values at those two points.

We assume the inequality holds for $n \in \mathbb{N}$ with $n > 2$. We show by induction that it still holds for $n = k + 1$.

If $t_{k+1} = 1$, then $t_i = 0$ for $i = 1, 2, \ldots, k$, and the inequality reduces to:

$$f(x_{k+1}) \leq f(x_{k+1}), \tag{5}$$

which is trivially true. Now, if $t_{k+1} \neq 1$, then we write

$$f\left(\sum_{i=1}^{k+1} t_i x_i\right) = f\left((1 - t_{k+1}) \sum_{i=1}^{k} \frac{t_i}{1 - t_{k+1}} x_i + t_{k+1} x_{k+1}\right). \tag{6}$$

Now, applying the result for $n = 2$, we have the upper bound on the right term as:

$$f\left(\sum_{i=1}^{k+1} t_i x_i\right) \leq (1 - t_{k+1}) f\left(\sum_{i=1}^{k} \frac{t_i}{1 - t_{k+1}} x_i\right) + t_{k+1} f(x_{k+1}). \tag{7}$$

Thus, applying the inductive hypothesis for $f\left(\sum_{i=1}^{k} \frac{t_i}{1-t_{k+1}} x_i\right)$, we get

$$f\left(\sum_{i=1}^{k+1} t_i x_i\right) \leq (1-t_{k+1}) \sum_{i=1}^{k} \frac{t_i}{1-t_{k+1}} f(x_i) + t_{k+1} f(x_{k+1}) = \sum_{i=1}^{k+1} t_i f(x_i). \tag{8}$$

Therefore, we conclude our proof.

ANNEX A – PUBLISHED PAPER AT CHAOS, SOLITONS AND FRACTALS, 181 (2024) 114694

Chaos, Solitons and Fractals 181 (2024) 114694

Contents lists available at ScienceDirect

Chaos, Solitons and Fractals

journal homepage: www.elsevier.com/locate/chaos

Entropy production on cooperative opinion dynamics

Igor V.G. Oliveira [a,b], Chao Wang [c,*], Gaogao Dong [d], Ruijin Du [e], Carlos E. Fiore [f], André L.M. Vilela [a,b,g,h], H. Eugene Stanley [h]

[a] Física de Materiais, Universidade de Pernambuco, Recife, PE 50720-001, Brazil
[b] Departamento de Física, Universidade Federal de Pernambuco, Recife, PE 50670-901, Brazil
[c] College of Economics and Management, Beijing University of Technology, Beijing, 100124, China
[d] School of Mathematical Sciences, Jiangsu University, Zhenjiang, 212013, China
[e] Center of Energy Development and Environmental Protection, Jiangsu University, Zhenjiang, 212013, China
[f] Instituto de Física, Universidade de São Paulo, São Paulo, SP, 05314-970, Brazil
[g] Data Science and Analytics, SUNY Polytechnic Institute, Utica, NY 13502, USA
[h] Center for Polymer Studies and Department of Physics, Boston University, Boston, MA 02215, USA

ARTICLE INFO

Keywords:
Complex systems
Consensus dynamics
Phase transition
Critical phenomena

ABSTRACT

As one of the most widespread social dynamics, cooperative behavior is among the most fascinating collective phenomena. Several animal species, from social insects to human beings, feature social groups altruistically working for a common benefit. This collaborative conduct pervades the actions and opinions of individuals, yielding strategic decision-making between political, religious, ethnic, and economic social puzzles. Here, we explore how cooperative behavior phenomena impact collective opinion dynamics and entropy generation in social groups. We select a random fraction f of community members as collaborative individuals and model the opinion dynamics using a social temperature parameter q that functions as a social anxiety noise. With probability q, regular individuals oppose their companions about a social decision, assuming group dissent. Collaborative agents experience a reduced effective social noise μq, where $0 < \mu < 1$ is the social anxiety noise sensibility parameter that enhances social validation. We perform numerical simulations and mean-field analysis and find the system undergoes nonequilibrium order–disorder phase transitions with expressive social entropy production. Our results highlight the effects of a social anxiety attenuation level in improving group consensus and the emergence of cooperative dynamics as a natural maximization of entropy production in noisy social groups, thus inducing exuberant collective phenomena in complex systems.

1. Introduction

In light of the pervasive influence of technology, the diverse and significant challenges surrounding information dissemination have propelled intense scientific research into Sociophysics models. Several dynamics regarding opinion formation on regular and complex networks were widely proposed to investigate social, financial, and professional interactions in groups of individuals or societies. Such physical models can capture the main features of complex collective phenomena in real societies. Similar to condensed matter systems, different opinion models exhibit intense critical dynamics and nontrivial nonequilibrium phase transitions [1–25].

Within the Sociophysics framework, the majority-vote model is an agent-based representation of interacting individuals in a contact network [24–45]. The model consists of a system of agents that hold opinions for or against some issue, and the stochastic variable σ_i, which assumes one of the two values ± 1, represents the opinion of an individual i at a given time. The majority-vote model evolves by an inflow dynamics, where each agent agrees with the majority of its neighbors with probability $1 - q$ and disagrees with chance q. The quantity q is called the noise parameter of the model, and it relates to a level of social anxiety, or social temperature, of the system.

Among several variations of this model, we highlight the investigation of majority-vote dynamics under the framework of random graphs and complex networks of interactions. In these studies, the authors find that group ordering, or opinion polarization in a society, is strongly related to the number of interacting neighbors [29–34], while additional investigations focus on social dynamics of systems composed of heterogeneous agents [35–38,41].

Inspired by real-world social group behavior, scientists developed further generalizations of the model, such as the three-state interpretation and different opinion functions, under the influence of regular and

* Corresponding author.
E-mail address: chaowanghn@vip.163.com (C. Wang).

https://doi.org/10.1016/j.chaos.2024.114694
Received 13 January 2024; Received in revised form 26 February 2024; Accepted 1 March 2024
Available online 11 March 2024

complex networks [43–48]. Nonetheless, based on opinion dynamics, examinations of this model rendered insights on second-order phase transitions, proposing criteria for the volumetric scaling of physical quantities at the critical point, yielding a universal relation for critical exponents regardless of the structure of the interaction network [48]. Recent studies on the economic behavior of brokers in financial markets reproduced real-world market features apprised by majority-vote dynamics [49–52].

Cooperative behavior is one of the most widespread collective social phenomena that still challenge scientists. Several animal species, from insects to human beings, exhibit social groups working for a joint benefit. Typical cooperative behavior, such as group hunting and reciprocity protection, makes species more competitive. Without this phenomenon, social institutions, non-governmental organizations, governments, culture, education, transport, health systems, among others, could be unattainable. Collaborative manners permeate the actions and opinions of individuals, imbuing strategic decision-making related to social dilemmas such as political, religious, ethnic, and economic challenges [53–55]. In this paper, we design an anisotropic social model to investigate the influence of cooperative voters on group opinion evolution.

We propose an agent-based model with two types of individuals, collaborative and regular, who exhibit different chances to adopt the dominant opinion expressed in a social group. We introduce a parameter $\mu \in (0, 1)$, named noise sensibility, to the standard majority-vote model to yield a distinct influence of social anxiety over individuals. Hence, a cooperative individual is under an effective attenuated social temperature μq, while a regular individual is subject to the regular noise q.

Our results show that the consensus is strongly related to the number of collaborative individuals and noise sensibility. Numerical and analytical results add a significant new twist to the remarkable observation of the entropy flux of the mean-field majority-vote model [56–58]. We achieve a general expression for isotropic and anisotropic cases and verify our results using numerical simulations in the mean-field formulation.

2. Model

In the isotropic majority-vote model (MVM), each agent occupies a node i of a given network of social interactions. A spin variable σ_i represents the opinion of the agent i about a particular subject or in a referendum in an instant t. In the isotropic version, an individual is under a probability $1 - q$ that its opinion σ_i follows the majority state of its interacting neighbors while assuming the minority state with probability q [24,25].

In this work, we analyze a square lattice opinion network with L^2 nodes, where a randomly chosen fraction f of agents have noise sensibility $0 < \mu < 1$, addressing the behavior of the cooperative individuals. In contrast, the complementary fraction $1 - f$ of regular voters follow the standard majority-vote dynamics, i.e., $\mu = 1$. Thus, for noise level q, we denote the flipping probability of a given opinion σ_i as

$$w_i(\sigma) = \frac{1}{2}\left[1 - (1 - 2\mu_i q)\sigma_i S\left(\sum_{\delta=1}^{4}\sigma_{i+\delta}\right)\right], \tag{1}$$

the summation runs over all the four first neighboring opinions that influence the individual i and $S(x)$ stands for the signal function, where $S(x) = -1, 0, 1$ for $x < 0$, $x = 0$, and $x > 0$, respectively. Furthermore,

$$\mu_i = \begin{cases} \mu, & \text{if } i \text{ is a cooperative agent.} \\ 1, & \text{if } i \text{ is a regular agent.} \end{cases} \tag{2}$$

That is, a cooperative individual agrees with the majority with probability $1 - \mu q$, and disagrees with probability μq. Thus, noise sensibility $\mu < 1$ increases the agreement probability by attenuating the effect of the noise parameter q on society.

The cooperative majority-vote dynamics with $f = 0$ capture the behavior of the isotropic majority-vote model with noise [24,25]. For $f = 1$, all individuals are cooperative, and the system also behaves as the standard MVM under the linear transformation $q \longrightarrow q/\mu$. In contrast, highlighting the effects of the noise sensibility μ, we recover the standard flip probability of the isotropic MVM when $\mu = 1$, in which all the agents are under the influence of the same social temperature q. The case for $\mu = 0$ corresponds to a bimodal distribution of noise, where a fraction f of the individuals are noiseless, always agreeing with its nearest interacting neighbors, scrutinized in previous investigations [36,41]. In this research, we perform numerical Monte Carlo simulations and a mean-field analytical procedure for the general cases of $0 < f < 1$ and $0 < \mu < 1$.

3. Cooperative stationary dynamics

To investigate the critical behavior of the model, we consider the order parameter m given by

$$m = \frac{1}{L^2}\left|\sum_{i=1}^{L^2}\sigma_i\right|. \tag{3}$$

We also consider magnetization $M_L(q, \mu, f)$, magnetic susceptibility $\chi_L(q, \mu, f)$, and Binder fourth-order cumulant $U_L(q, \mu, f)$

$$M_L(q, \mu, f) = \langle\langle m\rangle_t\rangle_c\,, \tag{4}$$

$$\chi_L(q, \mu, f) = L^2\left[\langle\langle m^2\rangle_t\rangle_c - \langle\langle m\rangle_t\rangle_c^2\right], \tag{5}$$

$$U_L(q, \mu, f) = 1 - \frac{\langle\langle m^4\rangle_t\rangle_c}{3\langle\langle m^2\rangle_t\rangle_c^2}, \tag{6}$$

where $\langle\ldots\rangle_t$ represents time averages taken in the stationary regime, and $\langle\ldots\rangle_c$ stands for configurational averages taken over independent realizations.

We perform Monte Carlo simulations on square lattice networks with L ranging from 40 to 200 and periodic boundary conditions. One Monte Carlo step (MCS) corresponds to the trial of updating N opinions randomly chosen accordingly to (1). Next, we discard 2×10^4 MCS to allow the system to reach the steady state and take the time averages over the subsequent 10^5 MCS. We repeat the process up to 100 independent samples to compute configurational averages. In our results, the statistical uncertainty is smaller than the symbol size.

In Fig. 1, we deliver snapshots of simulations for square lattices with $L = 200$, $q = 0.12$ and $\mu = 0.5$, for different values of collaborative fraction f: (a) 0.00, (b) 0.20, (c) 0.50 and (d) 1.00. White and black dots represent opinions $+1$ and -1, respectively. For fixed levels of μ and q, the collaborative agents increase the local consensus around them by supporting their contacts' opinions. This collective phenomenon yields a white cluster of agents with the same opinion, which increases with the fraction f of cooperative agents in figures (a) to (d), thus promoting social order.

Fig. 2 illustrates how the cooperative fraction of agents f improves social order when they have a 50% boosted chance of agreeing with their neighbors ($\mu = 0.5$). We plot (a) magnetization $M_L(q, \mu, f)$, (b) susceptibility $\chi_L(q, \mu, f)$, and (c) Binder cumulant $U_L(q, \mu, f)$ versus cooperative fraction f for $L = 200$, $\mu = 0.5$ and several values of q. Note that for each level of social anxiety q, the system undergoes a disorder–order transition for increasing values of f, agreeing with Fig. 1. We highlight the limiting cases $q = 0$ and $q = 0.3$ for $\mu = 0.5$ in Fig. 2(a), which are insensitive to f.

Fig. 3 shows how the nonconformity parameter q affects societies with different fractions of cooperative individuals for noise sensibility fixed at $\mu = 0.5$. We plot (a) magnetization $M_L(q, \mu, f)$, (b) susceptibility $\chi_L(q, \mu, f)$, and (c) Binder cumulant $U_L(q, \mu, f)$ versus social anxiety level q for $L = 200$. For small noise q, $M_L(q, \mu, f) = O(1)$ indicates the ordered phase of the social system with one dominant opinion. By

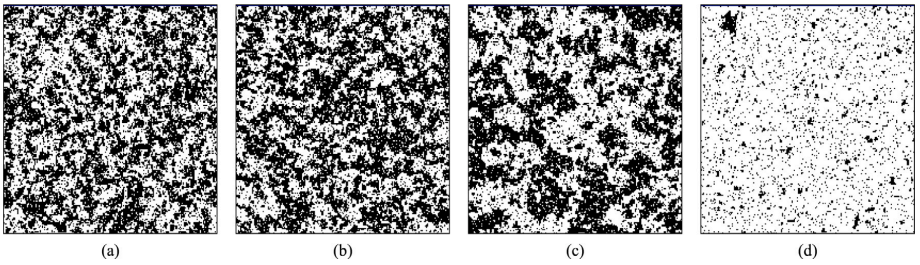

Fig. 1. Snapshots of a single simulation on a square network with $L = 200$, $q = 0.12$ and noise sensibility $\mu = 0.5$. (a) cooperative fraction $f = 0.00$, (b) $f = 0.20$, (c) $f = 0.50$, and (d) $f = 1.00$. Increasing f promotes social system consensus. White (black) dots represent +1 (−1) opinions.

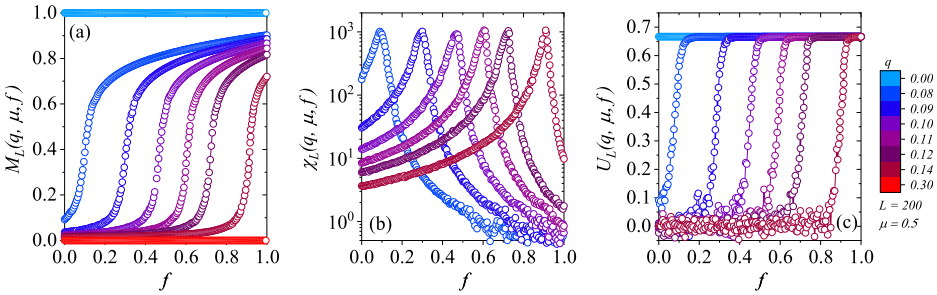

Fig. 2. Disorder–order transitions induced by the fraction of cooperative agents. In this configuration, $L = 200$ and $\mu = 0.5$ for different values of q. Figures (a), (b), and (c) stand for magnetization, susceptibility, and Binder cumulant, respectively. From left to right, $q = 0.08, 0.09, 0.10, 0.11, 0.12$ and 0.14. Results for $q = 0.0$ and $q = 0.3$ are insensitive to f for $\mu = 0.5$.

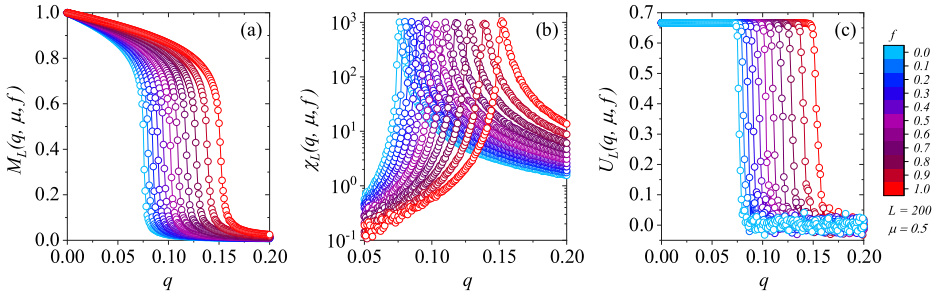

Fig. 3. Stationary averages of the cooperative majority-vote opinion dynamics. Square lattice simulations for $L = 200$, $\mu = 0.5$, and several values of f. Noise dependence of (a) average opinion (b) susceptibility, and (c) Binder cumulant. From left to right, f increases from 0.0 to 1.0 with $\Delta f = 0.1$ increments. The lines are guides to the eyes.

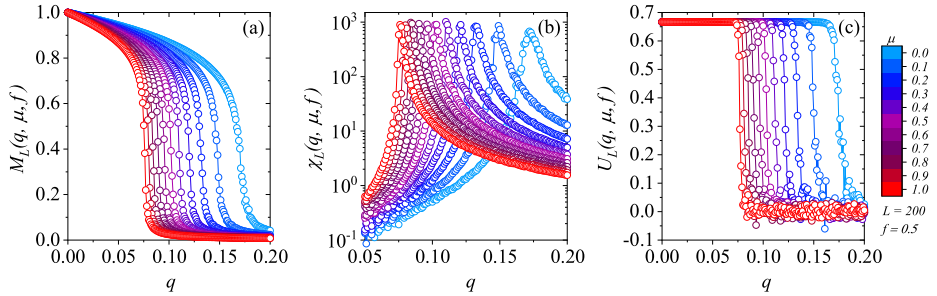

Fig. 4. Effects of the intensity μ of cooperative behavior on consensus robustness. (a) Magnetization $M(q,\mu,f)$, (b) magnetic susceptibility $\chi(q,\mu,f)$ and (c) Binder fourth-order cumulant $U(q,\mu,f)$ for diverse values of μ. From right to left, μ changes from 0.0 to 1.0 with $\Delta\mu = 0.1$ and $f = 0.5$. The lines are guides to the eyes.

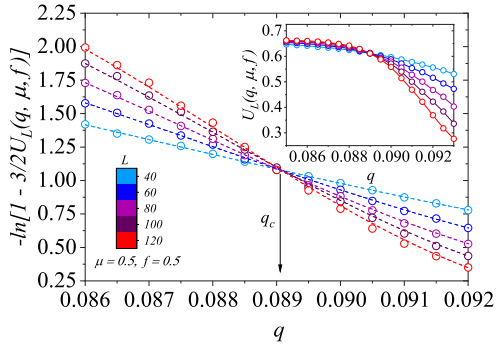

Fig. 5. Critical noise estimative. Binder fourth-order cumulant $U_L(q, \mu, f)$ for $\mu = 0.5$ and cooperative fraction $f = 0.3$. The point where the curves for different sizes L intersect provides an estimate for critical social temperature $q_c(\mu, f)$ in the thermodynamic limit $N \to \infty$. The dashed lines are cubic fits of the data points in critical region, and the continuous lines are guides to the eyes.

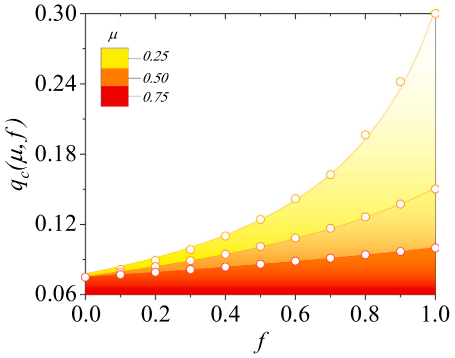

Fig. 6. Phase diagram of cooperative majority-vote opinion dynamics. The curves are descriptions of the phase boundary that separates the ordered and disordered phases for different values of noise sensibility μ. Circles represent the numerical estimates of critical points $q_c(\mu, f)$, obtained by the crossing point of the Binder cumulant curves for different system sizes. Lines are fits from Eq. (7).

increasing social temperature q, $M_L(q, \mu, f)$ decreases to zero for all values of the cooperative fraction f at a critical noise level $q = q_c(\mu, f)$. Systems with more cooperative agents support partial consensus for higher social temperatures, yielding a higher critical noise $q_c(\mu, f)$.

For $q > q_c(\mu, f)$, $M_L(q, \mu, f) \approx 0$, and the community exhibits two opinions approximately in the same share, not supporting consensus even with the presence of cooperative individuals. The system undergoes a second-order phase transition near a critical temperature $q_c(\mu, f)$, where the magnetic susceptibility $\chi_L(q, \mu, f)$ exhibits a maximum and the Binder cumulant $U_L(q, \mu, f)$ decreases swiftly. We remark that the critical noise value is an increasing function of the cooperative fraction f since such agents improve consensus.

In Fig. 4, we study how different intensities of the cooperative behavior phenomena influence consensus when half of the community is collaborative $f = 0.5$. We investigate the behavior of (a) magnetization $M_L(q, \mu, f)$, (b) susceptibility $\chi_L(q, \mu, f)$, and (c) Binder cumulant $U_L(q, \mu, f)$ as a function of q for $L = 200$ and diverse values of the noise sensibility μ. Decreasing μ stimulates the individuals to cooperate, reinforcing robustness to opinion disorder. Consequently, we observe that the critical noise $q_c(\mu, f)$ is a monotonically decreasing function of the noise sensibility μ for a non-zero fraction of cooperative agents.

Observe that as μ decreases, the range of social temperatures q for which the community exhibits a partial consensus increases. Indeed, each cooperative individual serves as a social influence on their neighbors, promoting the growth of a consenting cluster. This phenomenon directly affects the critical noise $q_c(\mu, f)$, in which $M(q_c) \to 0$. We conclude that the critical noise is a monotonically decreasing function of μ for a non-zero fraction of cooperative agents.

3.1. Phase diagram

To obtain a precise estimate of the critical social temperature $q_c(\mu, f)$ in the thermodynamic limit $N \to \infty$, which is independent of the society scale L, we calculate the Binder fourth-order cumulant for each pair (μ, f) with different system sizes. In Fig. 5, we exemplify this method by displaying the Binder cumulant for $\mu = 0.5$ and $f = 0.3$. We estimate the critical noise value $q_c(\mu, f)$ from the intersection point of Binder curves for different sizes L, since U does not depend on the system size only at $q = q_c(\mu, f)$. We find $q_c(\mu, f) = 0.0891(2)$ for $\mu = 0.5$ and $f = 0.3$. In Table 1, we summarize the results for the same process employing other values of f and μ, rendering the phase diagram shown in Fig. 6.

The interpolation of critical points $q_c(\mu, f)$ in Fig. 6 generates a description of the phase boundary that separates the ordered and disordered phases for each value of the noise sensibility μ. We note that consensus correlates with noise sensibility, and lower values of μ tend to yield higher values of q_c. Consensus robustness is also proportional to f since it controls the fraction under the influence of an effective noise reduction. From the data, we propose the phase boundary lines to obey an equation of type

$$q_c(\mu, f) = \frac{1}{a - bf}, \tag{7}$$

in which a and b are parameters that depend on μ. By conducting a non-linear curve fitting using Eq. (7), we estimate $[a, b] = [12.8(5), 9.4(5)], [13.2(1), 6.5(1)], [13.2(1), 3.3(1)]$, for $\mu = 0.25, 0.50$ and 0.75, respectively. From Table 1, we obtain $q_c(\mu, 0) = 1/a \approx 0.075$, in agreement with the isotropic MVM [24], and $q_c(\mu, 1) = 1/(a - b) \approx 0.075/\mu$ as expected from previous analysis.

3.2. Critical exponents

We examine finite-size effects on the social dynamics of the cooperative majority-vote model. In Fig. 7, we exhibit (a) magnetization, (b) susceptibility and (c) Binder cumulant for $f = 0.8$ and $\mu = 0.5$, with $L = 40, 60, 80, 100$ and 120. Note that at the critical point $q_c(\mu, f) \approx 0.13$ (see Table 1), $M \to 0$ as $L \to \infty$, remaining non-zero for noise values below $q_c(\mu, f)$. Also, the larger L, the more intense the magnetization fluctuations, yielding the highest peaks observed for the magnetic susceptibilities near $q_c(\mu, f)$.

To further analyze the behavior of M, χ, and U with system size L near the critical point, we estimate the critical exponents β/ν, γ/ν, and $1/\nu$ that characterize the phase transition of the model. Thus, we write the following finite-size scaling relations

$$M_L(q, \mu, f) = L^{-\frac{\beta}{\nu}} \widetilde{M}(\varepsilon L^{\frac{1}{\nu}}), \tag{8}$$

$$\chi_L(q, \mu, f) = L^{\frac{\gamma}{\nu}} \widetilde{\chi}(\varepsilon L^{\frac{1}{\nu}}), \tag{9}$$

$$U_L(q, \mu, f) = \widetilde{U}(\varepsilon L^{\frac{1}{\nu}}), \tag{10}$$

where $\varepsilon = q - q_c(\mu, f)$ is the distance from critical noise, and the universal scaling functions $\widetilde{M}$, $\widetilde{\chi}$ and $\widetilde{U}$ depend only on scaling variable $x = \varepsilon L^{\frac{1}{\nu}}$. Accordingly, we use these equations to obtain the phase transition critical exponents and capture the universal behavior of magnetization, magnetic susceptibility, and Binder cumulant.

In Fig. 8, we illustrate the numerical results for (a) M, (b) χ and (c) U versus the system size L at $q_c(\mu, f)$, with $\mu = 0.5$ and several values

Table 1
Critical social temperatures on square lattices and mean-field numerical estimates $q_c(\mu, f)$ and $q_c^{MF}(\mu, f)$, respectively, as a function of f and μ for the cooperative majority-vote dynamics.

f	$q_c(\mu = 1/4)$	$q_c(\mu = 1/2)$	$q_c(\mu = 3/4)$	$q_c^{MF}(\mu = 1/4)$	$q_c^{MF}(\mu = 1/2)$	$q_c^{MF}(\mu = 3/4)$
0.0	0.0750(1)	0.0750(3)	0.0750(1)	0.1665(1)	0.1665(1)	0.1664(3)
0.1	0.0816(2)	0.0791(2)	0.0771(1)	0.1802(1)	0.1753(1)	0.1711(2)
0.2	0.0894(1)	0.0839(1)	0.0792(1)	0.1957(3)	0.1851(1)	0.1750(1)
0.3	0.0986(1)	0.0891(2)	0.0814(1)	0.2149(1)	0.1961(1)	0.1799(2)
0.4	0.1101(2)	0.0947(2)	0.0837(1)	0.2376(4)	0.2077(3)	0.1848(1)
0.5	0.1243(1)	0.1011(1)	0.0861(2)	0.2667(1)	0.2224(2)	0.1904(1)
0.6	0.1420(3)	0.1085(2)	0.0886(2)	0.3031(3)	0.2373(1)	0.1955(1)
0.7	0.1626(3)	0.1167(2)	0.0912(2)	0.3507(1)	0.2566(2)	0.2018(2)
0.8	0.1963(3)	0.1264(2)	0.0941(2)	0.4163(4)	0.2768(2)	0.2076(1)
0.9	0.2418(3)	0.1374(1)	0.0970(1)	0.5128(1)	0.3033(3)	0.2152(1)
1.0	0.3002(1)	0.1503(2)	0.1000(1)	0.6664(1)	0.3332(2)	0.2221(1)

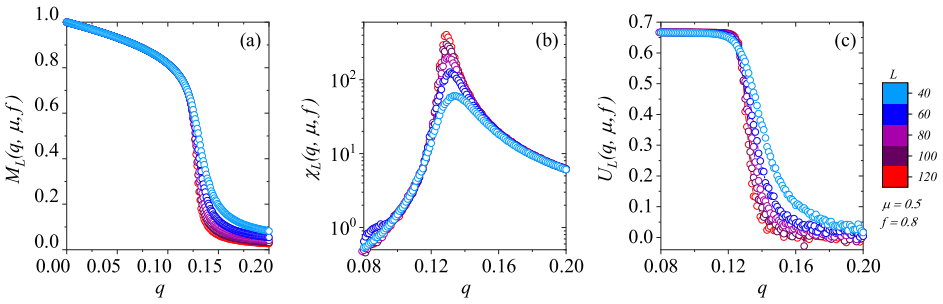

Fig. 7. Size dependence on consensus robustness versus noise parameter. In (a) average opinion, (b) susceptibility and (c) Binder cumulant U for system sizes $L = 40, 60, 80, 100,$ and 120. In this result, $f = 0.8$ and $\mu = 0.5$. The lines are guides to the eyes.

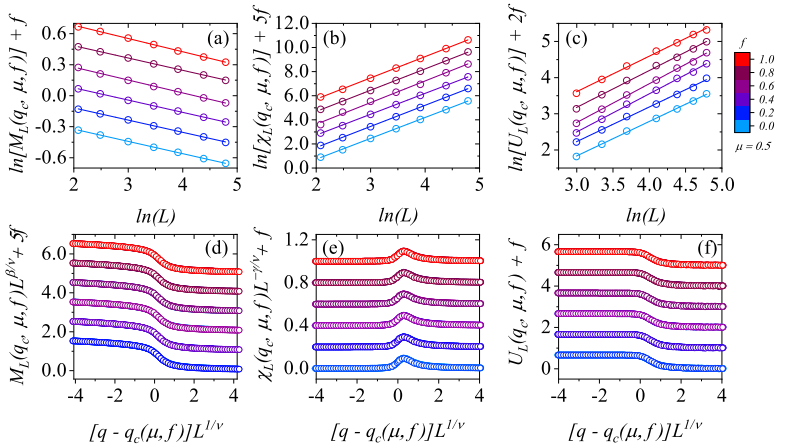

Fig. 8. Finite-size scaling analysis and universality. (a) Magnetization, (b) magnetic susceptibility, and (c) Binder fourth-order cumulant at the critical point $q = q_c(\mu, f)$ as functions of linear system size L in log–log scale for several values of the cooperative fraction f and $\mu = 0.5$. The lines represent linear fits to the data, yielding the standard Ising model critical exponents on square lattices considering error bars. We rescale all quantities, rendering one universal curve for critical exponents $\beta/\nu = 0.125$, $\gamma/\nu = 1.75$, and $1/\nu = 1$. We shift curves up to avoid overlap.

of f. By measuring the linear coefficient of each line in Fig. 8(a), (b) and (c), we estimate $\beta/\nu \approx 0.125$, $\gamma/\nu \approx 1.75$ and $1/\nu \approx 1$ considering the error bars. We confirm our results by performing a data collapse of rescaled versions (d) $\widetilde{M}$, (e) $\widetilde{\chi}$ and (f) $\widetilde{U}$ over the rescaled social noise using $\beta/\nu = 0.125$, $\gamma/\nu = 1.75$ and $1/\nu = 1$. Despite the different behaviors observed in Figs. 3 and 7, Fig. 8(d), (e), and (f) yield a single universal curve independently on f.

We further investigate critical exponents for $\mu = 0.25$ and $\mu = 0.75$, and the results also supply the same set of critical exponents. We conclude that the critical exponents of the cooperative majority-vote model are the same as those in an equilibrium two-dimensional Ising model and for the isotropic majority-vote dynamics [24], regardless of μ and f. This result is under Grinstein's criterion that states that nonequilibrium stochastic spin-like systems with up-down symmetry in

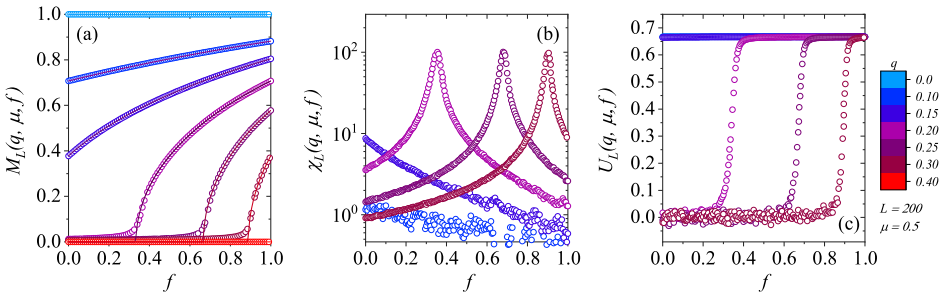

Fig. 9. Plots of the (a) magnetization, (b) magnetic susceptibility, and (c) Binder cumulant as a function of f for several values of the noise q for $\mu = 0.5$. The dashed lines on (a) stand for the analytical results given by Eq. (21), and the symbols are the numerical results for 20 samples with $L = 200$.

regular lattices fall into the same universality class of the equilibrium Ising model [59,60].

3.3. Mean-field analyses

A given configuration of opinions can be denoted by $\sigma = (\sigma_1, \sigma_2, \dots, \sigma_i, \dots, \sigma_N)$, with $N = L^2$. We obtain the behavior of the stationary magnetization m using the master equation that expresses the evolution of the probability $P(\sigma, t)$ of finding the system in the state σ at a time t [61,62]

$$\frac{d}{dt}P(\sigma,t) = \sum_{i=1}^{N}\left[w_i(\sigma^i)P(\sigma^i,t) - w_i(\sigma)P(\sigma,t)\right], \tag{11}$$

where the state σ^i can be obtained from state σ flipping the ith agent's opinion, i.e., $\sigma^i = (\sigma_1, \sigma_2, \dots, -\sigma_i, \dots, \sigma_N)$. Factor w_i is the flip rate of the ith individual $\sigma_i \to -\sigma_i$, given by Eq. (1) for the cooperative voter model. From Eq. (11), it follows that the time evolution of the average opinion of the agent σ_i is

$$\frac{d}{dt}\langle\sigma_i\rangle = -2\langle\sigma_i w_i\rangle. \tag{12}$$

Thus, for all Nf cooperative individuals, we write the following set of equations

$$\frac{d}{dt}\langle\sigma_j\rangle = -\langle\sigma_j\rangle + \Theta_\mu\left\langle S\left(\sum_\delta \sigma_{j+\delta}\right)\right\rangle, \tag{13}$$

for $j = 1, 2, \dots, Nf$, where we replace w_j using Eq. (1) with $\Theta_\mu = 1-2\mu q$ and $\sigma_j^2 = 1$. Similarly, for the remaining $N(1-f)$ agents, we have

$$\frac{d}{dt}\langle\sigma_k\rangle = -\langle\sigma_k\rangle + \Theta\left\langle S\left(\sum_\delta \sigma_{k+\delta}\right)\right\rangle, \tag{14}$$

where $\Theta = 1-2q$ and $k = Nf+1, Nf+2, \dots, N$. Adding Eqs. (13) and (14) and summing for all agents, we obtain

$$\sum_{i=1}^{N}\frac{d}{dt}\langle\sigma_i\rangle = -\sum_{i=1}^{N}\langle\sigma_i\rangle + N\left[f\Theta_\mu + (1-f)\Theta\right]\left\langle S\left(\sum_\delta \sigma_{i+\delta}\right)\right\rangle. \tag{15}$$

In the mean-field limit, a randomly chosen agent σ_i interacts with four neighbors also randomly selected. Labeling these neighbors as σ_a, σ_b, σ_c and σ_d, we write [57,58]

$$S\left(\sum_\delta \sigma_{i+\delta}\right) = S(\sigma_a+\sigma_b+\sigma_c+\sigma_d)$$

$$= \frac{3}{8}(\sigma_a+\sigma_b+\sigma_c+\sigma_d) - \frac{1}{8}(\sigma_a\sigma_b\sigma_c + \sigma_a\sigma_b\sigma_d + \sigma_a\sigma_c\sigma_d + \sigma_b\sigma_c\sigma_d). \tag{16}$$

In addition, in the stationary state, $m \approx \langle\sigma_i\rangle$ and $\langle\sigma_l\sigma_u\sigma_v\rangle \approx \langle\sigma_l\rangle\langle\sigma_u\rangle\langle\sigma_v\rangle \approx m^3$. Thus, we write

$$\left\langle S\left(\sum_\delta \sigma_{i+\delta}\right)\right\rangle = \frac{m}{2}(3-m^2). \tag{17}$$

By using this result in Eq. (15), we obtain

$$\frac{d}{dt}m = m\left\{-\epsilon - \frac{m^2}{2}\left[f\Theta_\mu + (1-f)\Theta\right]\right\}, \tag{18}$$

where

$$\epsilon = 1 - \frac{3}{2}\left[f\Theta_\mu + (1-f)\Theta\right]. \tag{19}$$

In the stationary state, $dm/dt = 0$. For $\epsilon > 0$, there is only one real solution, $m = 0$, representing the paramagnetic state (disordered). For $\epsilon < 0$, we obtain the ferromagnetic state (ordered) solution

$$m = \sqrt{\frac{2|\epsilon|}{f\Theta_\mu + (1-f)\Theta}}, \tag{20}$$

Then, using $\Theta_\mu = 1-2\mu q$ and $\Theta = 1-2q$ and Eq. (19), we write

$$m = \sqrt{\frac{1-6q\left[1-f\left(1-\mu\right)\right]}{1-2q\left[1-f\left(1-\mu\right)\right]}} \equiv \sqrt{\frac{1-6\bar{q}}{1-2\bar{q}}}, \tag{21}$$

with $\bar{q} = \bar{\mu}q = q[1-f(1-\mu)]$, valid for $q < q_c^{MF}$, the mean-field critical temperature. By imposing $m = 0$ in Eq. (21), we obtain

$$q_c^{MF}(\mu, f) = \frac{1}{6\left[1-f\left(1-\mu\right)\right]}. \tag{22}$$

Note that when $f = 0$, Eq. (21) yields the isotropic MVM mean-field result for m

$$m = \sqrt{\frac{1-6q}{1-2q}}, \tag{23}$$

with $q_c^{MF} = 1/6$ [63]. For $f = 1$, $q_c^{MF} = 1/6\mu$ as anticipated. Additionally, near the phase transition, $m \sim (|q - q_c^{MF}|)^\beta$, and we find exponent $\beta = 1/2$, indicating that the cooperative majority-vote model should belong to the mean-field Ising universality class.

3.4. Mean-field simulations

We confirm our mean-field analytical results by performing Monte Carlo simulations in the mean-field approach. In this formulation, we randomly select an agent whose four neighbors are also randomly chosen [38]. We consider systems of $N = L^2$ agents, with L ranging from 40 to 200. We skip 10^3 MCS to allow thermalization and evaluate the time averages over the next 10^5 MCS up to 100 different samples.

In Fig. 9, we show mean-field numerical estimates for (a) $M_L(q,\mu,f)$, (b) $\chi_L(q,\mu,f)$ and (c) $U_L(q,\mu,f)$ as functions of the fraction of collaborative individuals f for several values of the noise q. We evaluate the magnetization numerically (circles) and compare it with the

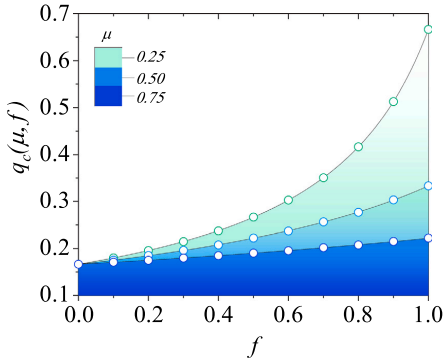

Fig. 10. Mean-field consensus-dissensus phase diagram. Lines denote analytical solutions given by Eq. (22), producing the phase boundaries that separate the ordered and the disordered phases for each noise sensibility μ. Circles represent numerical results for $q_c^{MF}(\mu, f)$, estimated by intersection points of Binder cumulant curves in mean-field simulations.

analytical solution of Eq. (21) (lines), exhibiting a satisfactory agreement. We note that mean-field results match the overall behavior displayed in Fig. 2 for square lattices, in which f improves consensus for different values of social noise q. The small divergence near the phase transition point results from the limited nature of the simulated mean-field network with $N = 4 \times 10^4$, whereas the analytical solution assumes the thermodynamic limit $N \longrightarrow \infty$.

The maximum value of each susceptibility curve in Fig. 9(b) denotes the critical values of f that yield an order–disorder phase transition. Additionally, the critical noise q necessary to vanish the order consensus increases with f, denoting a boost of social robustness. This result combines the behavior observed in Fig. 2(b) and Eq. (22), in which $q_c^{MF}(\mu, f)$ is a monotonically increasing function of f, validating our mean-field analysis.

Fig. 10 shows the mean-field phase diagram in the $q \times f$ parameter space, revealing the boundary between ordered and disordered phases as a function of f and μ. The lines represent the analytical solutions given by Eq. (22), and the circles represent the numerical data estimates obtained from the intersection points of Binder cumulant curves. The mean-field phase diagram shows the same qualitative characteristics of the square lattice scenario of Fig. 6. Numerical results are summarized in Table 1. Finally, we use finite-size scaling relations to plot in Fig. 11(a) magnetization, (*b*) magnetic susceptibility, and (c) absolute value of the Binder cumulant derivative at the critical temperature $q = q_c^{MF}(\mu, f)$ versus the system size for $\mu = 0.5$. The line slopes estimate critical exponents $\beta \approx 1/2$, $\gamma \approx 1$, and $\nu \approx 2$ for all values of the investigated f and μ. These results confirm the mean-field cooperative majority-vote dynamics belong to the mean-field Ising universality class.

4. Social entropy production

Entropy production is a manifestation of irreversibility dynamics. The cooperative majority-vote model generates entropy, even in the stationary regime; in contrast, reversible models reach thermodynamic equilibrium states without entropy production in the steady state [56–58]. In this context, we consider the Boltzmann–Gibbs entropy equation at time t

$$S(t) = -\sum_{\sigma} P(\sigma, t) \ln P(\sigma, t). \tag{24}$$

Combining Eq. (24) with the master equation of Eq. (11), we can express the time derivative of entropy as

$$\frac{d}{dt}S(t) = \frac{1}{2}\sum_{\sigma}\sum_{i}\left[w_i(\sigma^i)P(\sigma^i, t) - w_i(\sigma)P(\sigma, t)\right] \ln \frac{P(\sigma^i, t)}{P(\sigma, t)}, \tag{25}$$

We frame the rate of change of the entropy S of a system as two main components: entropy production rate Π and entropy flux Φ from system to environment. Thus, we write

$$\frac{d}{dt}S(t) = \Pi - \Phi. \tag{26}$$

Therefore, comparing Eqs. (25) and (26)

$$\Pi = \frac{1}{2}\sum_{\sigma}\sum_{i}\left[w_i(\sigma^i)P(\sigma^i, t) - w_i(\sigma)P(\sigma, t)\right] \ln \frac{w_i(\sigma^i)P(\sigma^i, t)}{w_i(\sigma)P(\sigma, t)}, \tag{27}$$

and

$$\Phi = \frac{1}{2}\sum_{\sigma}\sum_{i}\left[w_i(\sigma^i)P(\sigma^i, t) - w_i(\sigma)P(\sigma, t)\right] \ln \frac{w_i(\sigma^i)}{w_i(\sigma)}, \tag{28}$$

Note that Π is positive definite, but Φ can assume either sign depending on the direction of the flux. We write

$$\Phi = \sum_{\sigma}\sum_{i} w_i(\sigma)P(\sigma, t) \ln \frac{w_i(\sigma)}{w_i(\sigma^i)}, \tag{29}$$

that allows numerical estimates [64–69].

4.1. Flux on square lattices

The flux of entropy as a configurational average over the probability distribution in the stationary state from Eq. (29) is

$$\Phi = \sum_{i}\left\langle w_i(\sigma) \ln \frac{w_i(\sigma)}{w_i(\sigma^i)}\right\rangle. \tag{30}$$

The social entropy S remains constant in this state, therefore $\Pi = \Phi$. Hence, we calculate the stationary social entropy production by employing Monte Carlo simulations using Eq. (30).

In Fig. 12, we plot numerical results of entropy production $\varphi_L(q, \mu, f)$ in the stationary regime for several values of (a) system size L, (b) collaborative fraction f and (c) noise attenuation μ versus q. We observe in (a) that entropy flux has a weak sensibility with population size but a strong dependence on the fraction of collaborative agents and noise attenuation. Curves for $f = 0.0$ and $\mu = 1.0$ in Fig. 12(b) and (c), respectively, display the flux of entropy of the isotropic MVM [24,25], where a maximum flux occurs after the critical noise $q_c(\mu, f = 0.0) = 0.075$ and tends to zero for $q \to 0$ or $q \to 1/2$ in the isotropic case.

We highlight Fig. 12(b) also displays entropy flux that follows the isotropic system under the linear transformation $q \to q/\mu$, when $f = 1.00$ and $\mu = 0.5$. This flux vanishes for $q \to 0$ and $q \to 1/2\mu$. For $0 < f < 1$, after the maximum, instead of approaching zero, the entropy flux increases, supported by a discrepancy between the behavior of the cooperative and regular individuals. Indeed, (c) reveals this phenomenon intensifies as μ becomes smaller since the social temperature disparity among agents increases. We remark that, in general, a combination of cooperative and non-cooperative individuals increases the social entropy production of the society. Nonetheless, for small values of the social noise, the entropy generation is maximized when there is no cooperative behavior, $f = 0.0$.

For non-equilibrium systems, such as the cooperative majority-vote model, the Maximum Entropy Production Principle proposes that among all possible non-equilibrium steady states (NESS) that satisfy the system's constraints, the one with the highest entropy production rate is the most likely. The NESS with higher entropy production does not necessarily have more disorder but yields a dynamic balance that maximizes entropy production. Hence, if real-world societies follow this principle, the heterogeneity between cooperative and non-cooperative individuals could be a potential natural manifestation of the achieved NESS [70,71].

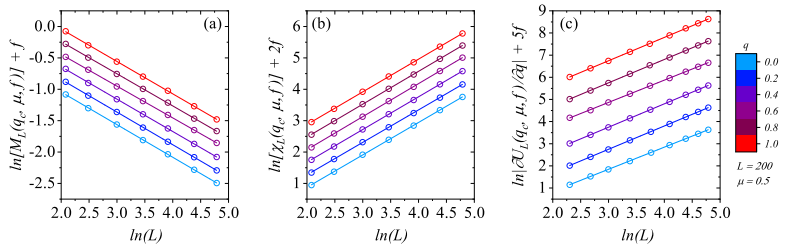

Fig. 11. Mean-field finite-size estimates for critical exponents. (a) $M(q,\mu,f)$, (b) $\chi(q,\mu,f)$ and (c) $|\partial U(q,\mu,f)/\partial q|$ with $q = q_c^{MF}(\mu,f)$ versus system size L for $\mu = 0.5$. Lines are linear regressions to the data, and their slopes equal the respective critical exponents in the mean-field limit.

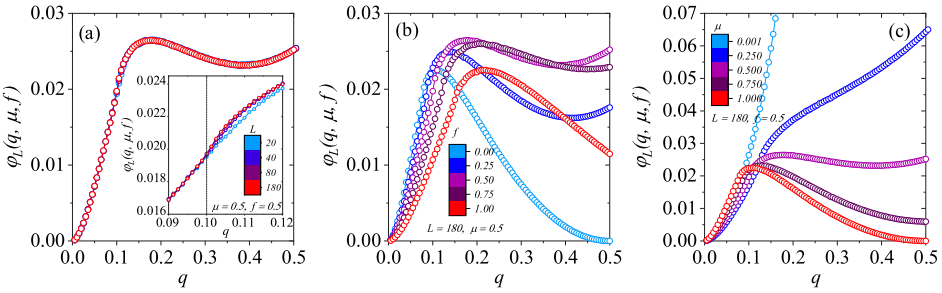

Fig. 12. Stationary social entropy flux production for collaborative majority-vote opinion dynamics versus noise parameter. We plot $\varphi_L(q,\mu,f)$ vs. q for several values of (a) system size L, (b) cooperative fraction f and (c) noise attenuation μ on square lattices. On (a) $\mu = 0.5$ and $f = 0.5$, while in (b) $\mu = 0.5$ and (c) $f = 0.5$ with $L = 180$. The lines are guides to the eyes.

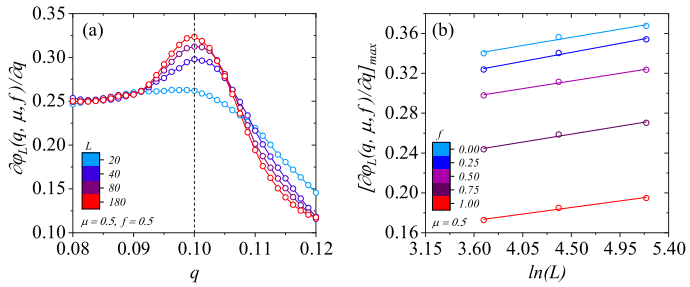

Fig. 13. Entropy flux Size dependence. (a) Derivative of entropy flux versus q for $\mu = 0.5$ and $f = 0.5$. (b) Maximum value of the entropy flux derivative at the critical point as a function of the natural logarithmic of the system size L. From top to bottom, line slopes are $\eta = 0.018(3), 0.020(2), 0.017(1), 0.018(2)$ and $0.015(2)$.

As a general pattern, the critical temperature does not coincide with the maximum of $\varphi_L(q,\mu,f)$. In fact, the critical noise is the point of inflection for φ that occurs before the maximum point. We display this behavior in the inset of Fig. 12(a), in which for $\mu = 0.5$ and $f = 0.5$, we obtain $q_c = 0.1011(1)$ (see Table 1). Therefore, in analogy with the entropy of equilibrium Ising model, the entropy flux exhibits a finite singularity at the critical point as

$$\varphi_L(q,\mu,f) = \varphi_L[q_c,\mu,f] + A_{\pm}\,|q - q_c|^{(1-\alpha)}\,, \tag{31}$$

where $A_{\pm}$ are amplitudes of regimes above and under the critical point $q_c = q_c(\mu,f)$ [57,58]. Hence, instead of a maximum in entropy flux, the second-order phase transition maximizes the derivative of entropy flux with respect to q, as we can observe in Fig. 13(a) for $q_c(0.5,0.5) = 0.1011(1)$. Indeed, from Eq. (31), we obtain

$$\frac{\partial\varphi_L(q,\mu,f)}{\partial q} \sim |q - q_c|^{-\alpha}\,, \tag{32}$$

where α corresponds to the same exponent associated with the specific heat of the Ising model. On square lattices, $\alpha = 0$, generating a singularity of the logarithm type. Hence, in analogy to the Ising model, we write

$$\frac{\partial\varphi_L(q,\mu,f)}{\partial q} \sim \ln|q - q_c|\,. \tag{33}$$

To verify our conjecture, we use the Savitzky-Golay Smooth algorithm with cubic polynomials to numerically estimate $\partial\varphi_L(q,\mu,f)/\partial q$ for several sizes L in Fig. 13(a). By finite-size scaling theory on Eq. (33), the maximum value of the partial derivative of entropy flux must diverge at the critical point as

$$\left[\frac{\partial\varphi_L(q,\mu,f)}{\partial q}\right]_{max} \sim \ln L^{\eta}, \tag{34}$$

with $\eta = (1-\zeta)/\nu$ and ν is the critical exponent associated to correlation length. Indeed, our results support $\nu = 1.0$, leading to $\zeta \approx 1.0$. Fig. 13(b)

confirms our assumption for $\mu = 0.5$ and several cooperative fraction values. We observe the same behavior for other values of μ and f.

4.2. Mean-field approach

The mean-field theory allows us to develop an analytical expression for entropy flux in the stationary regime. From Eq. (1), we write

$$\ln\frac{w_i(\sigma)}{w_i(\sigma^i)} = \ln\left[\frac{1-\sigma_i S\left(\sum_\delta \sigma_{i+\delta}\right)+2\mu_i q\sigma_i S\left(\sum_\delta \sigma_{i+\delta}\right)}{1+\sigma_i S\left(\sum_\delta \sigma_{i+\delta}\right)-2\mu_i q\sigma_i S\left(\sum_\delta \sigma_{i+\delta}\right)}\right].$$

Next, we note that the product $\sigma_i S\left(\sum_\delta \sigma_{i+\delta}\right)$ may assume only one of three possible values: $-1, 0$ and 1. Therefore,

$$\ln\frac{w_i(\sigma)}{w_i(\sigma^i)} = \begin{cases} \ln\left(\frac{\mu_i q}{1-\mu_i q}\right)\times(1), & \text{if } \sigma_i S\left(\sum_\delta \sigma_{i+\delta}\right) = 1, \\ \ln\left(\frac{\mu_i q}{1-\mu_i q}\right)\times(0), & \text{if } \sigma_i S\left(\sum_\delta \sigma_{i+\delta}\right) = 0, \\ \ln\left(\frac{\mu_i q}{1-\mu_i q}\right)\times(-1), & \text{if } \sigma_i S\left(\sum_\delta \sigma_{i+\delta}\right) = -1. \end{cases}$$

Thus, we obtain

$$\ln\frac{w_i(\sigma)}{w_i(\sigma^i)} = \ln\left[\frac{\mu_i q}{1-\mu_i q}\right]\sigma_i S\left(\sum_\delta \sigma_{i+\delta}\right). \tag{35}$$

Combining Eqs. (30) and (35)

$$\Phi = \sum_{j=1}^{Nf}\left\langle \ln\left[\frac{\mu q}{1-\mu q}\right]\sigma_j S\left(\sum_\delta \sigma_{j+\delta}\right) w_j(\sigma)\right\rangle + \sum_{k=Nf+1}^{N}\left\langle \ln\left[\frac{q}{1-q}\right]\sigma_k S\left(\sum_\delta \sigma_{k+\delta}\right) w_k(\sigma)\right\rangle. \tag{36}$$

Furthermore, in the stationary state, we obtain

$$\left\langle\left[S\left(\sum_\delta \sigma_{j+\delta}\right)\right]^2\right\rangle = \frac{1}{8}\left(5+6m^2-3m^4\right). \tag{37}$$

We divide Eq. (36) by the total number of individuals N and combine it with Eqs. (1) and (37) to derive an expression for entropy flux per site:

$$\begin{aligned}\varphi \equiv \Phi/N = f\ln\left(\frac{\mu q}{1-\mu q}\right)\times \left[\frac{1}{4}(3m^2-m^4)-\frac{\Theta_\mu}{16}(5+6m^2-3m^4)\right] \\ +(1-f)\ln\left(\frac{q}{1-q}\right)\times \left[\frac{1}{4}(3m^2-m^4)-\frac{\Theta}{16}(5+6m^2-3m^4)\right].\end{aligned} \tag{38}$$

We set $m = 0$ and get the disordered solution of the entropy flux, valid for $q > q_c^{MF}(\mu, f)$:

$$\varphi = \frac{5}{16} f\Theta_\mu \ln\left(\frac{1-\mu q}{\mu q}\right) + \frac{5}{16}(1-f)\Theta\ln\left(\frac{1-q}{q}\right). \tag{39}$$

On the ordered state, we have that magnetization behaves accordingly to Eq. (21), which is valid for $q < q_c^{MF}(\mu, f)$. Combining Eqs. (21) and (38), we obtain the entropy flux expression in the ferromagnetic state:

$$\varphi = \frac{f}{(1-2\bar{q})^2}\ln\left(\frac{1-\mu q}{\mu q}\right)\left\{\bar{q}\left[3-\Theta_\mu(2+\bar{q})\right]-\mu q\right\} + \frac{1-f}{(1-2\bar{q})^2}\ln\left(\frac{1-q}{q}\right)\left\{\bar{q}\left[3-\Theta(2+\bar{q})\right]-q\right\}, \tag{40}$$

with $\bar{q} = \bar{\mu} q = q[1-f(1-\mu)]$. For the particular case $f = 0.0$, we combine Eqs. (39) and (40) to obtain an expression for entropy production of the isotropic majority-vote model:

$$\varphi(q) = \left(\frac{q}{1-2q}\right)^2(3+2q)\ln\left(\frac{1-q}{q}\right)H(q_c-q)$$

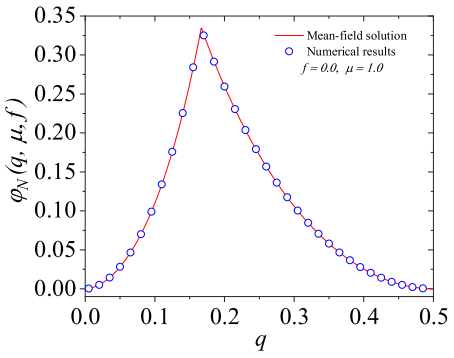

Fig. 14. Entropy production for mean-field isotropic majority-vote model. The red line denotes the results from Eq. (41) and blue circles are numerical estimations and $N = 180\times180 = 32400$.

$$+\frac{5}{16}(1-2q)\ln\left(\frac{1-q}{q}\right)H(q-q_c), \tag{41}$$

where $H(t)$ is the Heaviside function and $q_c^{MF}(\mu, f = 0.0) = 1/16$ is the isotropic mean-field MVM critical noise. We further investigate numerical simulations in the mean-field formulation to demonstrate this result.

Fig. 14 reveals mean-field entropy flux $\varphi(q, \mu, f)$ versus q, with $N = 180\times180 = 32400$, for the isotropic mean-field MVM simulation ($f = 0$ and $\mu = 1.0$). The red line represents results from Eq. (41), where blue circles represent numerical data in the mean-field formulation. Note that φ exhibits a singularity in mean-field critical noise $q_c^{MF} = 1/6$ and vanishes for $q \to 0$ and $q \to 1/2$.

We extend our investigation for mean-field stationary social entropy flux production $\varphi(q, \mu, f)$ versus noise q for several values of the cooperative fraction f and noise sensibility μ. In Fig. 15(a), we set $\mu = 0.5$ and $f = 0.00, 0.25, 0.50, 0.75$ and 1.00, while in Fig. 15(b), $f = 0.5$ and μ assume $0.25, 0.50, 0.75$ and 1.00. The open circles are mean-field numerical data for $N = 32400$ individuals, and the lines represent the analytical results given by Eqs. (39) and (40). There are slight deviations between mean-field solutions and Monte Carlo data in the ferromagnetic phase for entropy flux due to the finite nature of simulated systems, amplified as $\mu \to 0$.

Fig. 15(c) shows that φ does not approach zero when $q = 0.5$ in the mean-field limit for $0 < f < 1$ but remains finite independently of system size N. However, for any isotropic case ($f = 0$ or $\mu = 1.0$), φ tends to zero for $q = 0.5$, as expected. Distinguished from the square lattice case, in which φ reaches a maximum for $q > q_c$, in the mean-field framework, the maximum entropy flux point occurs at the mean-field critical temperature q_c^{MF}.

5. Final remarks

This work explores the impacts of collaborative behavior on majority-vote opinion dynamics and its social entropy production. We randomly select a fraction f of individuals of the society to represent cooperative agents, while the complementary fraction $1-f$ are regular voters. We introduce a social noise q such that with probability $(1-q)$, individuals agree with each other regarding a social issue subject, such as a political, professional, or economic matter. The cooperative agents retain a social temperature sensibility $0 < \mu < 1$, experiencing an effective social noise of μq, favoring social validation-based decisions. For $\mu = 0$ and $\mu = 1$, we recover bimodal [36,41] and isotropic majority-vote model [24,25], respectively.

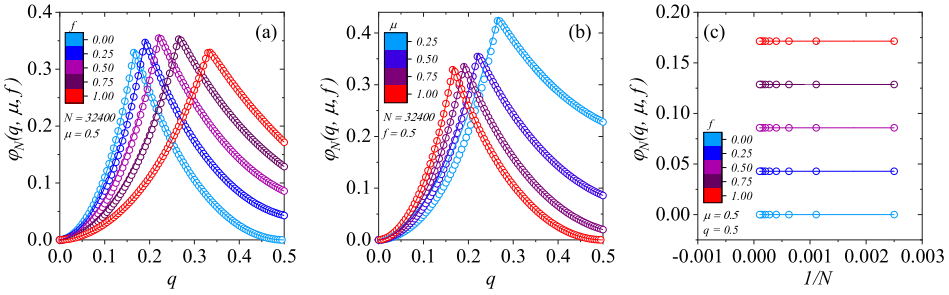

Fig. 15. Mean-field stationary social entropy flux production as a function of the social temperature. (a) Flux production dependence on cooperative fraction f for $\mu = 0.5$, (b) and several values of noise sensibility μ with $f = 0.5$. Open circles are numerical data from mean-field Monte Carlo simulations with $N = 32400$, and lines represent analytical results of Eqs. (39) and (40). Fig. (c) illustrates the finite behavior of entropy flux production for $q = 0.5$ which is independent of system size.

We employ Monte Carlo simulations and find that the system undergoes a second-order consensus-dissensus phase transition with the same universality class of 2D equilibrium Ising model for critical noise values $q = q_c(\mu, f)$. The critical exponents are not affected by the presence of collaborative agents, following Grinstein's criterion which states that nonequilibrium stochastic spin-like systems with up-down symmetry in regular lattices fall into the same universality class of the equilibrium Ising model [59,60].

For heterogeneous societies ($0 < f < 1$), there is a contrast between the effects of social temperature among regular and cooperative individuals, and $q_c(\mu, f)$ is a monotonically decreasing (increasing) function of noise attenuation μ (cooperative fraction f). Indeed, increasing the cooperative fraction f promotes the formation of a giant cluster of agreeing individuals that suppresses the phase transition. The collaborative behavior phenomena enhance the social robustness of society to opinion polarization. We highlight that if all individuals are cooperative ($f = 1.0$), the system behaves as if all individuals were regular ($f = 0.0$) under the linear transformation $q \longrightarrow q/\mu$.

Gibbs entropy and the master equation yield an expression that enables us to compute social entropy production in the stationary regime for square lattices. We observe that the entropy production of the isotropic majority-vote model has a maximum that occurs after the critical noise $q_c(\mu, f = 0.0) = 0.075$ and vanishes for $q \to 0$ or $q \to 1/2$. However, for cooperative societies, the entropy production increases after the local maximum and is non-zero for $q = 1/2$ due to the social temperature disparity between the collaborative and regular agents. Furthermore, combining cooperative and non-cooperative individuals yields higher social entropy production. Yet, for small social noise values, maximum entropy generation occurs in the absence of cooperative behavior, with $f = 0.0$.

Further generalizations of heterogeneous majority-vote opinion dynamics may consider complex network framework and the presence of non-compliance agents, in other words, $\mu > 1$. Exploring the influence of these dissenting agents within opinion dynamics can provide a deeper understanding of societal and (non)cooperative behaviors.

CRediT authorship contribution statement

Igor V.G. Oliveira: Writing – review & editing, Writing – original draft, Software, Methodology, Investigation, Formal analysis, Conceptualization. **Chao Wang:** Writing – review & editing, Writing – original draft, Validation, Investigation, Funding acquisition, Formal analysis, Conceptualization. **Gaogao Dong:** Writing – review & editing, Validation, Formal analysis. **Ruijin Du:** Writing – review & editing, Validation. **Carlos E. Fiore:** Writing – review & editing, Writing – original draft, Validation, Methodology, Investigation, Formal analysis, Data curation, Conceptualization. **André L.M. Vilela:** Writing – review & editing, Writing – original draft, Validation, Supervision, Software, Project administration, Methodology, Investigation, Funding acquisition, Formal analysis. **H. Eugene Stanley:** Supervision, Funding acquisition.

Declaration of competing interest

The authors declare that they have no known competing financial interests or personal relationships that could have appeared to influence the work reported in this paper.

Data availability

Data will be made available on request.

Acknowledgments

We thank M. J. de Oliveira for a critical reading of the manuscript. The authors acknowledge financial support from Brazilian and Chinese institutions and funding agents UPE, FACEPE (APQ-0565-1.05/14, APQ-0707-1.05/14), CAPES, CNPq (306068/2021-4), National Natural Science Foundation of China (72071006, 61603011, 62373169), and National Statistical Science Research Project (2022LZ03). The Boston University Center for Polymer Studies is supported by National Science Foundation, United States Grants PHY-1505000, CMMI-1125290, and CHE-1213217, by DTRA, United States Grant HDTRA1-14-1-0017, and by DOE, United States Contract DE-AC07-05Id14517.

References

[1] Ball P. The physical modelling of society: a historical perspective. Physica A 2002;314(1–4).
[2] Feng L, Li B, Preis T, Stanley HE. Linking agent-based models and stochastic models of financial markets. Proc Natl Acad Sci USA 2012;109(22).
[3] Hilbe C, Wu B, Traulsen A, Nowak MA. Cooperation and control in multiplayer social dilemmas. Proc Natl Acad Sci USA 2014;18(46).
[4] Schweitzer F. Sociophysics. Phys Today 2018;71(2).
[5] Galam S. Sociophysics: A review of galam models. Internat J Modern Phys C 2008;19(3).
[6] Galam S, Moscovici S. Towards a theory of collective phenomena: Consensus and attitude changes in groups. Eur J Soc Psychol 1991;21(1).
[7] Yeomans JM. Statistical mechanics of phase transitions. Clarendon Press; 1992.
[8] Galam S. Rational group decision making: A random field ising model at T=0. Physica A 1997;238(1–4).
[9] Tomé T, de Oliveira MJ. Role of noise in population dynamics cycles. Phys Rev E 2009;79(6).
[10] Schawe H, Hernández L. Higher order interactions destroy phase transitions in deffuant opinion dynamics model. Commun Phys 2022;5(32).
[11] Iacopini I, Petri G, Barrat A, Latorra V. Simplicial models of social contagion. Nature Commun 2019;10(2485).
[12] Centola D. The spread of behavior in an online social network experiment. Science 2010;329(5996).
[13] Stauffer D, de Oliveira SMM, de Oliveira PMC, de Sá Martins JS. Biology, sociology, geology by computational physicists. Elsevier; 2006.

[14] Lu Xi, Mo Hongming, Deng Yong. An evidential opinion dynamics model based on heterogeneous social influential power. Chaos Solitons Fractals 2015;73.
[15] Galam S. Application of statistical physics to politics. Physica A 1999;274(1–2).
[16] Sznajd-Weron K, Sznajd J. Opinion evolution in closed community. Internat J Modern Phys C 2000;11(06).
[17] Kononovicius Aleksejus. Supportive interactions in the noisy voter model. Chaos Solitons Fractals 2021;143.
[18] Nyczka P, Sznajd-Weron K. Anticonformity or independence?—insights from statistical physics. J Stat Phys 2013;151(1–2).
[19] Sznajd-Weron K, Szwabiński J, Weron R. Is the person-situation debate important for agent-based modeling and vice-versa? PLoS One 2014;9(11).
[20] Stone TE, McKay SR. Critical behavior of disease spread on dynamic small-world networks. Europhys Lett 2011;95(3).
[21] Sznajd-Weron K, Sznajd J. Who is left, who is right? Physica A 2005;351(2–4).
[22] Sznajd-Weron K, Weron R. How effective is advertising in duopoly markets? Physica A 2003;324(1–2).
[23] Galam S, Zucker J. From individual choice to group decision-making. Physica A 2000;287(3–4).
[24] de Oliveira MJ. Isotropic majority-vote model on a square lattice. J Stat Phys 1992;66(1).
[25] de Oliveira MJ, Mendes JFF, Santos MA. Nonequilibrium spin models with ising universal behaviour. J Phys A: Math Gen 1993;26.
[26] Chen H, Shen C, He G, Zhang H, Hou Z. Critical noise of majority-vote model on complex networks. Phys Rev E 2015;91(2).
[27] Chen H, Wang S, Shen C, Zhang H, Bianconi G. Non-markovian majority-vote model. Phys Rev E 2020;102(6).
[28] Lima JRS, Lima FWS, Alves TFA, Alves GA, Macedo-Filho A. Diffusive majority-vote model. Phys Rev E 2022;105(3).
[29] Campos Paulo RA, de Oliveira Viviane M, Brady Moreira FG. Small-world effects in the majority-vote model. Phys Rev E 2003;67(2).
[30] Choi J, Goh K. Majority-vote dynamics on multiplex networks with two layers. New J Phys 2019;21(3).
[31] Krawiecki A, Gradowski T, Siudem G. Majority-vote model on multiplex networks. Acta Phys Polon A 2018;133(6).
[32] Pereira Luiz FC, Brady Moreira FG. Majority-vote model on random graphs. Phys Rev E 2005;71(1).
[33] Lima FWS. Majority-vote on undirected barabási-albert networks. Commun Comput Phys 2007;2(2).
[34] Crokidakis N, de Oliveira PMC. Impact of site dilution and agent diffusion on the critical behavior of the majority-vote model. Phys Rev E 2012;85(4).
[35] Vilela André LM, Brady Moreira FG. Majority-vote model with different agents. Physica A 2009;388(19).
[36] Vilela André LM, Brady Moreira FG, de Souza Adauto JF. Majority-vote model with a bimodal distribution of noises. Physica A 2012;391(24).
[37] Lima FWS. Majority-vote model with heterogeneous agents on square lattice. Internat J Modern Phys C 2013;24(11).
[38] Vieira AR, Crokidakis N. Phase transitions in the majority-vote model with two types of noises. Physica A 2016;450.
[39] Encinas JM, Chen Hanshuang, de Oliveira Marcelo M, Fiore Carlos E. Majority-vote model with ancillary noise in complex networks. Physica A 2019;(516).
[40] Wu ZX, Holme P. Majority-vote model on hyperbolic lattices. Phys Rev E 2010;81(1).
[41] Vilela André LM, de Souza Adauto JF. Majority-vote model with a bimodal distribution of noises in small-world networks. Physica A 2017;488.
[42] Vilela André LM, Pereira Luiz FC, Dias L, Stanley HE, da Silva Luciano R. Majority-vote model with limited visibility: An investigation into filter bubbles. Physica A 2021;563.
[43] Vilela André LM, Stanley HE. Effect of strong opinions on the dynamics of the majority-vote model. Sci Rep 2018;8(1).
[44] Santos MA, Teixeira S. Anisotropic voter model. J. Stat. Phys. 1995;78(3–4).
[45] Costa LSA, de Souza AJF. Continuous majority-vote model. Phys Rev E 2005;71(5).
[46] Melo Diogo FF, Pereira Luiz FC, Brady Moreira FG. The phase diagram and critical behavior of the three-state majority-vote model. J Stat Mech Theory Exp 2010;2010(11).
[47] Lima FWS. Three-state majority-vote model on square lattice. Physica A 2012;391(4).
[48] Vilela André LM, Zubillaga Bernardo J, Wang Chao, Wang M, Du Ruijin, Stanley HE. Three-state majority-vote model on scale-free networks and the unitary relation for critical exponents. Sci Rep 2020;10.
[49] Vilela André LM, Wang Chao, Nelson Kenric P, Stanley HE. Majority-vote model for financial markets. Physica A 2019;515.
[50] Zubillaga Bernardo J, Vilela André LM, Wang Chao, Nelson Kenric P, Stanley HE. A three-state opinion formation model for financial markets. Physica A 2022;588.
[51] Granha Mateus FB, Vilela André LM, Wang Chao, Nelson Kenric P, Stanley HE. Opinion dynamics in financial markets via random networks. Proc Natl Acad Sci 2022;119(49).
[52] Zha Q, Kou G, Zhang H, Liang H, Chen X, Li C, Dong Y. Opinion dynamics in finance and business: a literature review and research opportunities. Financ Innov 2020;6(1).
[53] Capraro V. A model of human cooperation in social dilemmas. PLoS One 2013;8(8).
[54] de Jong G, Veijer J. Cooperative behavior in strategic decision making: Human capital and personality traits. Behav Strateg: Emerg Perspect 2014.
[55] Pennisi E. How did cooperative behavior evolve? Science 2005;309(5731).
[56] Tomé T, de Oliveira MJ. Entropy production in nonequilibrium systems at stationary states. Phys Rev Lett 2012;108(2).
[57] Hawthorne Felipe, Harunari Pedro E, de Oliveira MJ, Fiore Carlos E. Nonequilibrium thermodynamics of the majority-vote model. Phys Rev E 2023;(25).
[58] Fernández Noa CE, Harunari Pedro E, de Oliveira MJ, Fiore CE. Entropy production as a tool for characterizing nonequilibrium phase transitions. Phys Rev E 2019;(100).
[59] Grinstein G, Jayaprakash C, He Y. Statistical mechanics of probabilistic cellular automata. Phys Rev Lett 1985;55(23).
[60] Baxter RJ. The inversion relation method for some two-dimensional exactly solved models in lattice statistics. J Stat Phys 1982;28(1).
[61] Van Kampen NG. Stochastic processes in physics and chemistry. Elsevier; 2007.
[62] Tomé Tânia, Fiore Carlos E, de Oliveira Mário J. Stochastic thermodynamics of opinion dynamics models. Phys Rev E 2023;(107).
[63] Tomé T, de Oliveira MJ. Stochastic dynamics and irreversibility. Springer; 2015.
[64] Nicolis G, Prigogine Ilya. Self-organization in nonequilibrium systems: from dissipative structures to order through fluctuations. Wiley; 1977.
[65] Lebowitz JL, Spohn H. A gallavotti-cohen-type symmetry in the large deviation functional for stochastic dynamics. J Stat Phys 1999;95(1–2).
[66] Maes C. The fluctuation theorem as a gibbs property. J Stat Phys 1999;95(1).
[67] Maes C, Redig F, Moffaert AV. On the definition of entropy production, via examples. J Math Phys 2000;41(3).
[68] Maes C, Netočnỳ K. Time-reversal and entropy. J Stat Phys 2003;110(1).
[69] Lecomte V, Rácz Z, Van Wijland F. Energy flux distribution in a two-temperature ising model. J Stat Mech Theory Exp 2005;2005(2).
[70] Martyushev LM, Seleznev VD. Maximum entropy production principle in physics, chemistry and biology. Phys Rep 2006;426(1).
[71] Dyke J, Kleidon A. The maximum entropy production principle: Its theoretical foundations and applications to the earth system. Entropy 2010;12(3).